University of Hyderabad, Hyderabad, India

Università degli Studi di Trento, Trento, Italy

Optical Spectroscopic Characterization of Rare-earth activated conventional, non-conventional and nano-structured glasses for Integrated Optics

Thesis submitted for the degree of

DOCTOR OF PHILOSOPHY

Tesi di

DOTTORATO DI RICERCA IN FISICA

by

Krishna Chaitanya Vishnubhatla

Supervisors:

Prof. D. Narayana Rao……University of Hyderabad
Dr. Maurizio Ferrari…….....CNR-IFN
Prof. Maurizio Montagna……University of Trento

DECLARATION

I hereby declare that the matter embodied in this thesis entitled

"**Optical spectroscopic characterization of rare-earth activated conventional, non-conventional and nanostructured glasses for integrated optics."**

is the result of investigations carried out by me under the internationally co-tutored PhD programme at the School of Physics, University of Hyderabad, Hyderabad, India, and at the Department of Physics, University of Trento, Trento, Italy, under the supervision of Prof. D. Narayana Rao (University of Hyderabad), Dr. Maurizio Ferrari (CNR-IFN) and Prof. Maurizio Montagna (University of Trento).

Place: Hyderabad (**Krishna Chaitanya Vishnubhatla**)

Date:

CERTIFICATE

This is to certify that the work described in this thesis has been carried out by Mr. **Krishna Chaitanya Vishnubhatla.** under our collaborative supervision at the University of Hyderabad, Hyderabad, India, and at the Department of Physics, University of Trento, Trento, Italy, and this has not been submitted for any degree or diploma at this or any other University.

(Prof. D. NarayanaRao)

Place: Hyderabad
Date:

(Dr. Maurizio Ferrari)

Place: Trento
Date:

(Prof. Maurizio Montagna)

Place: Trento
Date:

Dean
School of Physics
University of Hyderabad

“Education is for life, not for living”
- Sri Sathya Sai Baba

To my Parents,

And my Brother

Contents

Chapter 1

Introduction

The activities presented in this thesis are performed in the framework of the Joint Research Program, India-Trento Bose-Romagnosi Program for Advanced Research Research & Development of Active Bulk and Planar Waveguides based on Nanostructured Glassy Systems at the School of Physics, University of Hyderabad and the C.S.M.F.O. (Caratterizzazione e Sviluppo Materiali per la Fotonica e l' Optoelettronica) group (CNR-IFN and Physics Department, University of Trento).

1.1 Motivation

The idea of using glass fiber for carrying out an optical signal for communications originated with Alexander Graham Bell [1]. However to be useful in practical applications, this idea had to wait 80 years for the discovery of glasses with low loss and cost-effective electronics. Development of fibers and devices for optical telecommunication began in the 1960s but the real change came in the 1985 with the discovery of optical fiber amplifier. With the advent of Wavelength Division Multiplexing (WDM) and Erbium Doped Fiber Amplifier (EDFA) technology replacing the electronic repeaters, the transmission capacity of a single fiber has increased by transmitting simultaneously through many channels in the same fiber. In standard EDFA the amplification bandwidth is limited to the emis-

sion bandwidth of Er^{3+} (1530 and 1560 nm). Hence various active glassy materials are being extensively explored as hosts for erbium ions and other rare-earths ions in order to increase their emission band and to exploit the entire low loss region (1300-1700 nm in new All Wave^{TM}Corning fibers). Moreover, this should be obtained both for long distance network and for Metropolitan Area Network (MAN), Local Area Network (LAN), to provide the final customer with fast data access. In fact, to favor the development of broadband MAN, low cost devices incorporating both active and passive functionalities are required. Planar technology that has the capability of creating optical waveguides on suitable substrates may offer a solution to this problem. Furthermore, the complexity and the interconnections of the networks will require subsystems incorporating many optical devices [2], which also have to be as compact as possible [3]. This led to the idea of integrated optics (IO) in which several functions are integrated on to a single chip. Unlike the EDFAs which are few tens of meters long, IO amplifiers should be as short as possible (few centimeters). Therefore higher rare-earth concentrations are required as compared to EDFAs [4]. This poses the challenge of controlling the energy transfer processes in the heavily doped materials used to achieve amplification and minimizing the non-radiative processes. An optimization of the dopant-matrix system is therefore necessary. Technology demands the capability of creating channel waveguide in such active material. Various technologies have been employed for the fabrication of silica-based IO components, including ion-exchange, sol-gel, rf-sputtering, flame hydrolysis, chemical vapor deposition, and pulsed laser deposition [5]. The new emerging technology of laser direct writing (LDW) of structures and buried waveguides inside the bulk, thin films, glasses, and polymers using a femtosecond laser promises to be a strong contender for such applications. In contrast to the above mentioned standard manufacturing methods such as physical-vapor deposition or ion exchange, the direct write approach is not restricted to the surface and can yield truly three-dimensional (3-D) structures. Femtosecond (fsec) pulses possess the unique ability to precisely deposit energy inside the

material. This ultrafast interaction does not require specially prepared or photosensitive materials and has the capability of realizing 3-D photonic structures in diverse materials at arbitrary depth inside the bulk substrate.

In this context, various novel host glass materials doped with Erbium are being investigated with much attention for development of gain elements involving the Er^{3+} intra-4f emission at 1.54 μ m, in the ultra-low loss telecommunication window. The research work was carried out on various novel active glasses with the following main objectives,

- to find novel suitable host material for Er^{3+} ions,
- to achieve Er^{3+} luminescence enhancement using Silver as sensitizer, and
- to fabricate waveguides, micro-structures by LDW in various glasses.

1.2 Thesis - outline:

The thesis has been written in way that each chapter is self-consistent and at the same time all chapters together present a collective picture envisioning the aims stated above. Apart from motivation and thesis outline, the later part of this chapter (**Chapter one**) gives a brief introduction, overview of glasses and rare-earths from the point of view of development of a suitable host material for Er^{3+}.

Second chapter discusses the results of the spectroscopic characterization of Baccarat glasses and Tellurite glasses and their merits. The Baccarat-modified silica glass with optimal Erbium (Er) activation, proves to be a valuable candidate for applications in telecommunication systems with good spectroscopic properties and high quantum efficiency close to 80%. Tellurite glasses have high refractive index compared to silicate glasses. This induces the increase of local field around the rare earth ion causing the enhancement of the radiative transitions and a wider splitting of Stark sublevels. Consequently greater efficiency and broadening of the emission shape is observed. These properties were proved to be valuable for WDM applications.

Third chapter concentrates on the energy transfer mechanism from silver to Erbium in Ag ion exchanged sodium silicate glasses and Er activated phosphate glasses, co-doped with silver. As the rare-earth ions have small absorption cross section, in order to improve luminescence yield several attempts were made to increase these ions excitation efficiency. Luminescence enhancement is obtained by energy transfer mechanism from a species with a large absorption cross section to the rare earth ion [6]. Enhancement of the Er luminescence was obtained in Ag-ion exchanged Silicate glass upon exciting at 476.5 nm. Silver and erbium co-doped sodium metaphosphate glasses were prepared by standard melt-quench technique. The excitation spectra of the 1.5 μ m luminescence of Er demonstrated energy transfer from Ag aggregates to Er, though it is weak as compared to Silicate glasses.

Fourth chapter focuses on Laser Direct Writing(LDW) of micro-structures, waveguides in glasses. The ability of LDW to pattern (process, deposit, dispense, or remove) materials in three dimensions and in a pre-determined manner is attractive for several important applications in photonics and microfluidics. A home built set-up for LDW of optical waveguides by femtosecond (fsec)laser was optimized and buried waveguides were written in various glasses. The fsec-laser used for LDW has a central wavelength of 800 nm, 100 fsec pulse duration, and 1 kHz repetition rate with the amplified pulses having output energy up to 1 m J. By optimizing the parameters like laser intensity, sample translation speed, and the input beam diameter waveguides with dimensions of 1- 10 microns were achieved. By placing a slit (of appropriate dimension) before the microscope objective, a structure of width 750 nm (less than diffraction limit) is written in Baccarat glass. Various micro-structures like hexagons, quadrilaterals, and gratings are inscribed in fused silica glass. The change in refractive index is measured to be of the order of 10^{-3} from the measurements of diffraction efficiency of the gratings in fused silica, Baccarat, GE124, tellurite and Foturan glasses. This chapter also presents the micro-raman characterization, absorption spectra and confocal photoluminescence study

of microstructures and waveguides inscribed into various glasses. Waveguiding is demonstrated in structures inscribed in Baccarat glass by beam shaping of the femtosecond laser by placing a rectangular slit before the focusing objective.

Fifth chapter summarizes the work done and lists the most significant results obtained along with a brief description of the future perspectives.

1.3 A brief overview of Glasses and Rare-earths

1.3.1 Glasses:

Glass can be defined as an amorphous solid completely lacking in long range, periodic atomic structure and exhibiting a region of glass transformation behavior [7] Glass was found more than 5000 years ago and since then it has been widely used in daily life. Glass is one of the most important materials in optics. As a passive component it is being used in optical fibers, lenses, mirror substrates and prisms etc.

With the development of integrated-optics glasses are being used with active functionalities, such as in light amplification, optical storage, ultrafast-optical switching and various modulations of light [6]

Glass belongs to the class of amorphous materials. This is a state of matter that possesses most of the macroscopic and thermodynamic properties of the solid state, while displaying the structural disorder and isotropic behavior of a liquid. It is also referred to as super cooled liquid. It lacks the periodic arrangement of constituent atoms. In a crystal, the atoms are arranged in a periodic pattern that repeats up to infinity.

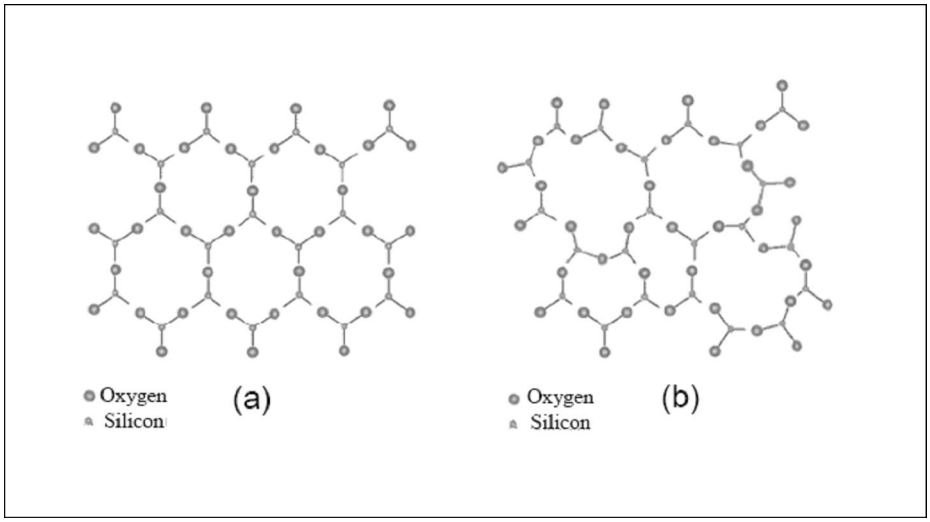

Figure 1.1: (a) Regular arrangement of SiO_2 in quartz, (b) arrangement of SiO_2 in glass

Quartz the major natural crystalline form of silica (SiO2) is a periodic structure of tetrahedron where Si atom occupies the center and oxygen atoms are on the apex. A regular network in a plane representation is given schematically below in Figure 1.1. Silica glass on the other hand is made from the same elemental tetrahedron except that there is no apparent regularity in the construction of this network. Many compounds, such as SiO_2, B_2O_3, and P_2O_5, readily form glasses by themselves and are called glass-formers or network formers [36, 37]. Some oxides, which are called network modifiers, cannot form a glass by themselves but they can form a glass when mixed with network formers. Oxides of alkali metals or alkali-earth metals are examples of typical network modifiers. When network modifiers are added to the glass they can modify the network, they break up the continuous network by introducing dangling or non-bridging oxygens (NBO). Though 99% of the practical glasses in terms of volume and types are produced by 'melt-quenching' technique [10], there are other processes by which glasses are realized. Some of the other main methods are (a)Vapor deposition (b) Sol-gel processing and (c) neutron irradiation of crystalline materials. Most of the traditional glasses are inorganic and non-metallic, but currently there are vast number of organic glasses in use and metallic glasses are becoming more common [7]. Some of the main features by which the glasses are qualified[10] are given below .

(1)Structural features:

- **Atomic arrangement:** Due to their peculiar arrangement of atoms, glasses can neither be classified into crystal nor into as liquids. This lack of regularity of atomic arrangement, has to be taken into account to understand the relevant physical and chemical features, by which glasses have some special properties. Since active ions doped in a glass occupy positions similar to the modifier ions, the absorption and emission spectra, if any, are broader than those from active ions doped in a crystalline materials, a feature which is often advantageous in preparation of special

glasses.

- **Chemical composition:** The other important feature attributed to the uniqueness of glass is the flexibility of the chemical composition. Unlike crystalline materials, there is no requirement of stoichiometry among constituents provided that there is electrical neutrality over the whole structure of a glass is maintained. Further the ability to modify the properties of a glass through ion-exchange, for example the movement of alkali ions within a glass structure gives us the flexibility to replace the alkali ions by other ions of same valence, i.e. Na^+ by K^+ or Ag^+ etc.

(2)Thermodynamic features:

- **Glass transition:** A glass is a thermodynamically metastable material which remains untransformed to its most stable state due to the hinderance of the atomic re-arrangement during the process of glass formation. The transition from a viscous liquid to a solid glass is called 'glass transition', and the temperature at which this occurs is called glass transition temperature (T_g). Conversely, T_g can also be thought as the temperature at which the solid begins to behave as viscoelastic solid on heating [7]. T_g is not a constant, it depends on thermal history of the sample.
- **Thermal stability and structural relaxation:** A glass obtained by cooling a liquid can be transformed into crystal when heated well above the T_g. If the temperature of heating is close to T_g, the glass remains un-crystallized but undergoes atomic re-arrangement called structural relaxation.

(3)Optical features:

- **Transparency:** As the intrinsic scattering losses of a glass is very small, the glass in principle, is transparent to light in the wavelength region where there is no intrinsic absorption. Glasses of oxides and fluorides systems that have a wide gap between the conduction and valence bands are generally transparent to light in the visible and near infrared regions, where as those of the chalcogenide system have narrower band gaps are generally translucent in visible region but transparent in the near infrared and infrared regions. The loss value is sum of the intrinsic loss and the extrinsic loss attributed to absorption by impure atoms and scattering loss due to compositional heterogeneity, etc. Majority of impurities that cause absorption loss are transitional metal ions and water.

- **Linear and non-linear refractive index and dispersion:** Refractive index is another important property to be considered with respect to the optical features of glass. It is correlated with electric dipole moment induced by the electromagnetic interaction of constituent atoms and molecules with light. The phenomenologically observed intensity dependant refractive index is given by, $n = n_0 + n_2^{"} I$, where I is the average beam intensity in units of (W / cm^2), n_0 is the linear refractive index and $n_2^{"}$ is the nonlinear refractive index.

1.3.2 Rare-earths:

The elements in the periodic table with the atomic number from 57 to 71 are known as the lanthanides. They belong to the broader class of elements known as the rare-earths, which also includes the actinides. The electronic configuration of the neutral lanthanides possess the common feature of a Xe configuration with three outer electrons $5d6s^2$ and n electrons in the 4f shell, with $1 \leq n \leq 13$. Lanthanides are chiefly trivalent and when ionized, the outer electrons $5d6s^2$ are removed and the triply ionized elements have the configuration [Xe] $4f^n$. Though other valance states are also known but they are much less stable. The closed 5s and 5p shells effectively shield the 4f shell. The ligand

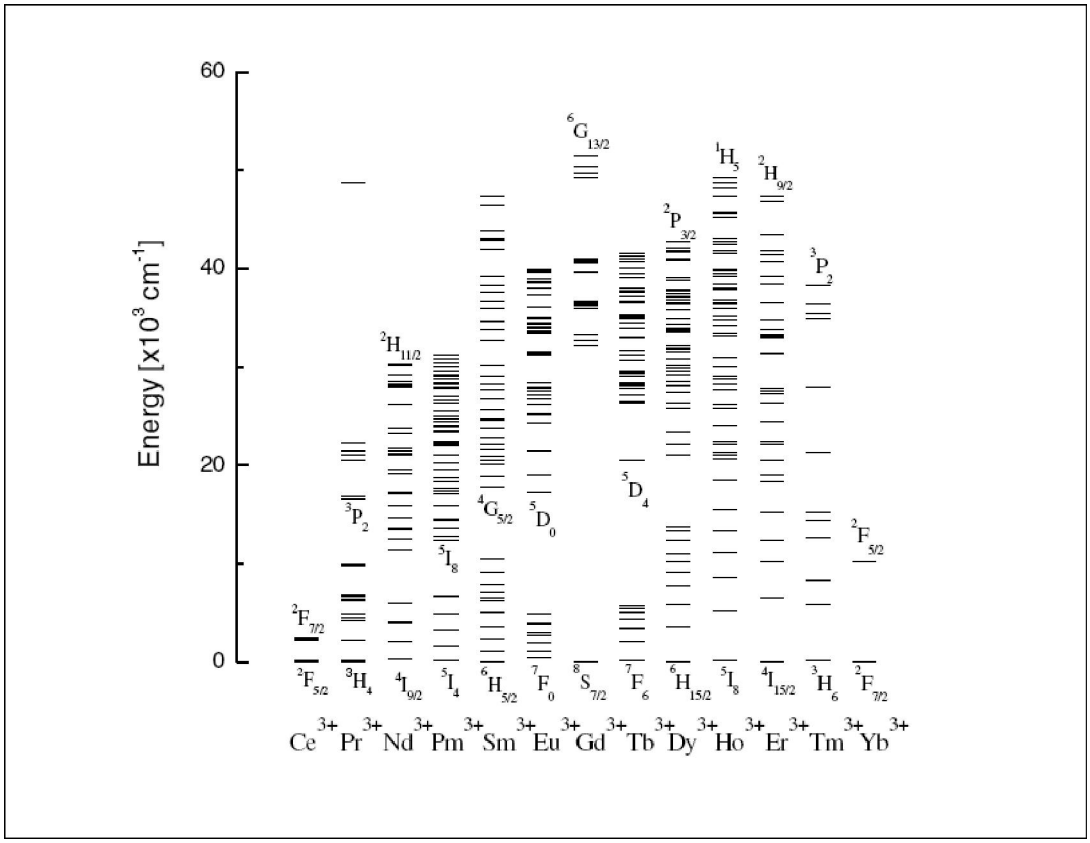

Figure 1.2: Energy Level diagram of Lanthanides [11]

field of the glass has only very weak influence on the electronic cloud of the lanthanide ion, which makes their spectroscopic properties very similar in all glassy and crystalline environments.

Figure 1.3.2 shows energy level diagrams for the isolated 3+ ions of each of the 13 lanthanides with partially filled 4f orbitals from cerium to ytterbium. As one progresses along this series, the average radius of the 4f shell slowly decreases. This phenomenon is known as lanthanide contraction. The observed absorption and fluorescence is because of the intra-configurational f-f transitions. The excited state lifetimes of rare-earths in glasses can be as long as 10ms and can have high fluorescence efficiencies Rare-earth ion luminescence is by no means a new field; sharp luminescence bands from the lanthanides

have been known since the beginning of the 20th century. The energy levels of the lanthanide ions in a range of crystals were extensively investigated and tabulated by Dieke and co-workers in 1968 [14], and the rare-earths have been widely used as the active ions in phosphors for several decades. The most common Cathode ray tube phosphors exploit the visible transitions of the triply charged ions of erbium (Er^{3+}), europium (Eu^{3+}), terbium (Tb^{3+}) and cerium (Ce^{3+}) to produce the saturated red, green and blue required for full colour display. There is therefore a substantial body of work on the use of rare-earth ions as phosphor activators, and this is a mature technology. Moving on from this, chronologically speaking, much research in the 1960s was concerned with the development of solid-state lasers exploiting the luminescence of rare-earth ions in glasses and crystals. The Nd:YAG laser is perhaps the most notable success from this period, and there is continued interest in novel rare-earth doped materials for lasers. Nd:glass lasers are widely used in very high power applications such as fusion research, and other rareearths such as holmium and praseodymium have found uses in fibre lasers and lasers for medical applications. More recently, however, optoelectronics has emerged as the principal area of research into rare-earth luminescence. This covers applications such as telecommunications, chip-to-chip and on-chip interconnects and optical memories. In recent years most of the interest in luminescent rare-earth ions has concentrated on one species: trivalent erbium, and in particular its emission band around 1.53 μ m. The reasons for this are clear if one considers the rapid growth in optical telecommunications and some of the materials limitations on this technology. The loss spectrum of silica fibre as seen in Figure 1.3.2 has two low loss windows : one between 1200 and 1350 nm, and a second (termed the ultra low-loss window) around 1450 1600nm. These are produced by the combined effects of losses due to Rayleigh scattering, overtones of the hydroxyl absorption, bending losses and infrared absorption due to the SiO species. The 1500nm window is the wavelength region of choice for telecommunications, and fortuitously coincides with the 1535nm intra-4f $^4I_{13/2}$ - $^4I_{15/2}$ transition of the Er^{3+} ion.

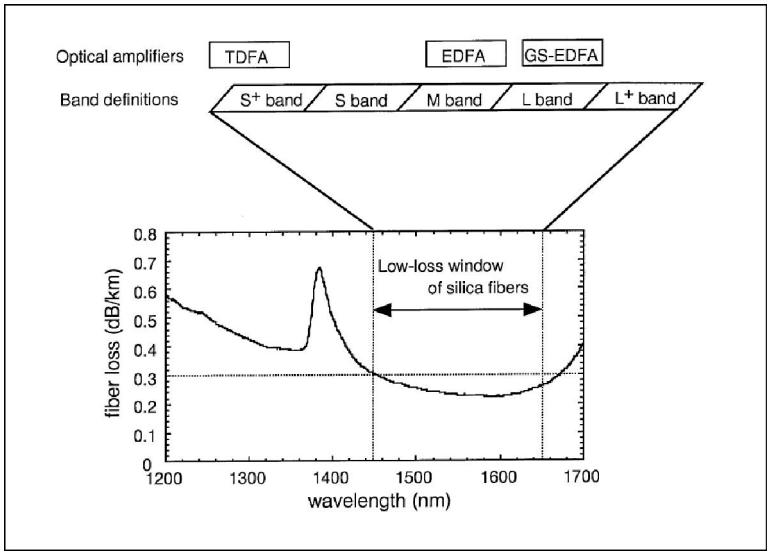

Figure 1.3: The loss spectrum of silica fibre depicting the ultra low-loss window at 1.5 μ m.

For this reason there has been intense interest in utilizing erbium doped materials for gain elements and sources in telecommunications systems. The development of the EDFA in the late 1980s [15, 16] exploited the $^4I_{13/2}$ - $^4I_{15/2}$ transition and allowed the transmission and amplification of signals in the 1530 $\leftrightarrow$ 1560 nm region without the necessity for expensive optical to electrical conversion [17]. It offered several advantages over electrical amplification, including the capability to produce gain at many different wavelengths simultaneously; a key requirement for WDM. The silica EDFA has been a tremendous success.

1.3.3 Rare-earths in glasses

Rare-earth luminescence was first reported in glasses and crystals, and rare earths (particularly erbium) in waveguide materials remain the most important and thoroughly researched application of rare-earth ions for optoelectronics. Oxide glasses are well known as excellent hosts for rare-earth ions: one of the first solid-state lasers was demonstrated in 1961 in Nd^{3+} - doped glass [16]. Lasing in a Nd^{3+} - doped multi-component glass

fibre was reported three years later [17]. The same material structure was exploited to demonstrate the first thin-film waveguide glass amplifier, in 1972 [18], and the first integrated optical glass laser, in 1974 [19]. The interest for Er^{3+} - doped glasses arose quite later, in the late 1980s, when the main operational wavelength for optical-fibre communication systems shifted towards the 1.5 μm band [20]. Since then, many remarkable results in the development of more efficient glass matrices and in the actual fabrication of rare-earthdoped glass integrated optical amplifiers have been achieved[11].

Limiting factors

Some of the most important limiting factors to be considered in case of the rare-earths being doped in solid hosts 9 glasses) are as follows [18, 22]

- **Phonon interactions:** Multiphonon relaxation can rapidly depopulate the upper excited state and therefore readily quench luminescence [18]. Such processes only occur when a small number of phonons are required to bridge the energy gap between the pair of electronic states of the rare-earth ion. As a guide, it is generally held that if the phonon cut-off energy of the matrix is greater than 25% of the energy gap (Δ E), rare-earth luminescence will be completely quenched. For phonon cut-off energies between 10% and 25% of Δ E, quenching will result in a temperature-dependent luminescence lifetime, whilst for phonon cut-off energies smaller than 10% the contribution of multiphonon relaxation will be negligible [19]. The importance of multiphonon processes therefore depends strongly on both the host material and the electronic structure of the rare-earth. In the case of erbium, the energy gap of the $^4I_{13/2}$ to $^4I_{15/2}$ transition is approximately 6500 cm^{-1}. The phonon cut-off energy of silica is 1100 cm^{-1}, and therefore the rare-earth luminescence at 1535 nm is only weakly quenched at room temperature. The presence of OH^- ion also leads to luminescence quenching. The bands characteristic of the OH^- groups in silicate glasses, are generally observed at 3670 and 3750 cm^{-1}. The $^4I_{13/2}$

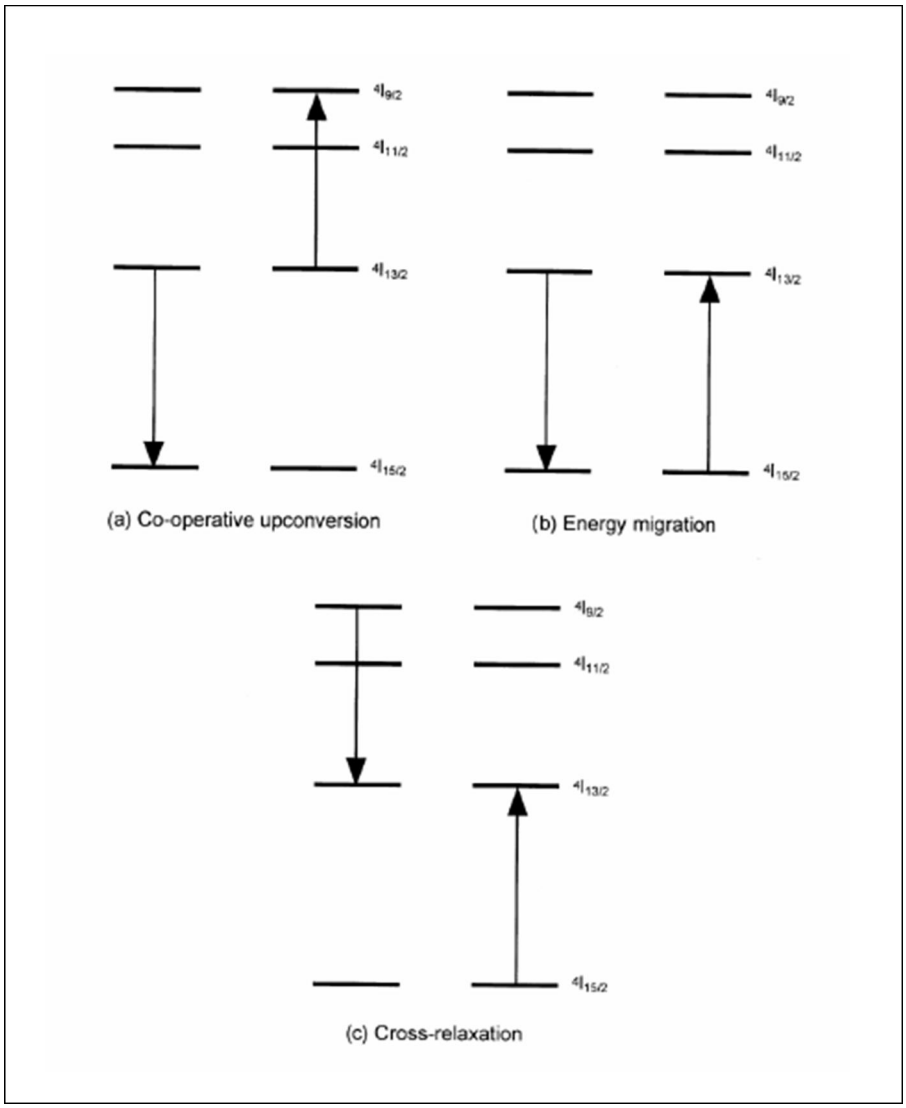

Figure 1.4: Ion - Ion interactions between two neighboring Er^{3+} ions [22]

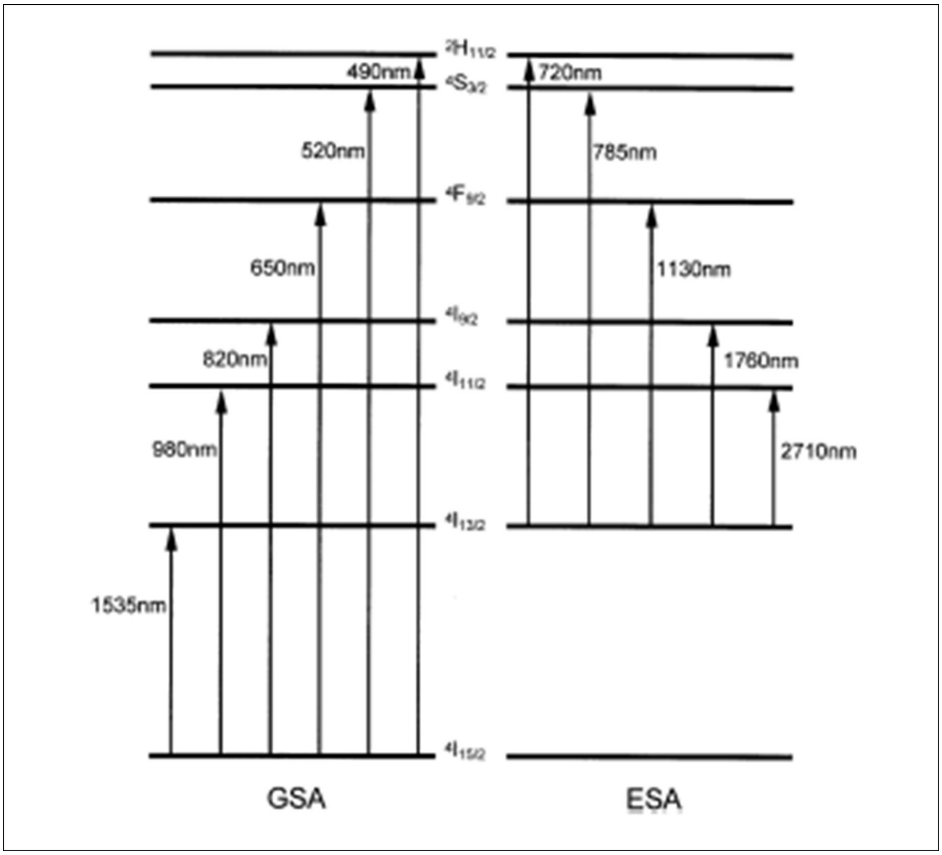

Figure 1.5: Ground and excited-state absorption transitions in erbium [22]

luminescence (at 6500cm^{-1}) of OH^--coordinated Er^{3+} ions is completely quenched by two phonon-OH mechanism.

- **Rare-earth solubility in solid hosts:** Beyond critical concentrations, rare-earth ions tend to form precipitates in most solid hosts. These can either take the form of clusters of rare-earth ions, as in the often macroscopic rare-earth aggregates observed in Er-doped silica, or can be compounds or alloys formed with one component of the host matrix. Upper limits are therefore placed on rare-earth concentrations in solid hosts.

- **Ion − ion interactions:** A characteristic of the rare-earth ions is their tendency to ion − ion interactions [18]. These can either be between ions of the same rare-earth (as is the case in clustered material), or between different ions (as in the sensitization of one rare-earth ion by another). The former constitutes a loss mechanism, increasing non-radiative decay channels or luminescence from unwanted transitions. The latter can be employed in novel pumping schemes whereby excitation is provided to one species and transferred to another, allowing a wider selection of pump sources to be used. Examples of such mechanisms are the Er/Yb co-doping schemes adopted to increase the luminescence efficiency of the Er^{3+} ion by coupling to the absorption bands of the Yb co-dopant. Introducing a second rare-earth dopant can also provide the added bonus of inhibiting aggregation of the emitting species through the formation of a solvation shell.

- **Co-operative upconversion:** Ions in the metastable state decaying to the ground state can couple in such a way that the decay of ion 1 promotes nearby ion 2 into a higher level (Figure1.4(a)). Once in the higher state, ion 2 may then decay rapidly and non-radiatively, or alternatively return to the metastable state and subsequently emits light. In the case of oxide glasses, the relaxation is rapid and non-radiative, and hence the result of co-operative upconversion is to lose an

excitation to heat.

- **Energy migration:** An ion in the metastable state can interact with a nearby ground state ion, promoting it to the $^4I_{13/2}$ level (Figure 1.4(b)). Although radiative emission may still occur from the second ion, the probability of non-radiative decay is increased with each successive transfer, and hence this constitutes a loss mechanism. Dipoledipole ForsterDexter interactions are responsible for this process, and therefore energy migration is again strongly dependent on rareearth ion concentration.

- **Cross relaxation:** This is the process whereby excitation energy from an ion decaying from a highly excited state promotes a nearby ion from the ground state to the metastable level. In erbium, the energy gap between the $^4I_{9/2}$ and $^4I_{13/2}$ levels is close to that between the $^4I_{13/2}$ and $^4I_{15/2}$ levels. As a result, at sufficiently high erbium concentrations, the population of the metastable state may be increased by the decay of an ion from the $^4I_{9/2}$ level and the consequent promotion of a nearby ion from the ground state (Figure 1.4(c)).

- **Excited state absorption:** Given a sufficiently long upper state lifetime, interaction with photons of the appropriate wavelength can promote electrons in the excited state to higher lying levels resonant with the incident photon energy. An ion can therefore be promoted to higher lying electronic levels from which it may return to the metastable state by multiphonon relaxation or radiative decay. However, in the process one of the two absorbed photons has been lost as either heat or emission at a different wavelength from the metastable-to-ground state transition. For the purposes of optical amplification, therefore, excited state absorption constitutes a loss mechanism: two photons are absorbed with only one emitted, and much research is therefore directed to it.

As optical transitions involving ions in the excited state originate from a level other than the ground state, the absorption spectrum of excited state ions is very different from that of those in the ground state. Energy gaps are in this case relative to the excited level rather than the ground state. Fig. 1.5 illustrates this for Er^{3+} by tabulating the major absorption bands originating on both the $^4I_{15/2}$ grant state and the $^4I_{13/2}$ metastable state. Note particularly the coincidence of the $^4I_{9/2}$ to $^4I_{13/2}$ transition at 800 nm and that at 790 nm due to the $^4I_{13/2}$ to $^4S_{3/2}$ transition. Excited state absorption at 800 nm depopulates the metastable state, and as a result, this is not widely used as a pump wavelength.

Bibliography

[1] H.J.R. Dutton, Understanding Optical Communications, IBM, 1998.

[2] E.J. Murphy, Integrated Optical Circuits and Components, Design and Applications, Marcel Dekker, New York, 1999.

[3] W. Huang, R.R. Syms, E.M. Yeatman, M. M. Ahmad, T.V. Clapp, and S. M. Ojha, IEEE Phot. Tech. Lett. 14, pp 959-961, 2002.

[4] H. Ogoshi, S. Ichino, and K. Kurotori, Furukawa Review 19, 17, 2000.

[5] Gines Lifante, Integrated Photonics: Fundamentals, JohnWiley & Sons Inc., 2003.

[6] K.Hirao, T.Mitsuyu, J.Si, J.Qiu (Eds.), Springer-Verlag, 2000.

[7] James E. Shelby, "Inroduction to glass science and technology", The Royal Society of Chemistry, U.K., 1997, chapter1.

[8] E.R. Elliott, Physics of Amorphous materials (Longman scientific technical) chapter 1.

[9] A.G. Guy, 'Introduction to material science', (Mc Graw-Hill, 1972), chapter 5.

[10] Masayuki Yamane, Yoshiyuki Asahara, 'Glasses For Photonics' , Cambridge University press, 2000.

[11] G. C. Righini and M. Ferrari, Rivista del nuovo cimento, Vol. 28, N. 12, 2005.

[12] G.H. Dieke, in: H.M. Crosswhite, H. Crosswhite (Eds.), Spectra and Energy levels of Rare-Earth Ions in Crystals, Wiley, New York, 1968.

[13] P.J. Mears, L. Reekie, I.M. Jauncey and D.N. Payne, Electron. Lett. 23, 1026 (1987).

[14] E. Desurvire, R.J. Simpson and P.C. Becker, Opt. Lett. 12, 888 (1987).

[15] E. Desurvire, Phys. Today 47, 20 (1994).

[16] Snitzer E., Phys. Rev. Lett., 7 (1961) 444.

[17] Koester C. J. and Snitzer E., Appl. Opt., 3 (1964) 1182-1186.

[18] Yajima H., Kawase S. and Sekimoto Y., Appl. Phys. Lett., 21 (1972) 407-409.

[19] Saruwatari M. and Izawa T., Appl. Phys. Lett., 24 (1974) 603-605.

[20] Digonnet M. J. F. (Editor), Selected Papers on Rare-Earth-Doped Fiber Laser Sources and Amplifiers, Vol. MS 37 (SPIE Press, SPIE, Bellingham) 1992.

[21] W. Miniscalco, IEEE J. Lightwave Technol. 9, 234 (1991).

[22] A.J. Kenyon, Progress in Quantum Electronics 26, 225284(2002).

[23] M.D. Shinn, W.A. Sibley, M.G. Drexhage and R.N. Brown, Phys. Rev. B 27, 6635 (1983).

Chapter 2

Optical Spectroscopic Characterization of glasses

INTRODUCTION

During the past decades, a great interest has been devoted to erbium-doped materials due to their availability for telecommunications applications [1-3]. In particular, much attention has been focused on erbium-doped glasses for the development of gain elements involving the Er^{3+} intra-4f emission at 1.54 μ m, in the so-called ultra low-loss telecommunication window, extending from around 1450 to 1600 nm. This research activity mainly aimed to identify the key parameters acting on the performance of fiber amplifiers [4]. Among these parameters, the host glass composition plays a crucial role on the amplification efficiency [1]. Actually, the performance of gain elements, such as erbium-doped glasses, is governed by the relevant electronic and optical properties of the active ion on which the host material has a significant influence: cross sections, spectral shapes of the emission and absorption bands, excited state lifetimes, interaction between active ions and their environment.

The results of optical spectroscopic characterisation of Er activated modified silicate glass

('Baccarat') and Zinc-Tellurite glass are presented in detail in the corresponding first and second sections of this chapter.

2.1 Baccarat: Modified silicate glass

Though solids of different natures have been employed as host for erbium ions, in view to obtain the signal amplification required in optical communication devices, silica glass still remains one of the more suitable hosts. In addition to a high transparency around 1.5 μ m and chemical durability, the long lifetime of the Er^{3+} $^4I_{13/2}$ metastable level permits the high-population inversions that are necessarily involved in the optical amplifiers claiming high-gain and low signal-to-noise.

2.1.1 Sample composition

The glasses have been produced at Cristallerie Baccarat by a conventional melt-quenching technique with the following molar composition: 77.29 SiO2: 11.86 K2O: 10.37 PbO: 0.48 Sb2O3. Two different sets of samples were produced, containing 0.2 and 0.5 mol% Er^{3+} ions, respectively labeled B02 and B05. The density of the samples has been measured by a gas pycnometer. The Er^{3+} concentrations have been determined in each case taking into account both the nominal composition and the measured density of the glass. Refractive index value at several wavelengths has been measured with an accuracy of 0.001 and a resolution of 0.0005, using a standard prism coupling method [6]. Refractive index, Er^{3+} concentration, and density of the Baccarat glasses are reported in Table 2.1.1.

Optical absorption experiments were performed at room temperature from the ultraviolet to the near infrared spectral range with a double beam spectro-photometer (UV-Vis-NIR Cary 5000 Varian). The Fourier Transform Infrared (FTIR) spectroscopy measurements were carried out by using a JASCO FTIR-660 plus spectrometer with a

Table 2.1: Refractive index, Er^{3+} concentration, and density of the Baccarat glasses B02, B05

Sample labeling	B02	B05
Density [g/cm3]	3.049 ±0.001	3.083±0.006
Er^{3+} -concentration [cm^{-3}]	8.9 1019	2.2 1020
Refractive index [± 0.0005]@		
457 nm	1.5762	1.5767
488 nm	1.5723	1.5732
514 nm	1.5688	1.5696
543.5 nm	1.5651	1.5657
632.8 nm	1.5602	1.5610
1319 nm	1.5448	1.5456
1542 nm	1.5427	1.5427

resolution set to 4 cm^{-1}. The polarized VV and depolarized HV Raman spectra were obtained by exciting the samples with the 488 nm line of an Ar^+ - ion laser. The signal was selected by a double monochromator and analyzed by a photon-counting system. The 514.5 nm line of an Ar^+ - ion laser and the 980 nm line of a Ti:Sapphire laser were used as excitation sources for near infrared photoluminescence (PL) spectroscopy measurements. A Triax 320-mm-focal-length single-grating monochromator was used to disperse the luminescence light onto an InGaAs photodiode and the signal acquisition was performed using a standard lock-in technique. To measure the PL decay of the excited $^4I_{13/2}$ level, the cw excitation laser was pulsed with a mechanical chopper and data were acquired with a digital oscilloscope

2.1.2 Results and Discussion

The refractive index dispersion of Baccarat glasses have been calculated using the conventional Sellmeier dispersion equation [6, 7] given as

$$n(\lambda) = \frac{A}{\lambda^4} + \frac{B}{\lambda^2} + C + D\lambda^2 + E\lambda^4 \tag{2.1}$$

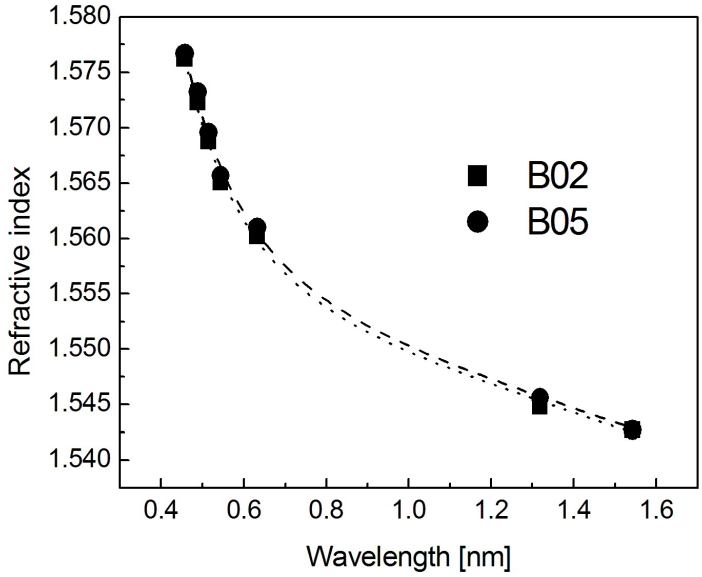

Figure 2.1: Refractive index dispersion of B02 (squares) and B05 (circles) glasses. The dot lines represent the result of the fit of the data to Sellmeier dispersion equation

where n(λ) is the refractive index measured at the wavelength λ. The measured values of the refractive index are substituted into the above dispersion equation and the coefficients A - E are determined by the least squares method. Figure 2.1 shows the refractive index dispersion curves for B02 and B05 glasses. Figure 2.2 shows the Raman spectra of the B02 sample collected in the VV and HV polarizations by exciting at 488 nm. The scattering of light was observed along a direction perpendicular to the laser beam. The Raman bands are characteristic of silica modified glasses exhibiting an intense Boson peak due to the high polarizability of the lead. The intensity of elastic scattering was relatively weak, so that it was possible to observe the Raman scattering from a frequency lower than 2 cm^{-1}. Furthermore, the intensity of elastic light scattering for crossed polarizations (polarization of scattered light perpendicular to that of incident light) was almost invisible in this configuration. That means that only the Rayleigh light was observed in the other configurations (parallel polarizations). This last point is a convincing test of the perfect

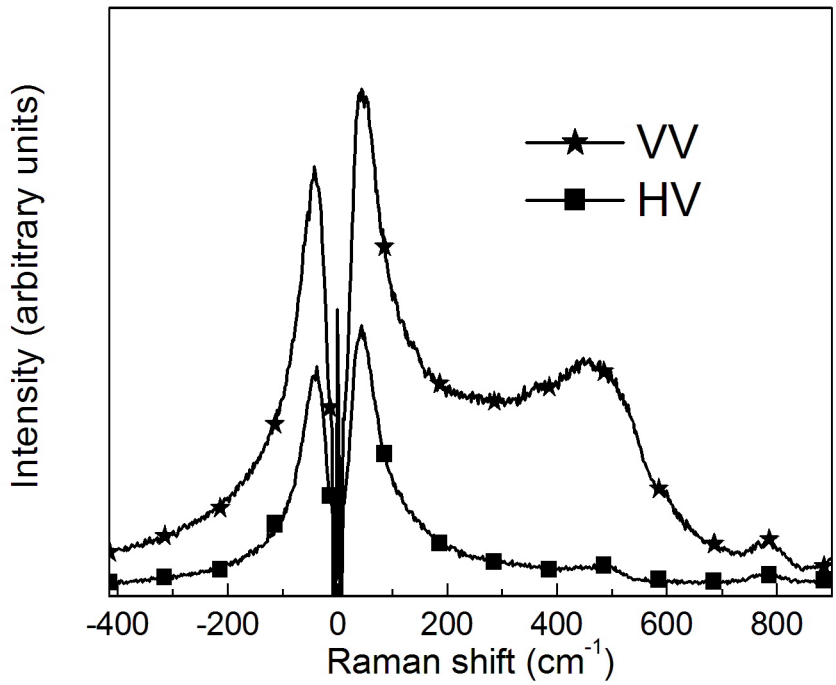

Figure 2.2: Raman spectra of the B02 sample collected in the VV and HV polarizations by exciting at 488 nm.

transparency of the Baccarat glass. The UV-Vis-NIR absorption spectrum obtained for the B02 glass is plotted on Figure 2.3(A). The spectrum is characteristic of Er^{3+}-doped oxide glasses [10]. The absorption bands are identified with the transitions from the $^4I_{15/2}$ ground state to the excited states of the Er^{3+} ions. In particular the band located at around 1540 nm is related to the $^4I_{15/2} \longrightarrow {}^4I_{13/2}$ transition of the trivalent erbium ion. Several Stark structures of the erbium absorption band at 1.5 μm are clearly resolved [10]. The absorption spectrum of the B02 glass sample reported in Figure 2.3(B) has been obtained from FTIR measurements in order to extend the previous plot to the infrared region up to the multi-phonon absorption edge which is, for this glass, at around 4500 nm. These samples present a wide transparency region extending from 350 up to 2700 nm. The absorption spectra obtained for the B05 sample are similar, except for the band intensities, which depend on the rare earths concentration. The spectrum of Figure 2.3(B) shows the multi-phonon tail of the absorption edge, which partially overlaps the wide band (3000-3700 cm^{-1}) assigned to the presence of hydroxyl groups in the glass matrix, centered at about 3570 cm^{-1} [13, 14]. The amplitude of this fundamental OH stretching band allows the estimation of the OH concentration by the Beer-Lambert law

$$C = (\alpha\ 0.434)\ (\frac{1}{\varepsilon}) \tag{2.2}$$

where C is the concentration of the bonded species whose vibrations induce the IR light absorption, α is the absorption coefficient and ε is the extinction coefficient. Unfortunately, shape and intensity of the OH absorption band strongly depend on the glass composition [13, 14] and as a consequence the evaluation of the extinction coefficient is not an easy task. However, we can give a rough estimation of water content assuming that the value of the extinction coefficient is comparable to what it is found for aluminosilicate glasses [13] and andesitic glasses [13, 14]. Taking a value of the extinction coefficient $\varepsilon_{3570nm} \sim 70\ l_{glass}\ /mol_{OH}\ cm_{glass}$ and $\alpha \sim 1\ cm^{-1}$ the resulting C_{OH} concentration is low as 6 x 10^{-6} mol cm^{-3}, which corresponds to an OH content of about 3.6

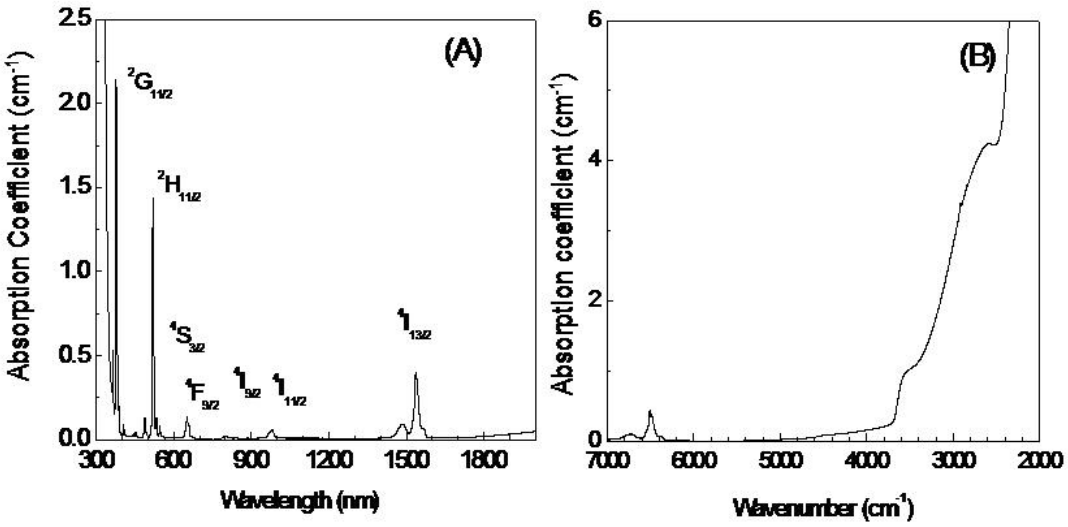

Figure 2.3: (A) Room temperature absorption spectrum in the UV-Vis-NIR spectral region of the B02 sample. Some of the final states of the $^4\mathrm{I}_{15/2} \longrightarrow {}^{2S+1}\mathrm{L}_J$ transitions are labeled; (B) extension of the absorption spectrum of the same sample in the IR region obtained from FTIR measurement.

x 10^{18} cm^{-3}. The PL spectra for the two samples in the region of the $^4I_{13/2} \longrightarrow {}^4I_{15/2}$ transition of Er^{3+} ions, obtained upon excitation at 514.5 nm with an excitation power of 180 mW, are shown in Figure 2.4. The PL spectra are almost identical and exhibit a main emission peak at 1537 nm. The spectral width of the two emission bands measured at 3 dB from the maximum of the intensity is 18 $\pm$ 1 nm. The spectral width of the emission bands is due to Stark splitting of the excited and ground states plus additional inhomogeneous and homogeneous broadening [3, 8] and the Stark structures at 1490, 1542, 1567 and 1617 nm appear well defined. This result indicates that Er^{3+} ions occupy sites characterized by similar local environment so that inhomogeneous broadening is not as important with respect to the amount of the Stark splitting. Moreover, it is recognized that the homogeneous broadening is dominant in silicate glasses [2]. No change in the spectroscopic features of the 1.5 μm emission was observed exciting at 980 nm.

No upconversion signal has been detected from Baccarat Er^{3+}-doped glass upon 980 nm excitation. Characteristic green upconverted luminescence was not observed, even exciting the more concentrated sample B05 at 980 nm, with a pump power of around 400 mW and a beam waist of about 50 μm. An important issue in the optimisation of material and component design is the reduction of the energy transfer upconversion (ETU) mechanism stemming from the clustering of the Er^{3+} ions. The intracluster ETU occurs on a submicrosecond time scale due to short interionic distance. The non-appearance of upconversion in Baccarat glasses indicate that most of Er^{3+} ions are homogeneously distributed and that interaction clusters as well as chemical clusters are practically absent [16, 18]. Figure 2.5 reports the luminescence decay curves from the $^4I_{13/2}$ state of Er^{3+} ion in B02 and B05 samples, obtained upon excitation at 514.5 nm with an excitation power of 180 mW. The same decay profile was measured upon 980 nm excitation. Both the decay curves exhibit a single-exponential behavior. For the B05 sample doped with 0.5 mol % of erbium a lifetime of 11.5 $\pm$ 0.1 ms was measured and the sample B02 doped with 0.2 mol % of erbium exhibits a lifetime of 14.2 $\pm$ 0.1 ms. Such a measured lifetime

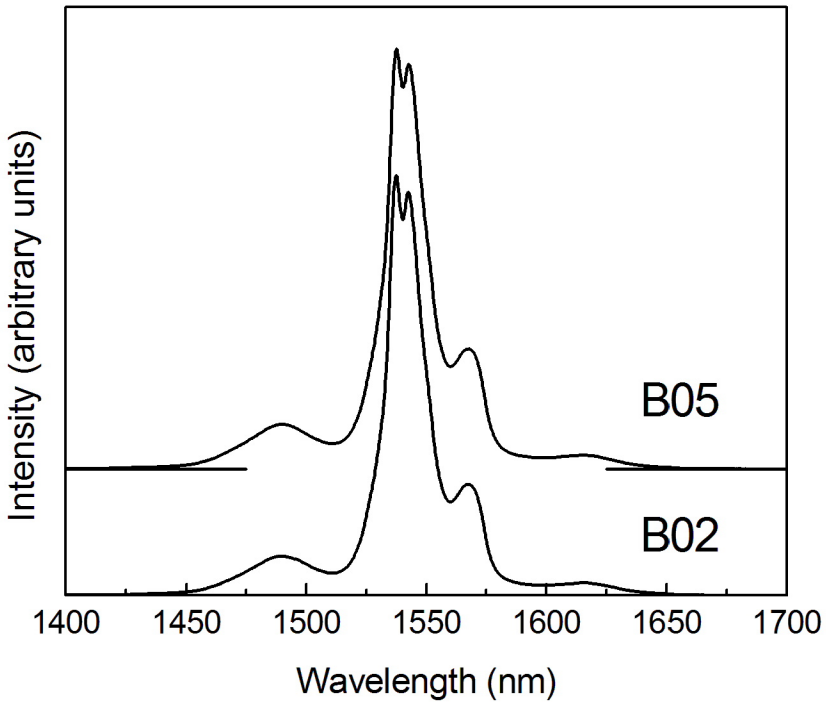

Figure 2.4: Normalized room temperature photoluminescence spectra of the $^4I_{13/2} \longrightarrow {}^4I_{15/2}$ transition of Er^{3+} ion for the B02 and B05 samples, obtained by exciting at 514.5 nm.

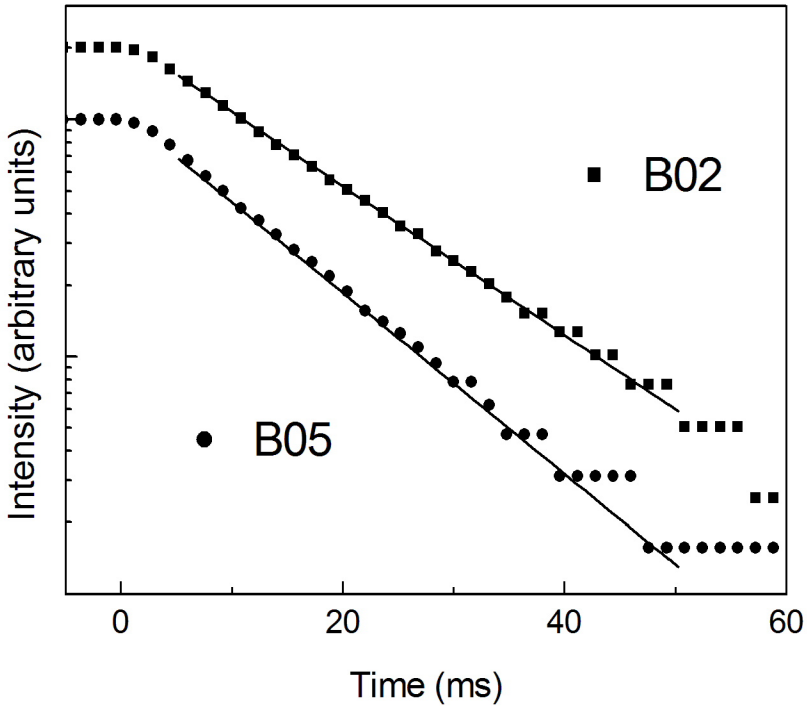

Figure 2.5: Room temperature luminescence decay curve from the $^4I_{13/2}$state of Er^{3+} ion in of B02 (squares) and B05 (circles) samples obtained after pumping at 514.5 nm with an excitation power of 180 mW. The solid lines represent single exponential decay fit to the experimental data.

is very close to the highest values which have already been reported for erbium in silicate glass hosts: 14.5 ms in Silicate L-22 [1] and 14.7 ms in Silicate [15] are typical values found in the literature. The measured lifetime (τ_{mes}) must be compared with the radiative lifetime, τ_{rad}, to obtain the radiative quantum efficiency QE defined by the ratio of the measured to the radiative lifetime:$QE = \frac{\tau_{mes}}{\tau_{rad}}$. The value of τ_{rad} can be calculated via different theoretical approaches and numerical analysis. The so-called Judd-Ofelt [16, 17] theory yields an estimation of the oscillator strength characterizing the intensity of a transition between two $^{2S+1}L_J$ multiplets. The intensity parameters Ω_q, called Judd-Ofelt parameters, are obtained by the chi-square method [18, 19]. The radiative lifetime of the Er^{3+} $^4I_{13/2}$ metastable state are obtained from the oscillator strength of the $^4I_{13/2}$

Table 2.2: Intensity parameters Ω_q (in units of 10-20 cm2) Baccarat glass activated by 0.2 mol% Er^{3+} (sample B02) and 0.5 mol% Er^{3+} (sample B05).

Sample	Ω_2	Ω_4	Ω_6	r.m.s.
B02	3.36	0. 75	0. 17	$1.38\ 10^{-7}$
B05	3.19	0.56	0.16	$6.5\ 10^{-8}$

$\longrightarrow {}^4I_{15/2}$ transition. Both electric and magnetic dipole contributions of the spontaneous emission probability are considered in the calculation of the radiative lifetime.

Table 3.2 reports the obtained Judd-Ofelt parameters together with the root mean square (r.m.s.) deviations of the oscillator strengths [18]. The radiative lifetimes obtained from the Judd-Ofelt theory are given in Table 3. The second approach consists in a two-level system for which g1 and g2 are the degeneracies of the lower state 1 and the upper state 2, respectively.

For such a degenerate system one condition has to be satisfied: either the sublevels making up each level are all equally populated, or the transition strengths between the sublevels are all equal. Taking into account only the decay pathway via the spontaneous emission for the 2$\longrightarrow$1 transition, and denoting A21 as the corresponding transition rate (Einstein A coefficient), the radiative lifetime of the upper state 2 is given by [20]:

$$\frac{1}{\tau_{21}} = A_{21} = \frac{8\pi}{\lambda^2}.\frac{g_1}{g_2}\int \sigma_{12}(\nu)d\nu \tag{2.3}$$

where $\lambda = \frac{\lambda_o}{n}$ is the wavelength of transition in the medium (λ_o is the wavelength, n refractive index in vacuum) and $\sigma_{12}(\nu)$is the absorption cross section at a frequencyν. Although the conditions involved in the two-level model are not satisfied in the case of the ${}^4I_{13/2} \longrightarrow {}^4I_{15/2}$ Er^{3+} transition, the radiative lifetimes calculated from this model are in good agreement with the ones obtained from the Judd-Ofelt theory (see Table 2.3), like it has already been verified in various erbium-doped glasses such as germanate, phosphate, silicate or tellurite [21]. The last method employed here to access to a quantitative

Table 2.3: Calculated τ_{rad} lifetimes and radiative quantum efficiency of the Er^{3+} $^4I_{13/2}$ metastable level from various methods: the standard Judd-Ofelt analysis, a simple method based on the Einsteins relation for the emission probability of a two-level system and the approximate McCumber procedure.

Sample label	Measured lifetime τ_{mes} (ms)	Judd- Ofelt model τ_{rad} (QE)	Einstein Model τ_{rad} (QE)	McCumber model τ_{rad} (QE)
B02	14.2±0.1	17.8 (79.8%)	18.9 (75.1%)	20.1(70.6%)
B05	11.5±0.1	18.4 (62.5%)	17.9 (64.2%)	19.3 (59.6%)

estimation of the Er^{3+} $^4I_{13/2}$ level lifetime is based on the Mc Cumber theory [22] and developed by Miniscalco and Quimby [23]. The absorption cross section, σ_{abs}, and the emission cross section, σ_{em}, are related according to the following relationship [22]:

$$\sigma_{em}(\nu) = \sigma_{abs}(\nu)e^{(\varepsilon - h\nu)/KT} \tag{2.4}$$

where ε is the $^4I_{15/2} \longrightarrow {}^4I_{13/2}$ transition energy at temperature T. The radiative lifetime of the Er^{3+} $^4I_{13/2}$ level can then be calculated from

$$\frac{1}{\tau_{rad}} = \frac{8\pi n^2}{c^2} \int \nu^2 \sigma_{em}(\nu) d\nu \tag{2.5}$$

The emission cross section obtained for the B02 glass is plotted in Figure 2.6, as function of wavelength, together with the absorption cross section for comparison. In Table 2.3 are reported calculated rad lifetimes of the Er^{3+} $^4I_{13/2}$ metastable level from various methods: the standard Judd-Ofelt analysis [16, 17], a simple method based on the Einsteins relation for the emission probability of a two-level system [21] and the approximate McCumber procedure [4, 22, 23].

As seen in Table 2.1.2, the lifetimes that have been calculated using the approximate treatment based on the McCumber theory are slightly higher than the ones estimated

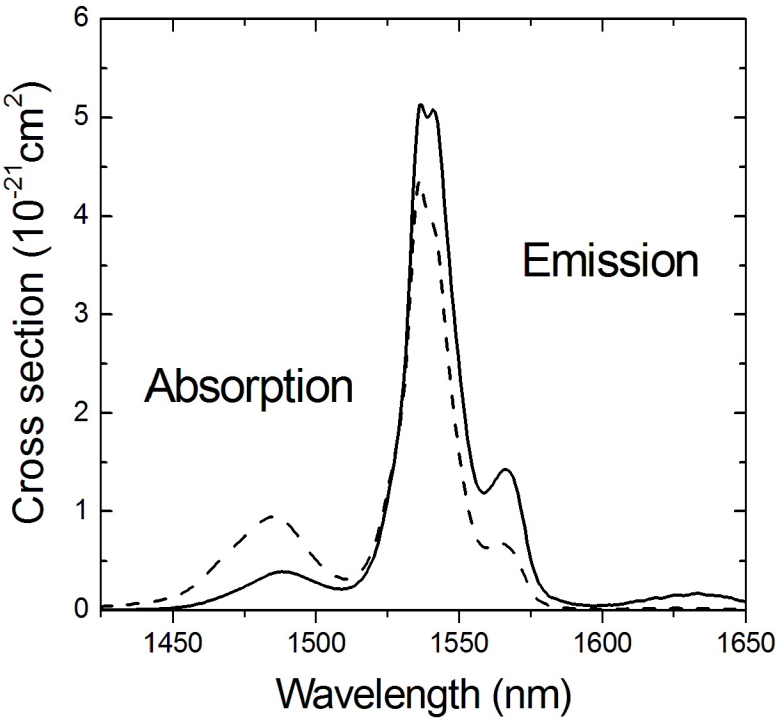

Figure 2.6: Absorption and calculated emission cross sections of Er^{3+} ion at 1.5 μm in the B02 glass.

with the previous methods, especially for the B02 glass. However, the various methods considered here for calculating τ_{rad} gives some results in good agreement between them in despite of the different treatments employed from one method to the other. The average between the result of the three model give a radiative QE of the Er^{3+} $^4I_{13/2}$ metastable level of about 62 % for the B05 glass and of about 75 % for the B02 glass. For the B02 glass, QE reaches very high values, up to 79.8 % in the case of a calculation based on the Judd-Ofelt theory. Such high quantum efficiency has already been observed in Er^{3+}-doped tellurite glasses [19], but remains among the highest quantum efficiencies estimated in pure or modified-silica host glasses.

Figure 2.6 shows the calculated absorption and emission cross sections for the B02 Baccarat glass. The calculated emission cross sections are very similar to those calculated

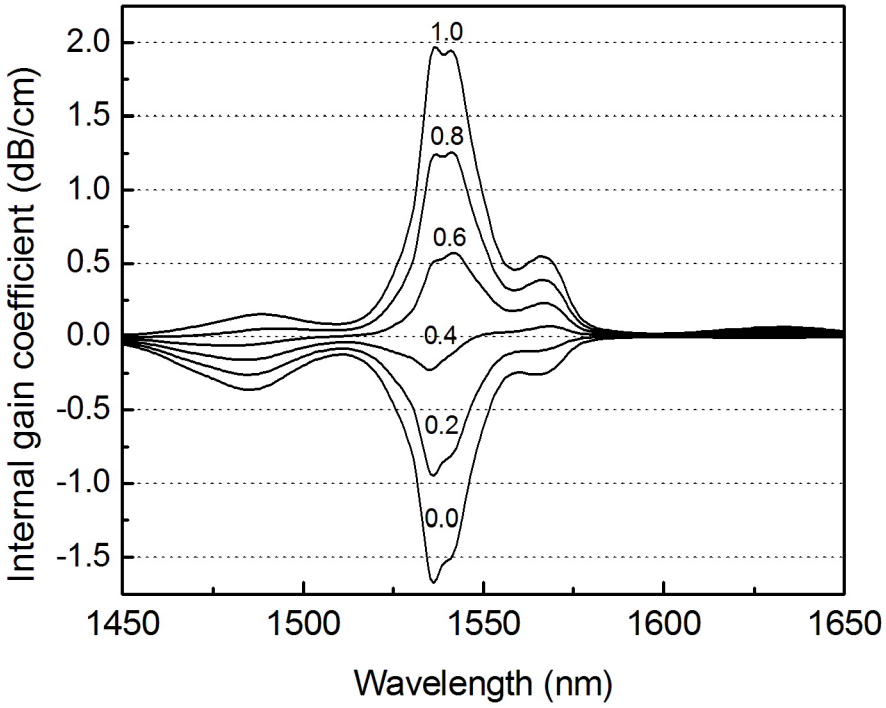

Figure 2.7: Calculated internal gain coefficient versus wavelength in the B02 glass for different values of the fractional upper-state population N2/N indicated on the graph for each curve.

for other silicate systems [1, 4]. The internal gain coefficient g at wavelength λ can be estimated by means of the formula [4] $g(\lambda) = \sigma_{em}(\lambda)N2\sigma_{abs}(\lambda)$ N1 where N1 and N2 are the densities of ions in the ground state and the excited state, respectively. (N1+ N2 = N, N being the density of erbium ions). In the case of total inversion (N2 = N), at 1537 nm we obtain a internal gain coefficient of about 2.0 dB. Figure 2.7 report the internal gain curves versus wavelength for the B02 glass at different values of the fractional upper-state population $N2/N$. The change in the upper-state population strongly modifies the internal gain coefficient of the glass in the full 1460-1580 nm spectral range, in fact, for low values of the population inversion, the glass is like an absorber of the light for the shorter wavelengths, while it amplifies the longer wavelengths [4].

2.2 Zinc-Tellurite glasses

Erbium-doped tellurite glasses have optical and chemical properties suitable for optical applications . High linear and non-linear indices of refraction, relatively low phonon energy spectra, many valence states of tellurium, good infrared transmittance, and chemical durability make them promising candidates for fiber laser and optical amplifier devices [25] In pure tellurite glasses, the main structural unit consists of a TeO4 trigonal bypyramid (figure 2.8) [26, 27], where the two atoms of oxygen at the vertex of the pyramids are called axial and the other two equatorial. The glassy network is created by the fact that any oxygen atom is shared between two different bypyramids, once in equatorial and once in axial position. However, modifier ions are usually added in the glass fabrication; they play a role in breaking the oxygen bonds (figure 2.8 (b)), (in particular elements of the first and second group Na, Li), and also in creating new structural units (Zn, Pb, W) [26, 28, 29]. In both the cases, the increased disorder allows an easier vetrification process.

The interest in rare earth activated tellurite glasses as materials for optical amplifiers in the second and third telecommunication windows dates from the work of Wang et al.[30], who compared the features of tellurite glasses with those of silicate and fluoride. Two physical properties are mainly responsible for this interest: the high value of the refractive index (around 2) and the low maximum phonon energy (around 700 cm^{-1}) (depending on the modifier ions). In fact, the higher refractive index induces an increase of the local electric field that rare earth ions experience [31]. In turn, this causes both an enhancement of the radiative transition rates and a wider splitting of Stark sublevels. The first effect leads to a greater efficiency of photon emissions with respect to other non radiative decays, the second one to a broadening of the emission shape, which for erbium ions extends in the L-band. Moreover, the already discussed complex structure of the tellurite glasses allows a great variety of sites for the active ions increasing the inhomogeneous broadening of the lines [32]. In this section we will investigate the spec-

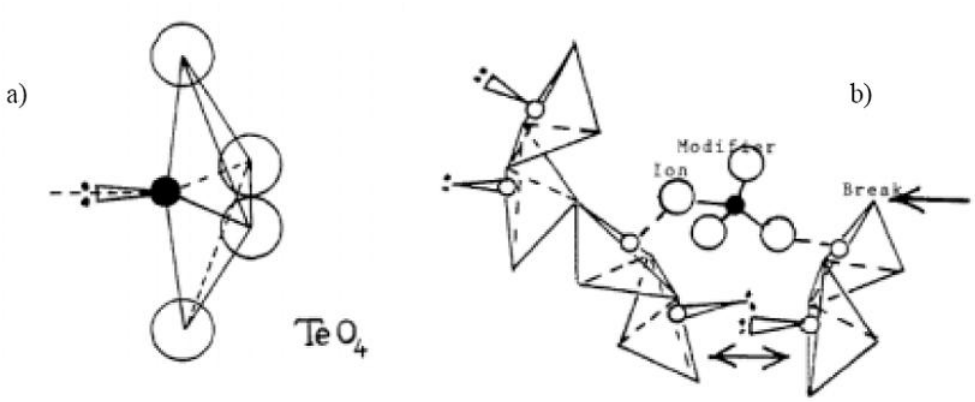

Figure 2.8: Basic coordination polyhedron in vitreous TeO2. b) Deformation and breaking of the TeO2 chains by a modifier.

troscopic properties of Er^{3+} activated TeO2 ZnO glasses. Presence of self-absorption is also discussed.

2.2.1 Sample composition

Glasses were prepared from oxide powders of TeO2, ZnO and Er2O3 as starting materials using the conventional melt-quenching method. The nominal composition of the glasses is 65 TeO_2 - 35 ZnO, the amount of dopant was varied from 0.5 molar % to 3 molar % The refractive index of the glasses were measured by prism-coupling method and the values at the indicated wavelength are given in the table 2.4.

Table 2.4: Density, Er^{3+} concentration, and Refractive index of the Zinc-Tellurite glasses

Sample label	ZT	ZT05	ZT10	ZT20	ZT30
Er Molar%	0	0.5	1	2	3
Density	5476	5519	5624		
Refractive Index : @ wavelength (nm)	-	-	-	-	-
543.5 (nm)	2.0492	2.076	2.0748	2.0657	2.0561
632.8 (nm)	2.0302	2.055	2.0542	2.0454	2.0374
1319 (nm)	1.9894	2.006	2.0053	1.9982	1.991
1542 (nm)	1.9872	2.002	2.0015	1.9938	1.9866

2.2.2 Results and Discussions

The figure 2.9 is the absorption spectrum of ZT30 (doped with highest Er^{3+} [3 molar %]) and ZT the undoped glass. All the major final states of the $^4I_{15/2} \longrightarrow {}^{2S+1}L_J$ transitions were identified and labeled following ref. [33]. The other samples presented very similar absorption spectra, except for the intensities of Er^{3+} electronic transitions that were roughly proportional to the activating ion concentration.

The figure 2.2.2 reports the polarized Raman spectra of the ZT, ZT30 samples. The Raman spectra are very similar with minor difference discussed in the following. The Raman spectra were normalized relative to the maximum intensity of the band at of 660 cm^{-1}, in order to draw qualitative inference of the effect of Er^{3+} ion (if any) on the structural properties of the glass without the Er^{3+} activation. The band at 660 cm^{-1} is assigned to the stretching vibrations of the TeO_4 trigonal bypiramidal groups. They are linked through TeOTe, with O in a position alternatively axial and equatorial, and form the backbone of pure TeO_2. The presence of a modifier ion such as Zn leads to the creation of TeO_3 and TeO_{3+1} polyhedra that are responsible for the band at 740 cm^{-1} in ZT, 750cm^{-1} in ZT30 (similar band was observed at 770cm^{-1} by [34]). N.Jaba et.al [25]noted that with increasing concentration of Er ion concentration the band intensity at 750cm^{-1} increases (the band intensity was significantly more even for sample with Er ion concentration of 3 molar %) in 70TeO_2 - 30ZnO glasses. The increase in intensity observed

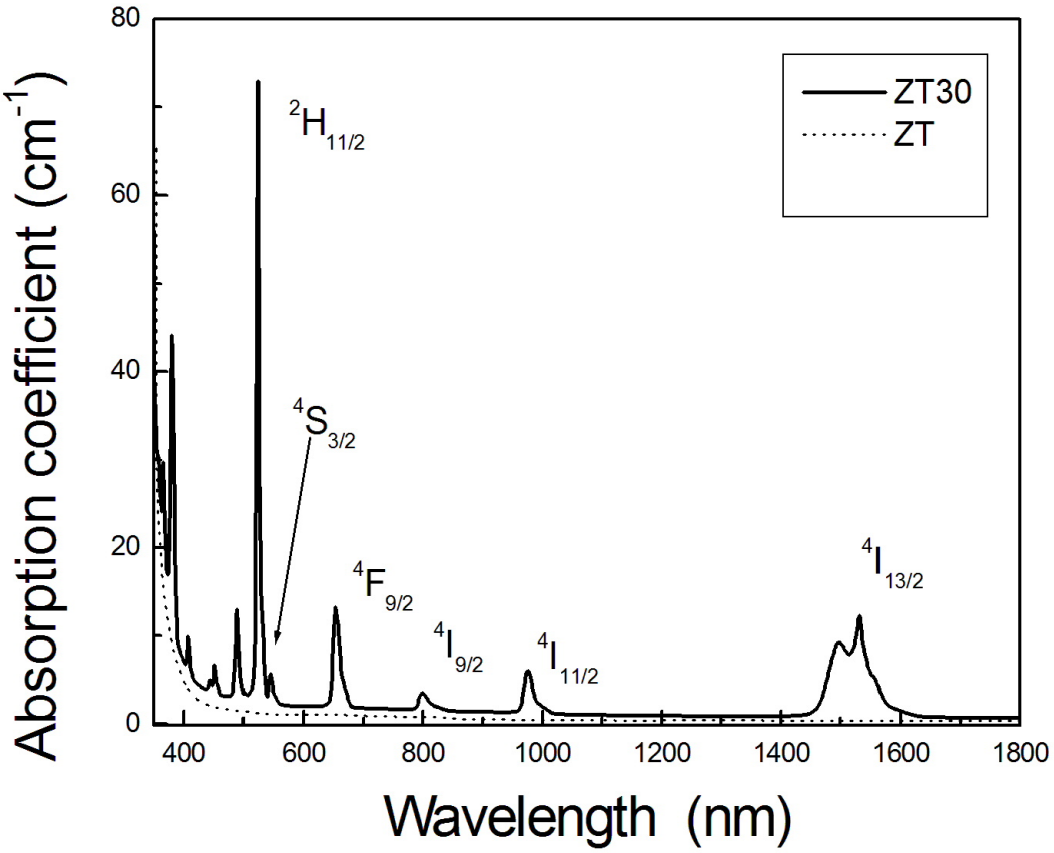

Figure 2.9: Absorption spectrum of (Solid line)ZT30 (doped with highest Er^{3+} [3 molar %]) and (dottedline) ZT the undoped glass.

for the 750 cm^{-1} band with erbium concentration was found to be consistent with the destruction of TeO4 groups. The attributed that introduction of erbium oxide into the glass network induces a gradual reduction of tellurium coordination ($4 \longrightarrow 3+1 \longrightarrow 3$), thus leading to a substantial change in the glass structure. The intensity of the band doesnot vary in the sample as shown in the figure 2.2.2 and no disruption of the glass structure. The presence of the erbium, even in such a high concentration, appears not to give rise to the development of structural peaks, indicating a very good dispersion of the rare earth ions, with no evidence of the formation of clusters .

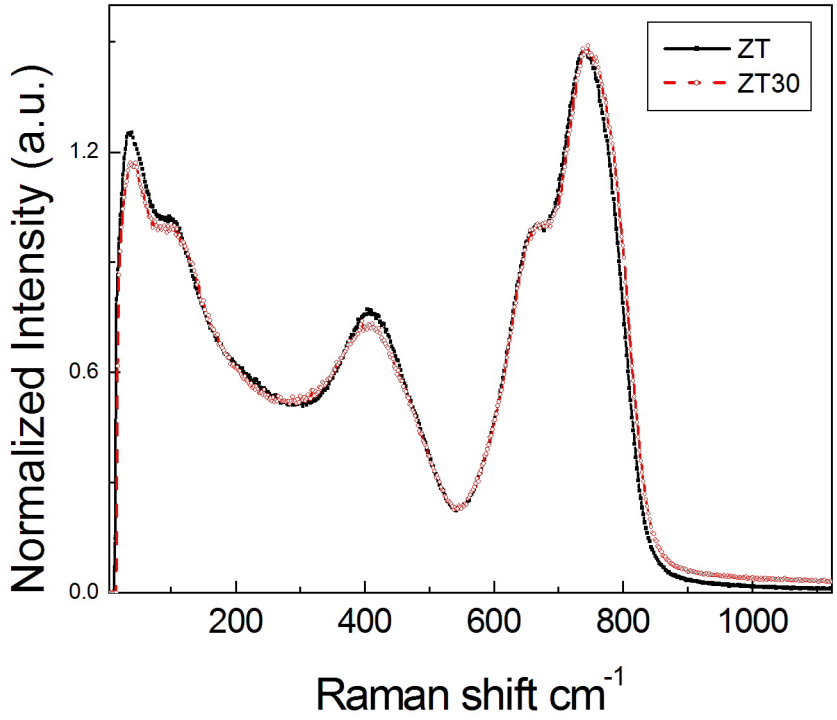

Figure 2.10: Raman spectra of sample ZT and ZT30, normalized relative to the maximum intensity of the band at 660 cm^{-1}

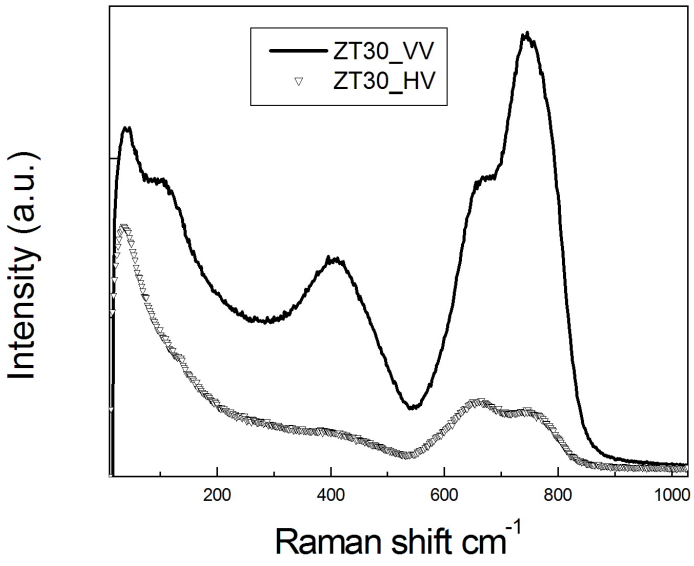

Figure 2.11: Polarised (VV) and un-polarised Raman spectra of sample ZT30

The band at 410 cm^{-1} is assigned to bending vibrations of the TeOTe bonds at corner sharing sites. Its intensity can be considered a measure of the connectivity of the network [32]. In the low frequency range, we distinguish the boson peak at 35 cm^{-1} and a shoulder, at 110 $^{-1}$. In literature [35] the shoulder has been assigned to vibrations due to $TeO_4ZnO_6TeO_3$ chain structures, where Zn plays a glass network-forming role, in agreement with the vibrational frequencies of $ZnTeO_3$ and $Zn_2Te_3O_8$ crystals. This shoulder is absent in the un-polarised spectra as seen in the figure 2.2.2

(PL) spectra for the samples ZT05, ZT10, ZT20 and ZT30 are normalized to their relative intensities at the peak 1535nm. The photoluminescence spectra are shown in the figure 2.2.2, all the samples are excited by 514 nm laser line. The normalised absorption spectra of ZT05 and ZT30 are also reported. The FWHM of the PL appears to be increasing from 79 nm in the least doped sample (ZT05) sample to 117nm in most doped one (ZT30)sample. These results could lead to think that the increasing of the Er^{3+} concentration is associated with the occupation by the active ions of more and more

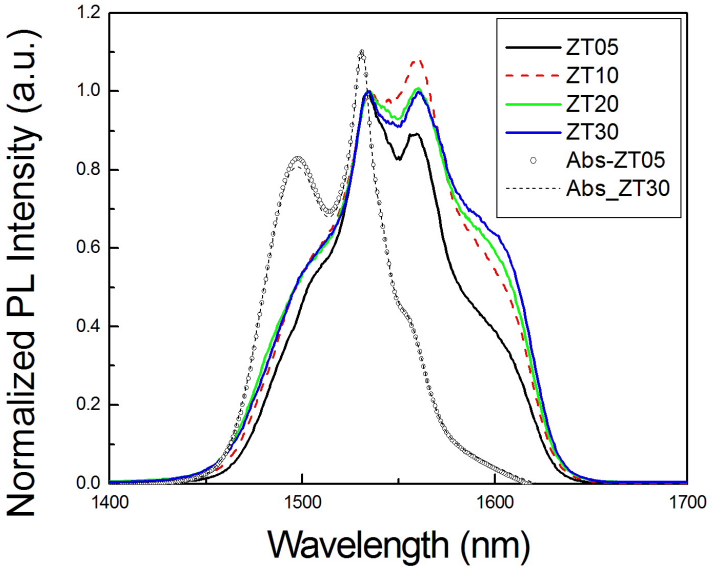

Figure 2.12: Normalized IR, PL spectra of ZT05, ZT10, ZT20 and ZT30; Absorption spectra of ZT05 and ZT30 are also presented

different microscopic environments, giving rise to a greater inhomogeneous broadening. However, this explanation contrasts with the evidences presented in the absorption spectra (Fig.2.2.2) where the shape of the electronic transition does not change with the doping level.

The observed broadening of the emission can instead be attributed to a self absorption effect that, as reported in [36], leads to overestimate the real emission bandwidth. In order to investigate the existence of such an effect, the fluorescence intensity emitted at right angle from the incident beam was monitored varying the penetration depth, i.e. the distance between the focused beam and the exit face. The sample were irradiated with 514 nm and the PL is collected in the IR at two positions a)the laser beam was near the exit face and b)the laser beam was 1.5 mm away from the exit face of the sample. The results for the ZT30 sample are shown in figure 2.13, this effect is found to be negligible in ZT05 (the least doped), as expected it is maximum (the laser beam was 2.5 mm away

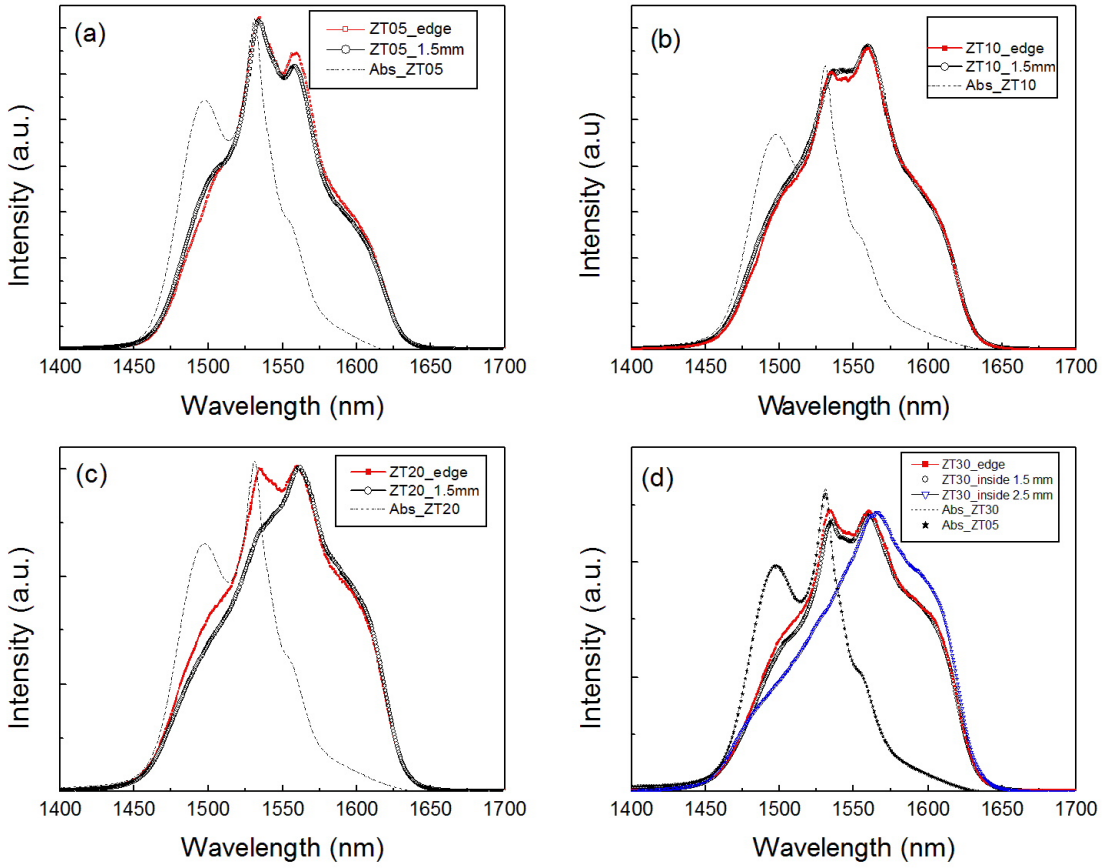

Figure 2.13: Normalized emission spectra of the $^4I_{13/2} \longrightarrow {}^4I_{15/2}$ transition for ZT30 sample at different penetration depth

from the exit face) in the sample ZT30 (highest doped sample).

Table 2.5: Measured life times of the PL collected at 1535 nm w.r.t geometry of excitation

Sample label	near the exit face	1.5 mm inside the sample from exist face
ZT05	4.2 m sec	4.2 m sec
ZT10	2.59 m sec	2.55 m sec
ZT20	1.38 m sec	1.38 m sec
ZT30	0.89 m sec	0.84 m sec

The life times of the PL (collected 1535nm) were measured w.r.t the geometry of excitation for the samples ZT05, ZT10, ZT20 and ZT30, and the values are given in the table 2.5.

The plots of the life times of Er PL at 1535 of the samples ZT10, ZT30 are shown in the figure 2.14. The lifetimes of the Er PL in IR were found to decrease with increase in the concentration implying a strong presence of concentration quenching in these samples. In case of self absorption the PL bandwidth is expected to increase with increase in the depth at which the sample is excited by laser beam w.r.t to the exit face of the sample (sample surface closer to collection system). Also, the life-time are expected to increase in such cases. The minimal effect of the excitation geometry on the life-times again proves that self-absorption though present, the concentration quenching is dominant in the samples.

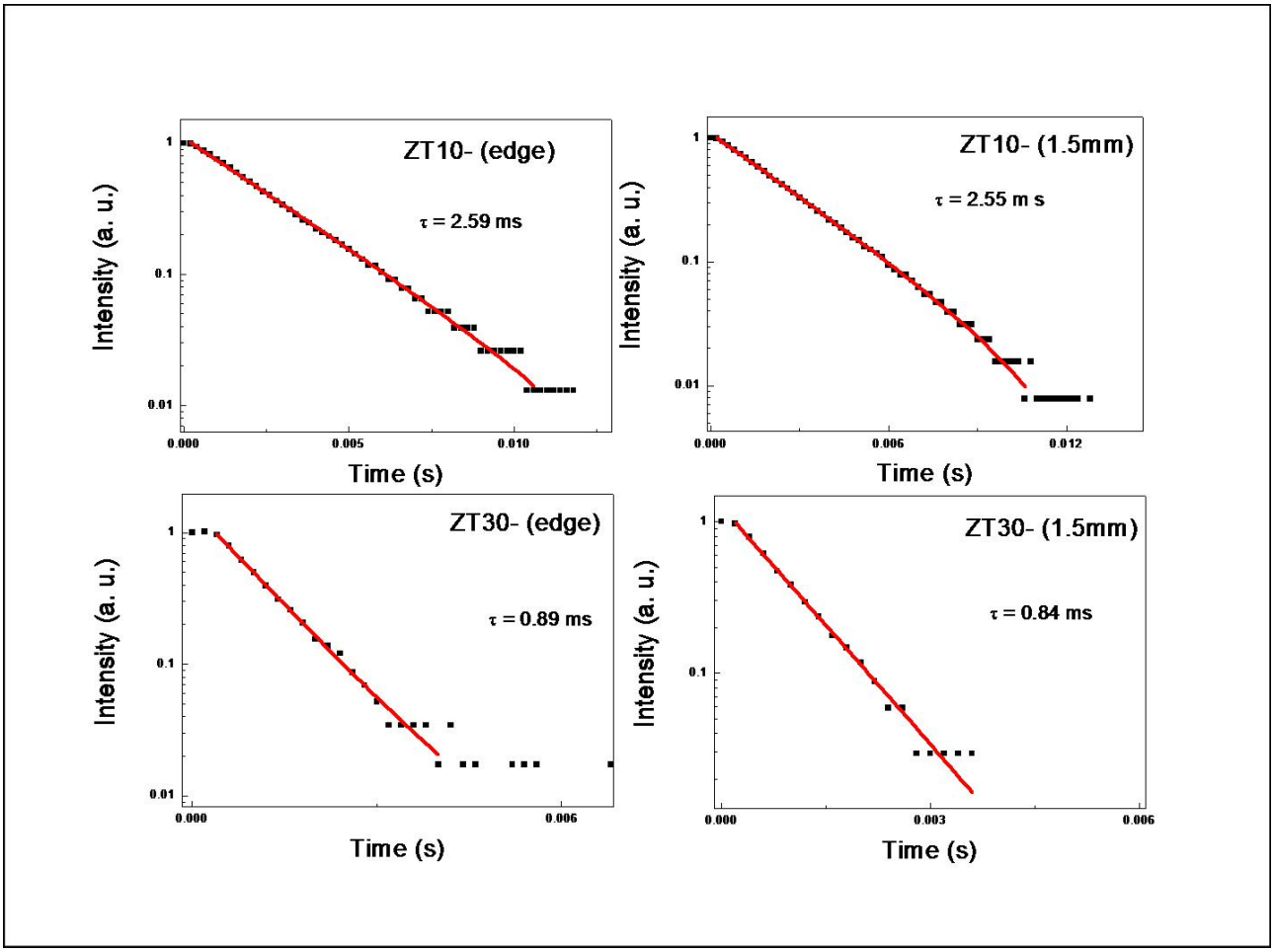

Figure 2.14: PL life times of samples w.r.t. geometry of excitation (as indicated in respective sub plots; The solid line is the result of fitting and the squares are the data point

2.3 Conclusions

(a)Baccarat glass:

The glasses, with molar composition: 77.29 SiO2: 11.86 K2O: 10.37 PbO: 0.48 Sb2O3, have been produced at Cristallerie Baccarat by a conventional melt-quenching technique. Two different sets of samples were produced, containing 0.2 and 0.5 mol% of Er^{3+} ions. The refractive index was measure at several wavelengths. Raman and absorption measurements indicate the high transparency of the Baccarat glass. The water content of these glasses is very low and we estimate a C_{OH} concentration low as 3.6 x 10^{18} cm-3. Luminescence at 1.5 μ m with a spectral width of 18 nm observed on both the glasses. No changes in the spectral width as a function of the excitation wavelength were observed and no NIR-to-visible upconversion signal has been detected. The non-appearance of upconversion in Baccarat glasses indicates that most of Er^{3+} ions are homogeneously distributed and that interaction clusters as well as chemical clusters are practically absent. The $^4I_{13/2}$ metastable state of the Er^{3+} ions decay curves present a single exponential profiles, with a lifetime value of 11.5 ms for the sample doped with 0.5 mol % of erbium and a lifetime of 14.2 ms for the sample doped with 0.2 mol % of erbium. Radiative lifetime were calculated with different models and compared between the experimental measured lifetimes. For the 0.2 mol % Er^{3+}-activated glass, quantum efficiency reaches very high values, up to 79.8 % in the case of a calculation based on the Judd-Ofelt theory. Such high quantum efficiency has already been observed in Er^{3+}-doped tellurite glasses, but remains among the highest quantum efficiencies estimated in pure or modified-silica host glasses. Stimulated emission cross sections in the 1.5 μm region were obtained by using McCumber theory and internal gain curves resulting from absorption and stimulated emission cross sections are calculated. The optical and spectroscopic properties of this modified-silica glass make it well adapted as host medium for the light propagation and a good candidate for many applications in telecommunication systems. The laser action shown by the micro-spheres of Baccarat glass fabricated by plasma torch method (

work of C.Arnaud et.al. [24]) amply demonstrates the fact that Baccarat is a good glass system. The inscription of micro structures, devices like micro-gratings and waveguides in the Baccarat glasses by femto-second laser directwriting method (presented in chapter 4.) further corroborates this fact.

(b) Zinc-Tellurite glasses

Optical spectroscopic properties of Er^{3+} activated 65TeO2 35ZnO glasses were characterized, studying the effects of doping ion concentration on PL characteristics. Raman spectra show that the addition of ZnO has no detrimental effects on the glass structure. No trace of the formation of cluster containing erbium is evidenced. The self-absorption process affects considerably the measurement of the emission properties of Er^{3+} tellurite glasses, leading to a broadening of the observed line shape. This broadening of line shape increased with increase in the doping level. From the life time measurements with respect to geometry of excitation suggest that the concentration is more dominant as compared to self absorption. As an example of the application and use of these glasses, the results of micro-grating inscribed into the Zinc-tellurite glass by laser directwriting method are presented in chapter 4.

Bibliography

[1] W. J. Miniscalco, J. Lightwave Technol., **9**, pp. 234-250(1991).

[2] A. J. Kenyon, Prog. Quant. Elect. 26, pp.225-284, (2002).

[3] A. Polman, J. Appl. Phys. 82, 1-39, (1997).

[4] E. Desurvire, Erbium-Doped Fiber Amplifiers, Principles and Applications, John Wiley, New York, (1994).

[5] http://www.metricon.com/

[6] T. Mito, S. Fujino, H. Takebe, K. Morinaga, S. Todoroki, and S. Sakaguchi, J. Non-Cryst. Solids 210, pp. 155-162, (1997).

[7] S. Fujino and K. Morinaga, J. Non-Cryst. Solids 222, pp. 316-320, (1997).

[8] M.P. Hehlen, N.J. Cockroft, and T.R. Gosnell, Phys. Rev. B 56, pp. 9302-9318, (1997).

[9] S.N. Houde-Walter, P.M. Peters, J.F. Stebbins and Q. Zeng, J. Non-Cryst. Solids 286, pp. 118-131, (2001).

[10] C.W. Mandeville, J.D. Webster, M.J. Rutherford, B.E. Taylor, A. Timbal, and K. Faure, American Mineralogist 87, pp. 813-821, (2002).

[11] P.L. King, T.W. Vennemann, J.R. Holloway, R.L. Hervig, J.B. Lowenstern, and J.F. Forneries, American Mineralogist 87, pp. 1077-1089, (2002).

[12] F. Auzel and P. Goldner, Opt. Mat. 16, pp. 93-103, (2001).

[13] J.L. Philipsen, J. Broeng, A. Bjarklev, S. Helmfrid, D. Bremberg, B. Jaskorzynska, and Plsdttir, IEEE J. Quantum Electron. 35, pp. 1741-1749, (1999).

[14] P. Mislinski, D. Nguyen, and J. Chrostowski, J. Lightwave Tech. 15, pp. 112-120, (1997).

[15] F. Auzel, Ann. Telecomm. 24, pp. 199-229, (1969).

[16] B. R. Judd, Phys. Rev. 127, pp. 750-761, (1962).

[17] G. S. Ofelt, J. Chem. Phys. 37, pp. 511-520, (1962).

[18] K. A. Gschneidner and L. Eyring, Handbook on the Physics and Chemistry of Rare Earth, vol. 25, Elsevier, (1998).

[19] R. Rolli, M. Montagna, S. Chaussedent, A. Monteil, V. K. Tikhomirov, and M. Ferrari, Opt.Mat. 21, pp. 743-748, (2003).

[20] P. C. Becker, N. A. Olsson and J. R. Simpson, Erbium - Doped Fiber Amplifiers: Fundamentals and Technology, P. L. Kelly, I. Kaminow and G. Agarwal, Academic Press, San Diego, (1999).

[21] B. J. Chen, G. C. Righini, M. Bettinelli and A. Speghini, J. Non-Cryst. Sol. 322, pp. 319-323, (2003).

[22] D.E. McCumber, Phys. Rev. 134, A299-A306, (1964).

[23] W. J. Miniscalco and R. S. Quimby, Opt. Lett. 16, pp. 258-260, (1991).

[24] C. Arnaud, M. Boustimi, M. Brenci, P. Frona M. Ferrari, G. Nunzi Conti' S. Pelli, G. Righini, Proc. of SPIE Vol. 5622, 315-320 (2004).

[25] N. Jaba, A. Mermet, E. Duval, B. Champagnon b, Journal of Non-Crystalline Solids, 351, 833837(2005).

[26] R. El Mallawany, Mater. Chem. Phys, 53, 93(1998).

[27] T. Sekiya, N. Mochida, A. Ohtsuka and M. Tonokawa, J. Non-Cryst. Solids 144 (1992) 128.

[28] T. Sekiya, N. Mochida and A. Ohtsuka, J. Non-Cryst. Solids 158, 106, (1994).

[29] C. Duverger, M. Bouazaoui and S. Turrell J.Non-Cryst. Solids 220, 169, (1997).

[30] J. J. S. Wang, E. Vogel M and E. Snitzer, Opt. Mater. 3, 187, (1994).

[31] G. Manoj Kumar, D. Narayana Rao and G.S. Agarwal, Phys. Rev. Lett. 91 (2003)203903.

[32] A. Jha, S. Shen, and M. Naftaly, Phys. Rev. B 62, 6215, (2000).

[33] R. Reisfeld and Y. Eckstein J. Non-Cryst. Solids 15, 125, (1974).

[34] Shaltout I, Tang Y, Braumstein R, and Abu-Elazm, J. Phys. Chem. Sol. 56(1) 141, (1995).

[35] M. Mazzuca, J. Portier, B. Tanguy, F. Romain, A. Fadli, S. Turrell, J. Mol. Struct., 349, 413, (1995).

[36] X. Feng, S. Tanabe, and T. Hanada, J. Am.Ceram. Soc. 84, 165, (2001).

Chapter 3

Silver To Erbium Energy Transfer Mechanisms

INTRODUCTION

The small absorption cross sections of rare earth ions such as erbium or neodymium have spawned numerous attempts to increase the ions' excitation efficiency. Most concepts rely on energy transfer from a species with a large absorption cross section to the rare earth ion in question. In the specific case of erbium, codoping with ytterbium (although itself a rare earth ion, it has a reasonably high absorption cross section at 980 nm) has found its way into application in lasers and optical amplifiers for 1540nm light and broad-band sensitisation in the visible via organic complexes and silicon nanocrystals have been demonstrated.

Particular attention has been devoted to metal-dielectric nanostructured materials [1], due to the well-known surface plasmon resonance, which originates from a confinement effect on the electronic properties in metal systems of finite size[2]. The phenomenon of plasmon resonance is classically described as the oscillation of the free electrons with respect to the ionic background of the nanoparticle, when they are collectively excited by laser irradiation. Glasses containing metal nanoparticles have been exploited since

the Medieval Ages, for the fabrication of colored stained glasses in cathedrals, but they are now attracting a novel interest for photonic applications [3]. The strong absorption crosssection related to the surface plasmon excitation in noble-metal nanoparticles and/or the large local field enhancement, that is generated around the excited nanoparticle make it possible to use such metal nanoparticles for the enhancement of the luminescence intensity emitted by rare-earth ions.

The study of the interactions between rare earths (RE) and metals obtained large interest in the recent years [4] because it connects the scientific interest of understanding the effect of changing the photonic mode density (PMD) on the fluorescence properties of the ions, with the technological appeal of increasing both pumping efficiency and radiative decay rate by suitably enhancing the electric field near the ions. As a matter of fact, several studies showed that the presence of metal surfaces or nanoparticles modifies the PMD, which can be regarded as vacuum fluctuations or as supported electromagnetic modes. In turn, by virtue of the well-known Einstein relation [5], the PMD is proportional to the probability of spontaneously emitted radiation, which therefore is affected both in the decay rate and in the spatial distribution. This happens for any inhomogeneity in ε_r: a remarkable effect is in photonic band gap materials where certain k transitions may be completely inhibited [6]. Also, for metals, the closeness between active centers and metals can induce an important non radiative decay through the coupling of the excited energy levels of the RE to the surface plasmon polaritons [7]. These properties might be exploited in the design of devices activated with RE; in fact, the technological interesting 4f transitions of these ions have weak oscillation strengths, prohibited by Laporte rule, and the possibility to increase the electric field near them could allow 1) to reduce the pumping energy density required to invert population and 2) to favor the radiative decay with respect to the non radiative in order to increase the quantum efficiency.

These motivations stimulated in 1985 O.L. Malta and coworkers to investigate the effect of the nucleation of silver nanocrystals on the spectroscopic properties of an eu-

ropium doped borosilicate glass[8]. They found that the visible luminescence of europium increased after the introduction of silver in the matrix. In analogy with surface enhanced Raman scattering (SERS) [9], they attributed the result to the increase of the electric field in proximity of the metal nanoparticles. Their results were confirmed by Hayakawa et al. [10, 11], but recently [12, 13, 14, 15] it was shown that the excitation occurs also out of resonance, leading to think to energy transfer as the responsible for the increased luminescence. In such a controversial scientific context, we decided to investigate the optical and spectroscopic properties of Er co-doped Ag-ion exchanged thin plates of silicate and sodium phosphate. These ion-exchanged glasses were subjected to heat treatments, and Er luminescence enhancement was observed only in the Sodium-Silicate thin plates. This motivated to investigate further the absence of the luminescence enhancement in Phosphate thin plates. Ag doped phosphate bulk glasses were fabricated. The bulk phosphate glasses when subjected to Laser Treatment showed some enhancement which was mainly due to radiative transfer. With the aim of better understanding the mechanism of the enhancement in the Ag ion- exchanged Sodium-silicate, the effective role of silver concentrations and the contributions of different silver species, sodium-silicate samples were ion-exchanged varying silver concentration. The spectroscopic study reveals that the enhancement of the erbium luminescence in a silver doped glass is due to a energy transfer process from silver species, especially dimers. The sample preparation, the experimental details and the discussion of the results are presented in detail in the following sections of this chapter.

3.1 Sample Preparation

The composition of the rare-earth doped silicate glass we decided to use for our tests is (mol%): 71.5 SiO_2, 15 Na_2O, 10.4 CaO, 1.2 Al_2O_3, 0.4 P_2O_5, 0.6 K_2O, 0.3 Er_2O_3 and 0.6 Yb_2O_3; it was one of a set of glasses we had developed for the fabrication of

ion-exchanged integrated optical amplifiers [16]. From this glass, five plates were cut, thinned down to 200 m, and optically polished. One of these plates was kept as reference (labeled as Ref) while the second plate was fully ion-exchanged. The silicate glass plate was exchanged by keeping it for 67 hours in a molten salt bath of molar concentration 0.5% $AgNO_3$, 99.5% $NaNO_3$ at 390^o C. This ion-exchanged plate will be referred to as SAgEr0 hereafter. The remaining three plates were also kept in the bath for ion exchange with similar conditions but by varying molar concentration (0.5, 1.5 and 5%) of $AgNO_3$. These ion-exchanged plates will be referred to as AgEr5, AgEr15, AgEr50, respectively

The phosphate glass has the following composition (mol%): 65 $NaPO_3$, 20 Nb_2O_5, 15 Ga_2O_3 and 3 mol% of Er_2O_3 was added to the glass. From this glass two plates were cut, thinned down to 200 m, and optically polished. One of these two plates was kept as reference (labeled as Ref) while the other was fully ion-exchanged. The bath used for the ion-exchange of the phosphate glass was 0.5 $AgNO_3$, 49.75 $NaNO_3$, 49.75 KNO_3 mol % and the exchange temperature was fixed to 280C for 65 hours. This ion-exchanged plate will be referred to as PAgEr0 hereafter.

The exchanged depth was estimated to be around 100 μ m from each side of the glass plate, so that silver ions should be present along its whole thickness. The index profile on each side of the plate, reconstructed under the assumption that the distribution is Gaussian (because it provided the best fit of the experimentally measured effective indices in waveguides supporting a much lower number of guided modes).

Preparation of Bulk Sodium Phosphate glasses by melt-quench:

Powders of AgO_2, HPO_3, $NaPO_3$ and $ErCl_3$ were mixed and melted in alumina crucibles at 700 ^{o} C in air for 4 h with a resulting nominal composition of $10(AgPO_3)$ $89(NaPO_3)$ $1(ErO_{3/2})$. By pouring the melt on a metal mould of cylindrical shape, four glass pieces were obtained with height of 2.5 mm and diameter of 15 mm. After annealing at 200 ^{o} C for 2 h to remove the stress, the samples were optically polished. A sample

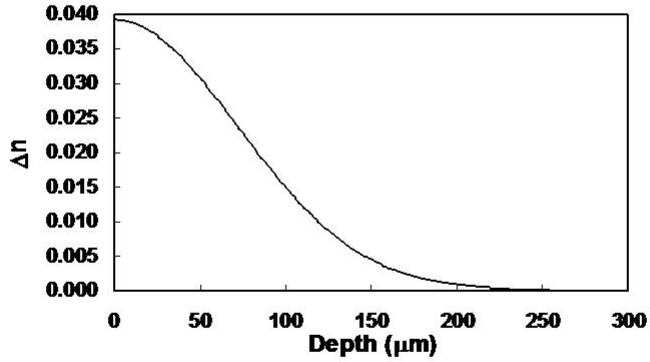

Figure 3.1: Numerically reconstructed Gaussian refractive-index distribution produced on each side of the SAgEr0 sample by the Ag^+/Na^+ ion-exchange at 390C for 67 hours in a molten salt bath of molar concentration 0.5% $AgNO_3$, 99.5% $NaNO_3$

.

of 99($NaPO_3$) 1 ($ErO_{3/2}$) composition, hereafter NaPh, was obtained with the same procedure and kept as a reference.

Absorption measurements were performed using a Cary 5000 UV-Vis-NIR spectrophotometer in dual beam mode. Excitation spectra were recorded using a Xe lamp coupled to a single grating monochromator as excitation source, in a spectral range extending from 360 nm to 750 nm. Simultaneously to the PL signal from the Er^{3+} - doped glass, the signal from a photodiode placed in the light beam close to the sample was acquired for each excitation wavelength in order to correct the excitation spectra by taking into account the spectral characteristics of the excitation source. All excitation spectra were recorded by collecting the Er^{3+} PL signal at 1.53 μ m [17]. The photoluminescence band corresponding to the $4I_{13/2} \longrightarrow 4I_{15/2}$ transition of the Er^{3+} ion was

observed using several excitation wavelengths. Great care was taken in these experiments to keep unmodified the experimental conditions when measuring the PL intensity from the Ag-exchanged glass plate and from the corresponding reference one, in order to have quantitative comparison the PL intensities.

3.2 Ag ion-exchanged Sodium Silicate and Sodium Phosphate glasses

The ion exchanged plates were subjected to heat treatments in air at different temperatures and for different periods were performed on SAgEr0, PAgEr0 and respective Ref plates. The sequence of annealing treatments performed on SAgEr0 is summarized in Table 3.2, and the sequence of annealing treatments performed on PAgEr0 is summarized in Table 3.2.

Table 3.1: Temperature and time for the additive heat treatments of the Ag-exchanged silicate glass plate

Temperature(^{O} C)	Time of Annealing (min.)	Sample Label
-	As prepared	SAgEr0
500	30	SAgEr1
500	30 + 30	SAgEr2
500	30+ 70	SAgEr3
500	30 + 30 + 60	SAgEr4
500 600	30+70 +60	SAgEr5

Table 3.2: Temperature and time for the additive heat treatments of the Ag-exchanged phosphate glass plate

Temperature(^{O} C)	Time of Annealing (min.)	Sample Label
-	As prepared	PAgEr0
500	30	PAgEr1
500	30 + 30	PAgEr2

3.2.1 Absorption, Excitation, PL spectra of the Ion-exchanged glasses

Figure 3.2 shows the luminescence spectra of the reference and as-prepared Ag-exchanged plates of silicate (figure 3.2(a)) and phosphate (figure 3.2 (b)) glass. Photoluminescence spectra in IR region, obtained by excitation at 980 nm. These spectra have been normalized and vertically shifted for clarity.

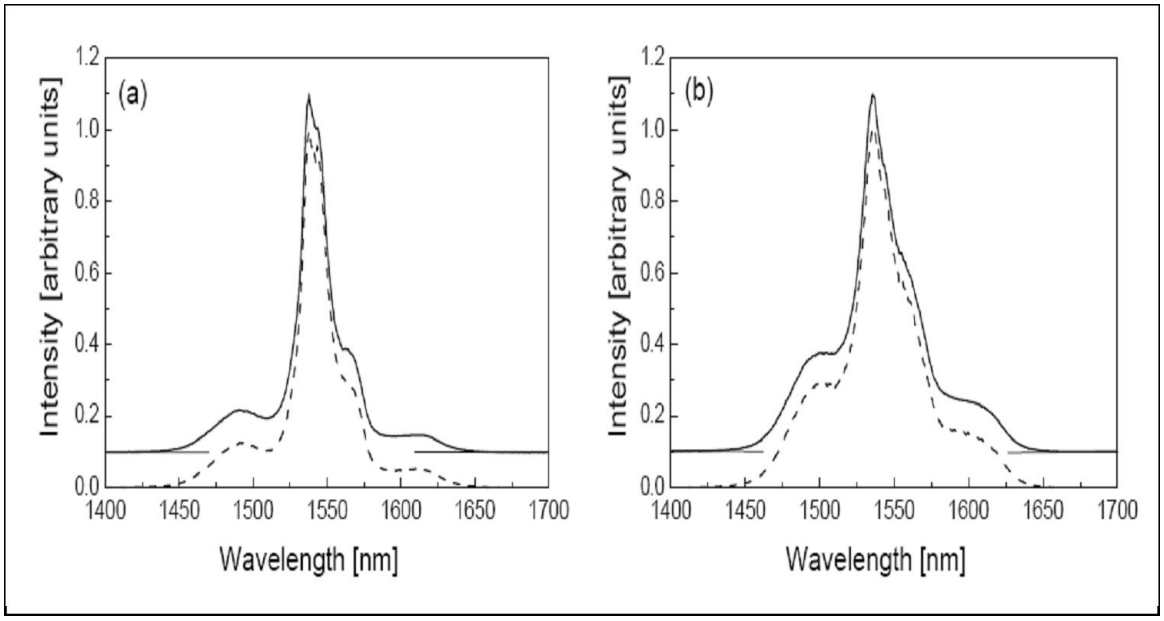

Figure 3.2: Photoluminescence spectra in IR region, obtained by excitation at 980 nm. In the figure 2(a)silicate glasses: Ref (dashed line) and SAgEr0 (continuous line) plates of Er^{3+}-doped silicate glasses; in the figure 2(b)Phosphate glasses:Ref (dashed line) and PAgEr0 (continuous line)

No effect of the Ag-exchange on the profile of the Er^{3+} PL band at 1.5 μm was

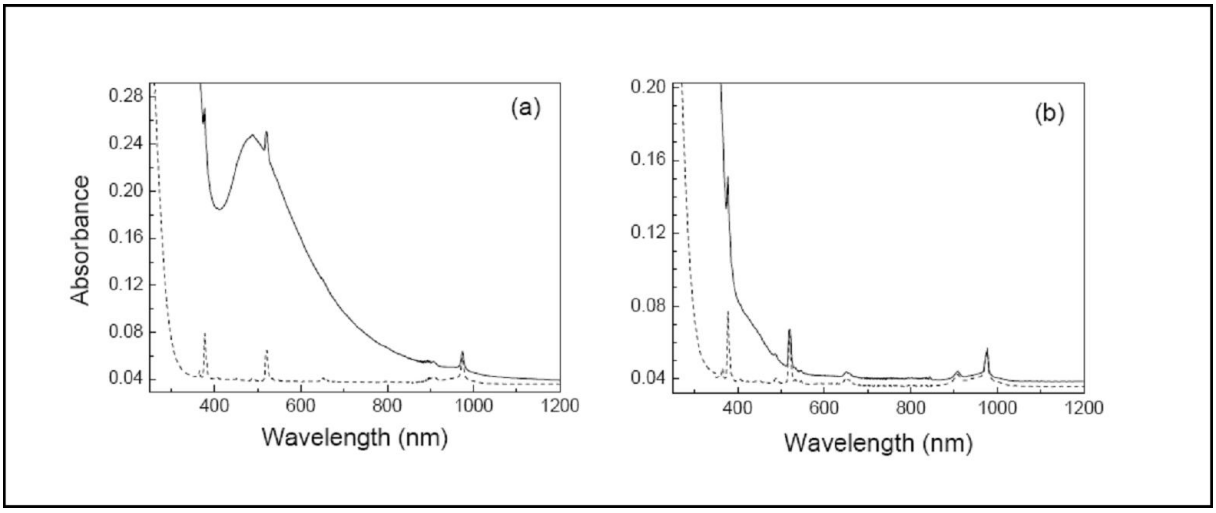

Figure 3.3: Absorption spectra of silver-exchanged (continuous line) and Ref (dashed line) silicate plates, (a) after annealing at 500C for 30 min (SAgEr1); (b) after a second annealing at 500C for 30 min (SAgEr2).

observed. Figure 3.3 (a) shows the absorption spectra of the Ref and SAgEr1 glasses. The Ref sample is transparent in a wide range, down to 300 nm, and the sharp peaks observed in its absorption spectrum are due to transitions of Er^{3+} ions, from the $^4I_{15/2}$ ground state to excited states. In the spectrum of the SAgEr1 glass the band due to the surface plasmon resonance of Ag0 nanoparticles, usually centered around 400 nm [2], is not visible. Instead of the typical plasmons band, a red-shifted broader band, centered at about 480 nm, is observed. After a further heat treatment of the samples, performed in the same conditions as the first ones, the absorption spectrum was drastically modified, as shown in figure 3(b). The broadband centered at 480 nm is no more present. A shoulder appears at around 420 nm, in the region of the Urbach edge of the spectrum of SAgEr2. The absorption spectra of the SAgEr3 and SAgEr4 samples looked very similar to that of the SAgEr2 plate. Figure 3.4 shows the absorption spectrum of the SAgEr5 glass, where a strong band is clearly observed in the blue region, with a maximum at 417 nm. Let us underline that such a band was not visible in the absorption spectra of the SAgEr2, SAgEr3 and SAgEr4 samples, that had been annealed at 500C, as indicated in

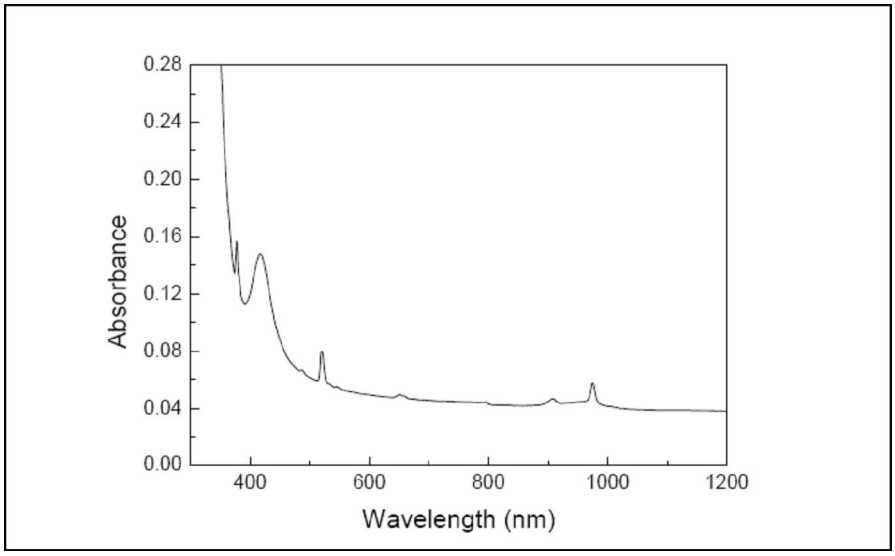

Figure 3.4: Absorption spectrum of the SAgEr5 glass after annealing at 500C for 30 + 70 min and at 600C for 60 min.

Table 1. The shape of the $4I_{13/2} \longrightarrow 4I_{15/2}$ PL band remained the same for all subsequent heat treatments performed on the Ag-exchanged silicate sample.

Figure 3.2.1 shows the excitation spectra of the Ref and SAgEr2 glasses. The excitation spectra of the other annealed silver-exchanged samples are similar to the spectrum of the SAgEr2 glass. After annealing, an enhancement of the Er^{3+} emission intensity at 1532 nm was detected in the exchanged sample, with respect to the reference one, for excitation in the spectral range from 400 to 500 nm.

The spectra reported in the inset have all the same shape, typical of the $4I_{13/2} \longrightarrow 4I_{15/2}$ transition of Er^{3+}. For instance, there are not background or additional structures, thus indicating that the detected PL is only originating from Er^{3+} $4I_{13/2} \longrightarrow 4I_{15/2}$ transition and excluding any spurious emissions that, in principle, could be induced by the Ag-exchange process. Their relative intensities are related to those already observed in the excitation spectra. Therefore, they do not provide additional information, but clearly indicate that the detected PL in the excitation spectra is only originating from Er^{3+} luminescence. Regarding the phosphate glasses an absorption broadband similar

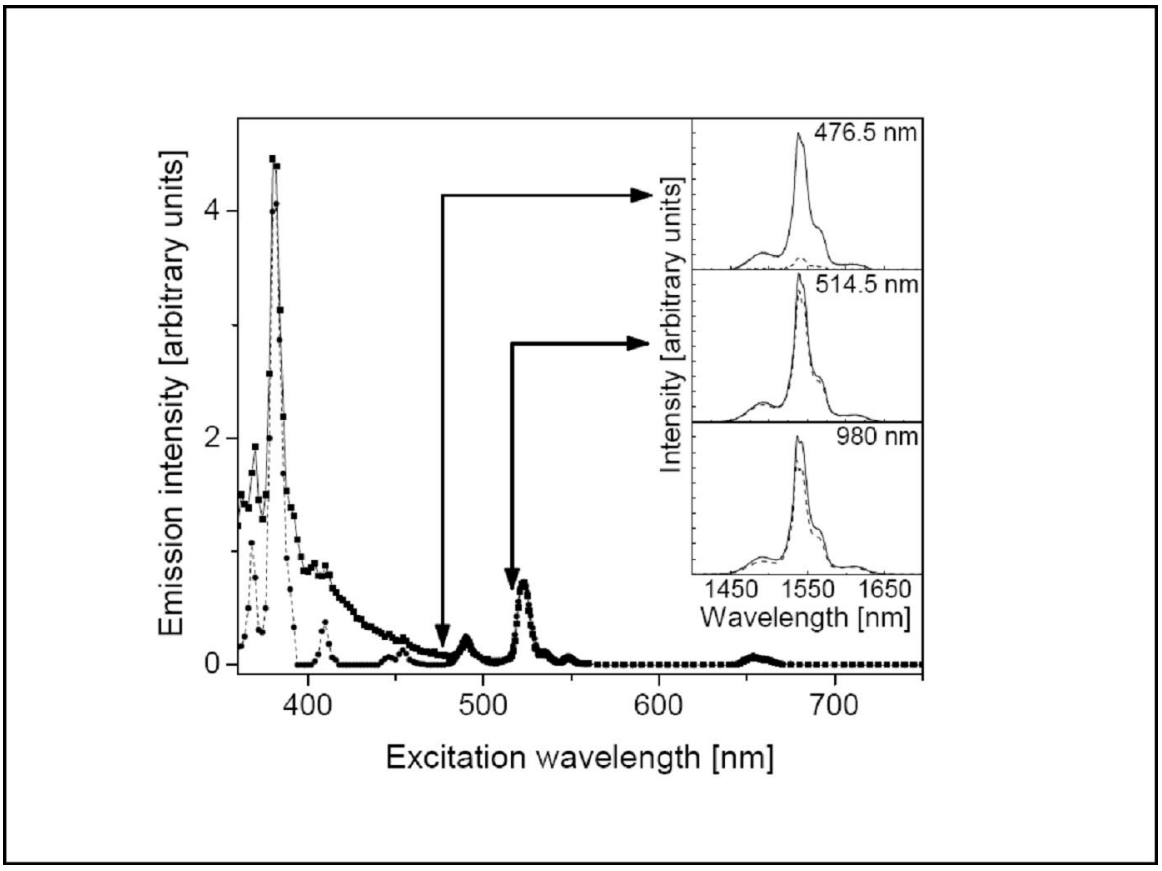

Figure 3.5: Excitation spectra from 360 to 750 nm of the Ref (circles + dashed line) and SAgEr2 (squares + continuous line) silicate plates. The wavelength of the detected light was set to 1532 nm. The inset gives a comparison of the Er^{3+} emission band at 1.53 μ m measured in the Ref (dashed line) and silver-exchanged (continuous line) silicate plates for three different excitation wavelengths (indicated by the arrows on the excitation spectra): 476.5, 514.5 and 980 nm.

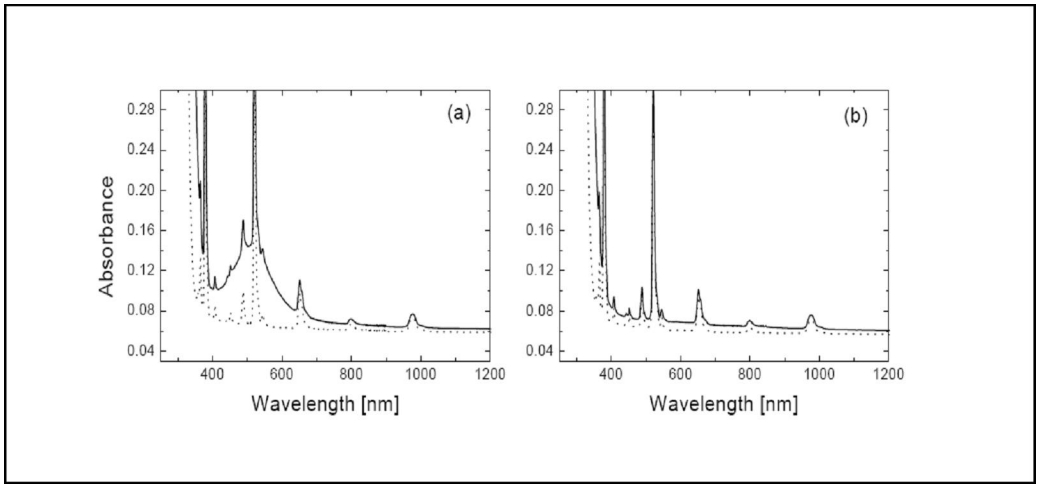

Figure 3.6: Absorption spectra of silver-exchanged (continuous line) and Ref (dashed line) phosphate plates, (a) after annealing at 400C for 30 min (PAgEr1); (b) after a second annealing at 400C for 30 min (PAgEr2).

to the broadband observed at 480 nm in the figure 2a is also observed in figure 3.6(a), related to the phosphate glass annealed at 400C for 30 min (PAgEr1). In this case, the band is weaker and the position of its maximum pointed at 510 nm.

After a further heat treatment of the phosphate samples, the absorption spectra are drastically modified as shown in figure 3.6(b). As for the silicate glasses the broad band centered 510 nm is no more present but no shoulder appears at around 420 nm, in the case of the phosphate glass annealed at 400C for 30 min (PAgEr2). Contrary to the case of the silicate glass excitation spectra evidence no change of the Er^{3+} emission intensity at 1532 nm detected in the Ag-exchanged phosphate glass, with respect to the silver-free glass, even after performing subsequent heat treatments at 400C.

From the present experimental results, some enlightenment is brought in the understanding of the sensitization of erbium by silver. The excitation spectrum of figure 3.5 clearly shows the tail of a band in the blue region, extending to about 500 nm. Such an excitation band seems to be associated with the absorption shoulder observed in figure 3.3 (b), and is not correlated with the broadband at 480 nm revealed in figure 3.3 (a). This last point is supported by the following arguments:

(i) A similar broadband has been observed in an Ag-exchanged phosphate glass after heat treatment at 400C for 30 min (figure 3.6(a)), but in this case also, no enhancement was detected.

(ii) The absorption broadband in the Ag-exchanged silicate glass (SAgEr1) extends from the violet (400 nm) up to the NIR (1000 nm), which corresponds to a range much wider and extended to the red than the region where enhancement of the Er^{3+} emission intensity is detected (from 400 to 500 nm).

(iii) In the sample annealed for twice 30 min (SAgEr2), the absorption broadband, observed in the SAgEr1 sample, disappears (figure 3.3 (b)), while the excitation spectrum remains the same. On the other hand, a correlation of the Er^{3+} PL enhancement with the absorption shoulder observed in figure 3.3(b) can be pointed out when comparing figure 3.3(b) and figure 3.5. The tail of the excitation band and the shoulder seem to extend on a common spectral range.

Let us remark that this shoulder could be already present after the first annealing at 500^o C for 30 min (figure 3(a)). Its contribution could be covered by the presence of the more intense broadband at 480 nm. This could explain why all the excitation spectra of the annealed silver-exchanged samples are identical, whereas their absorption spectra appear so different. Up to now, the origin of the broadband in the absorption spectra of the SAgEr1 glass (figure 3(a)) has not yet been determined and still remains under investigation. Nevertheless, it could be related to the presence of very small silver aggregates, i.e. like multimers [15], and/or silver-induced matrix defects. The shoulder in the region of the Urbach tail of the absorption spectrum of the SAgEr2 sample (figure 3(b)) is observed approximately between 400 and 500 nm. This could be assigned to the emergence of the surface plasmon absorption band, which in turn is a good indicator of the presence of silver nanoparticles inside the silicate matrix. These nanoparticles would be formed by migration and aggregation of silver atoms in the glass during the successive phases of annealing. Such a migration-aggregation process strongly depends on the char-

acteristics of the heat treatment as illustrated by figure 4 through the appearance of a strong band in the absorption spectrum of the SAgEr5 glass after the annealing temperature is increased from 500 ^{o} C to 600^o C. From its shape and its spectral characteristics, this band is attributed without any doubt to the surface plasmon resonance of silver nanoparticles. At this point, it is worth to note that, in all the annealed silver-exchanged glasses, even if a fraction of silver exchanged had participated to the growth of nanoparticles, a large part of silver probably remained under the form of ions, atoms, charged or neutral dimers and multimers. Consequently, the contribution of the latter species to the Er^{3+} PL enhancement cannot be excluded. Finally, it is important to note that the Er^{3+} PL at 1.53 μ m is enhanced nearly for all excitation wavelengths from 400 nm to 500 nm, with a slightly lower efficiency for the resonant Er^{3+} excitations, indicating that such an enhancement is mainly effective for non-resonant excitation of the active ions. Considering the slight weakness of the peaks due to absorption by Er^{3+} ions in the Ag-exchanged silicate plates with respect to those in the reference plates (figure 3), the following crucial information is deduced about the mechanism from which silver can act as a sensitizer for erbium: the Er^{3+} PL enhancement does not originate from an increase of the absorption cross section in Er^{3+} ions when they are subject to the strong local electromagnetic field generated by the surface plasmon excitation of silver nanoparticles, but it is very likely promoted by energy transfer from silver nanoparticles or multimers to the Er^{3+} ions.

3.2.2 TEM, XPS analysis of the Ion exchanged Silicate glasses:

Specimens for TEM observations were prepared by scraping off thin films in absolute ethanol using a diamond knife. A drop of the suspension was deposited onto and dried on a carbon coated copper grid. TEM study of the scraped samples was performed using a 200 kV side entry JEOL 2010 transmission electron microscope. XP spectra were acquired using a 200 mm Scienta (GammadataUppsala) hemispherical analyser.

Table 3.3: Composition of the samples analysed given in atomic abundances (%).

Atom	Reference	SAgEr1	SAgEr2	SAgEr3	SAgEr4	SAgEr5
Si	30.8	33.0	30.4	32.3	30.6	31.1
Na	2.1	1.5	2.2	1.7	1.8	2.13
Ca	2.4	0.4	0.5	0.9	0.8	0.9
Al	2.3	1.8	2.6	1.6	2.7	2.7
K	1.4	1.1	0.8	1.1	1.2	1.3
O	61.1	61.8	62.9	61.7	62.1	61.3
Ag	0	0.3	0.5	0.6	0.6	0.5

The vacuum was in the region of 10-8 Pa. For each sample a wide scan, 0 1200 eV, was acquired to detect the chemical elements together with the possible contaminations. Core lines were acquired using a pass energy of 150 eV. In this condition the energy resolution of the analyser at the Fermi edge is about 0.4 eV. With this energy resolution, chemical shifts due to different bonds may be distinguished. Glasses being strong insulators need charge compensation during spectra acquisition. The value of 285 eV for the core line of the CH_x components was chosen as a reference for determining the correct binding energy (BE) values of the other glass chemical elements. Atomic concentrations were obtained from the intensities of the spectral components. Linear background subtraction and Gaussian components were used to perform peak fitting. For each chemical element, the core line was deconvoluted into components pertinent to the chemical bonds formed.

In figure 3.7 (a) and 3.7 (b) show the effect of annealing on the Ag dispersion in the glassy network. In particular the TEM image presented in figure 3.7 (a) is the image obtained from sample SAgEr1 as an example of mild thermal treatment. The image shows silver condensed into a few clusters of dimension 10 nm and the arrows in the magnified portion provide evidence of the possible presence of smaller silver aggregates of dimensions around 1 to 3 nm. In panel B is reported the TEM image obtained from SAgEr5, the sample annealed for longer time and at higher temperature. Again silver is present in clusters having now a higher diameter of about 15 nm. Let us switch now to the XPS analysis.

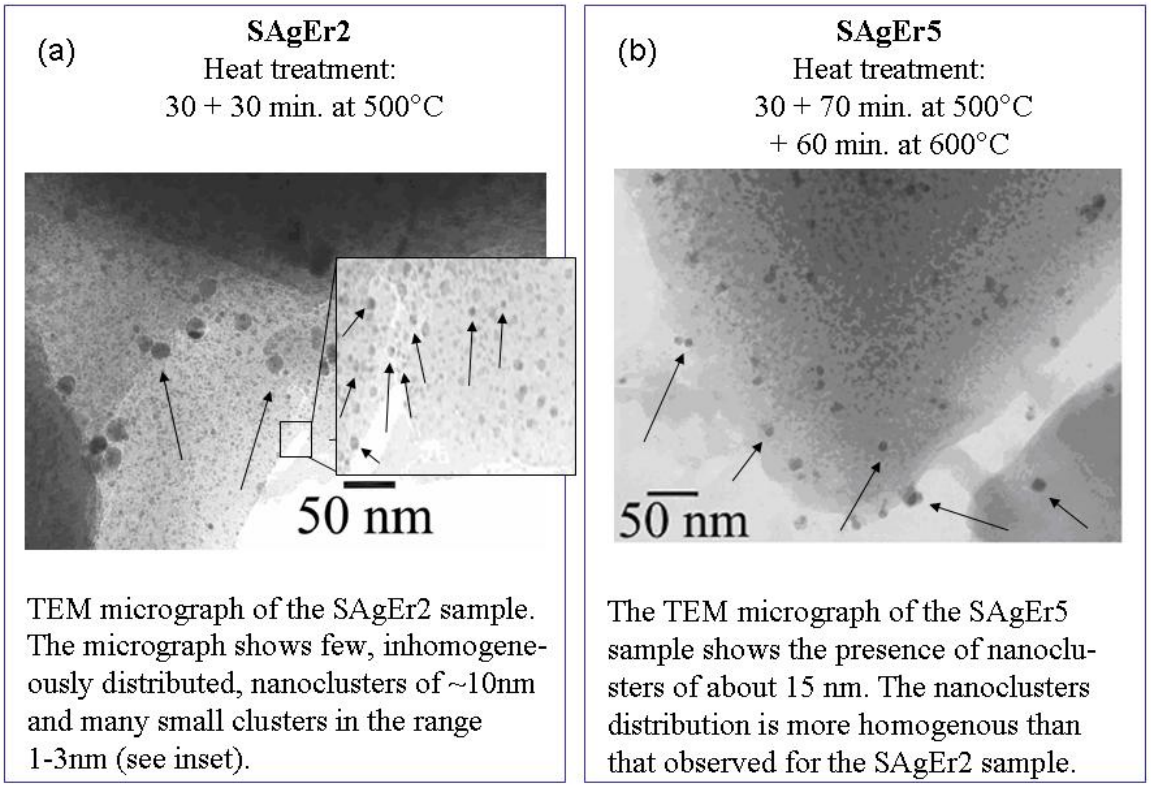

Figure 3.7: (a): TEM image obtained for an Ag exchanged soda-lime glass annealed at 500^o C for 30 min. Silver aggregates into a few clusters of 10 nm size and probably into small clusters of 1 to 3 nm size. (b): TEM image obtained from an Ag exchanged soda-lime glass annealed at 500^o C for a total of 100 min plus a second treatment at 600^o C for 60 min. Now the dimensions of the Ag cluster are about 15 nm. Arrows indicate Ag clusters.

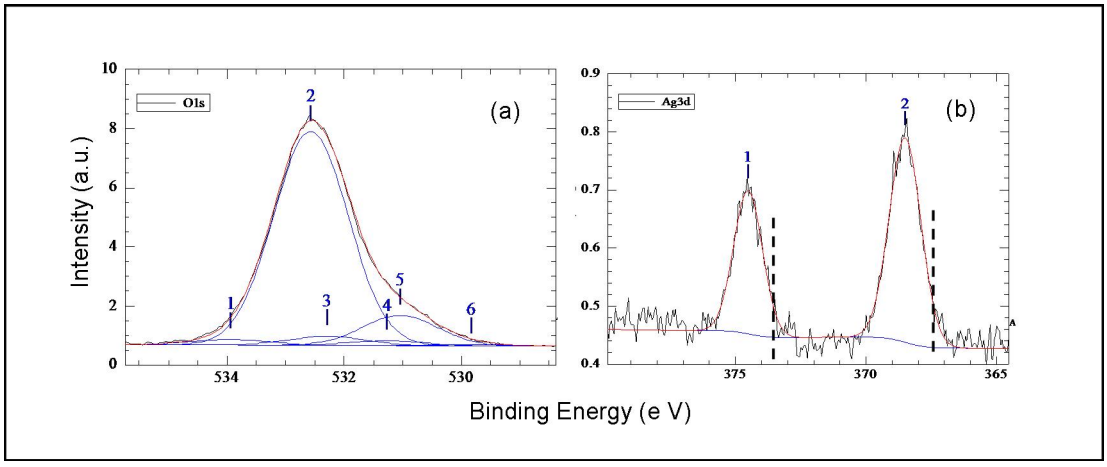

Figure 3.8: (a): XP spectrum of the O 1s core line deconvolved into the Gaussian components. The numbers indicate different chemical bonds (see the text).(b): the Ag 3d 3/2 and Ag 3d 5/2 core lines. Broken lines indicate the positions of silver oxide.

In table 3 the chemical elements are summarized revealed by our instrument and the relative total atomic abundance. It is worth remembering that XP spectra show the composition related to the material surface. For this reason some of the glass component elements are not detected because their concentration is below the instrumental sensitivity (preferential superficial arrangement of Si, Al, K and C due to contamination). The atomic concentration of Ag is almost constant among the samples and around 0.5%.

In figures 3.8 (a), (b) are shown examples of the core line spectra of oxygen and silver respectively. Oxygen is decomposed into six components. Each of them is associated with a specific chemical bond formed by oxygen with the other chemical elements of the soda-lime glass. Peak fittings are performed linking component integrals to the stoichiometry an optimizing the χ^2. Component 1 at 534 eV is related to (C=O)O* (* indicates the oxygen atom whose BE is referred to). Component 2 at 532.6 eV is related to the bridging oxygen in SiO2 while component 5 at 531 eV is related to the non-bridging oxygen atoms in agreement with [18]. Components 3, 4, 6 at 532.3, 531.3 and 529.8 eV correspond to COC, (C=O*)C and $Na_2O + K_2O$ respectively. In figure 3.8 (b) shows the

silver core line split in the two spinorbit components 3d3/2 at higher BE and 3d5/2. A pure Gaussian component was used to fit each peak. Broken lines indicate the position of silver oxide. Finally in figure 3.9 shows the position of the Ag 3d5/2 as a function of the annealing time. The dashed line represents the BE relative to that of metallic silver. A small decrease of the Ag 3d5/2 BE value is observed, increasing the annealing time. The inset of figure 3.5 clearly shows an enhancement of the Er^{3+} fluorescence when a laser excitation at 476.5 nm impinges on the Ag exchanged soda-lime glasses. Despite this effect being observed also by other authors [8, 12, 14, 19] the mechanism underlying the process of erbium excitation leading to the radiative $4I_{13/2} \longrightarrow 4I_{15/2}$ transition is not well established. In this respect we can give some hints. First of all Ag plays a fundamental role in this emission process. Some authors [8, 19] related the enhancement of the Er^{3+} fluorescence to the presence of the well known Ag surface plasmon. In brief, due to the high Ag cross section, a large portion of the exciting energy is converted into free electron plasma oscillations. The strong local field enhancement around the rare earth ion promotes energy transfer from the Ag nanoparticle to the Er^{3+} and then the emission at 1532 nm. To verify this model it is of paramount importance to determine the chemical state of the Ag atoms. Unfortunately the composition of the glassy network is too complex and the concentration of Ag too small for detecting the presence of silver oxide from the oxygen core line peak (see figure 3.8(a)). Nonetheless inspection of the 3d core lines of Ag gives us some clear indications [20]. The dashed lines in figure 3.8(b) point to the BE of silver oxide. Ag enters in the glassy network via ion exchange as Ag^+ which could form Ag_2O. Our spectra do not show any deformation at low BE: pure Gaussian lineshapes perfectly describe the peaks. We can conclude that silver is present in our glasses in a non-oxidized form. As a consequence the electrons on the surface of the Ag nanoparticles are not involved in strong chemical bonds with oxygen and free to oscillate when excited by laser radiation. Other information may be gained from the analysis of the Ag spectra. It is known that the XP lineshapes of metallic system are

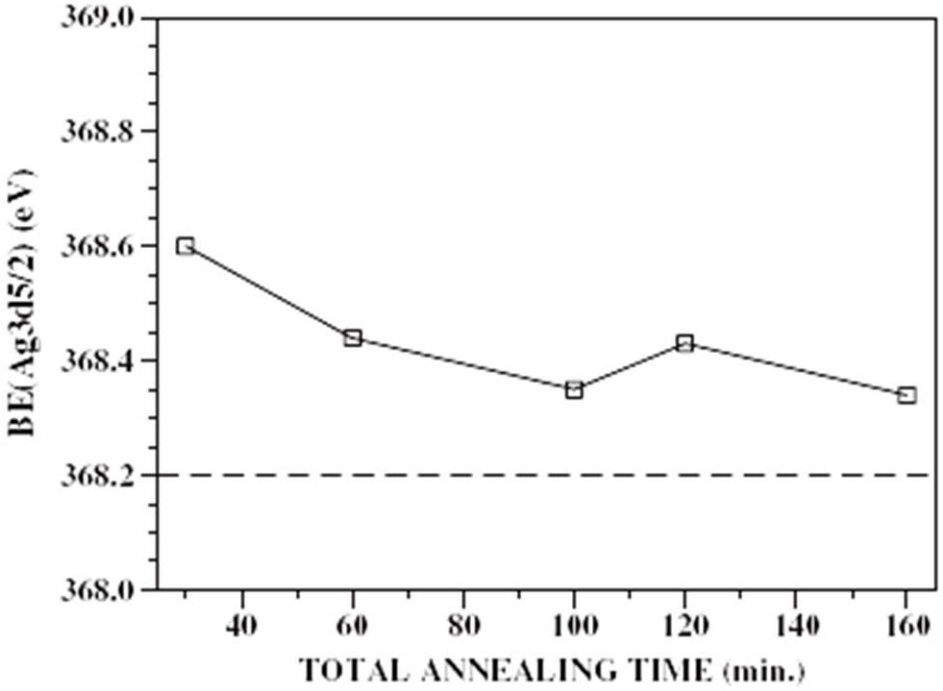

Figure 3.9: Trend of the Ag binding energy as a function of the total annealing time. The dashed line indicates the BE relative to that of pure metallic Ag.

asymmetric. In metals the presence of the core hole screening introduces a tail on the high BE side of the core line [21]. The spectra from each of the SAgEr samples have symmetric shapes fitted with simple Gaussian components. This reflects the loss of the Ag metallic character due to condensation in nanoclusters. In fact, known from the literature is a tendency to electronic quantum confinement when the dimensions of metal clusters scale down to the nanometre size [22]. This effect is confirmed also by the energy shifts towards higher BE of the Ag 3d peaks.

The results shown in figures 3.8(a), (b) and 3.9 tell us that the lower the Ag nanocluster size the higher the BE shift. The dependence of the BE on the metallic nanoparticle size was already observed by other authors [23] and explained theoretically [22]. So XPS enables us to relate electronic quantum confinement to the strength of the thermal treatment. It is known that heating induces a condensation of Ag into clusters. Figure 3.9

indicates that there is a progressive increase of the average Ag nanoparticle size up to 100 min of annealing. In agreement with TEM images, further thermal treatments are likely to induce an increase of the nanoparticle dimensions with a loss of the electron localization and an increase of the metallic character of the Ag aggregates.

3.3 Er activated Sodium Phosphate glasses co-doped with silver

The matrices where the enhancement of Er PL has been observed were silicate glasses. On the contrary, silver exchanged sodium phosphate glass, a matrix broadly used in application because of the high solubility of rare earths and its advantageous mechanical properties, has shown no energy transfer and therefore no significant increase of Er^{3+} luminescence at 1.5 μ m [13] . This has motivated us to do a further and deeper study into the effect of the phosphate matrix on such energy transfer processes.

The Erbium activated bulk Sodium Phosphate glass (co-doped with silver) samples underwent different heat treatments at 300 ^{O} C and 400 ^{O} C in air for 30 min to promote the formation of silver clusters (and hereafter they are called AgPh3 and AgPh4, respectively, while the untreated one is called AgPh2). A sample (labeled as AgPhLT), was laser treated with a 10 Hz pulsed Nd-YAG laser operating at 355 nm, with 6 ns pulse and energy of 29 mJ. The laser was focused onto an area of 0.3 cm^2 for 20 minutes. Optical absorption spectra were obtained in the $0.2 - 3.2$ μm range using a double beam spectrometer with a resolution of 1 nm. Photoluminescence measurements in the visible and infrared were obtained upon several excitation wavelengths. The set-up for the detection of the infrared signal consisted in a 320 mm single-grating monochromator with a resolution of 2 nm connected to an InGaAs photodiode, while for the visible range it consisted in a double monochromator with a resolution of 0.5 nm connected to a photon counting system. Excitation spectra were excited by a Xe lamp coupled to a

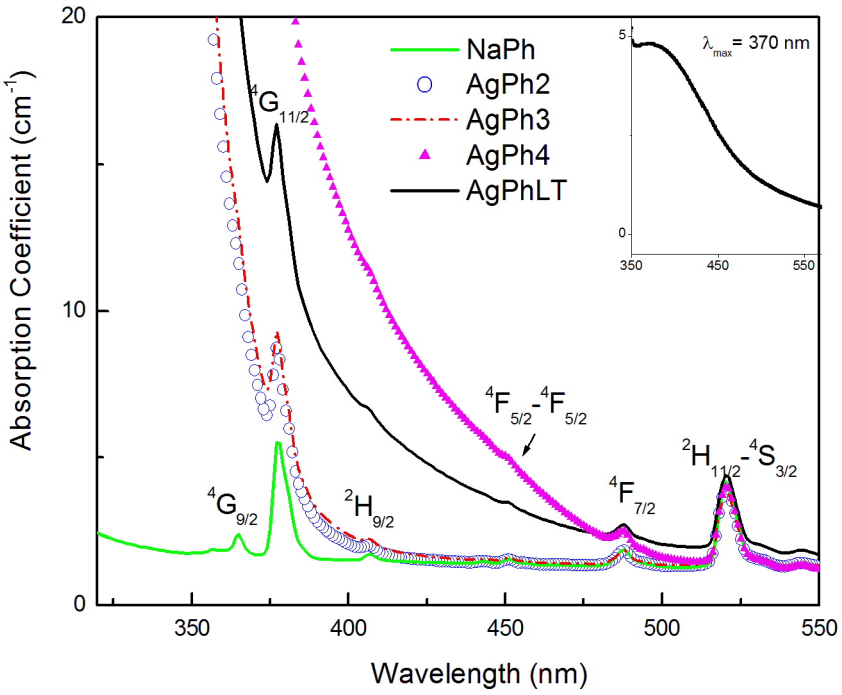

Figure 3.10: Room temperature absorption spectra of the phosphate samples. The inset shows the difference between the spectra after and before the laser treatment.

single-grating monochromator, in a spectral range extending from 320 nm to 750 nm, with a resolution of 5 nm. The signal was collected at several wavelengths in visible and IR range. The absorption spectra of the samples are shown in figure 3.10 . The NaPh sample has a wide transparency window down to the NUV. Many sharp lines of the Er^{3+} appear in the spectrum. In the samples containing silver, the intense absorption due to the $4d^{10} \longrightarrow 4d^9 5s1$ transition of Ag^+ ions shifts the energy gap. The samples are too thick for showing the absorption band shape, whose maximum should be at 250 nm [24]. The sample annealed at 400 ^{O} C becomes slightly opaque: a beginning devitrification process is probably active, since $NaPO_3$ has a low glass transition, around 300 ^{O} C [25]. The laser treatment also produces red-shifts of the absorption that can be ascribed to a clustering of Ag^+ ions. This has been evidenced in the inset, where the differential ab-

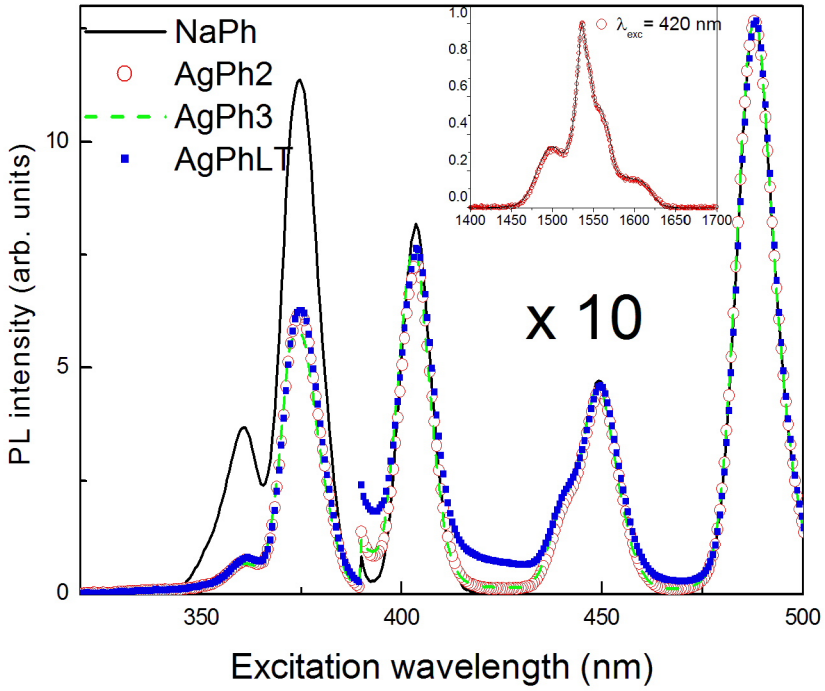

Figure 3.11: Excitation spectra obtained collecting the erbium luminescence at 1.53 μ m. The spectra have been multiplied by a factor 10 for wavelengths higher than 390 nm. The inset shows the PL spectrum of the $^4I_{13/2} \longrightarrow {}^4I_{15/2}$ erbium transition upon 420 nm excitation by Xe lamp.

sorption coefficient of AgPhLT, before and after the laser treatment, has been reported. The broad band centered at about 370 nm, reported in the inset of figure 3.10, has been observed also in AgPO3 crystals and assigned to Ag^+Ag^+ dimers [26]. Figure 3.11 shows the excitation spectra collected at 1532 nm, on the maximum of the $^4I_{13/2} \longrightarrow {}^4I_{15/2}$ erbium emission. In addition to the erbium excitation sharp bands, a weak broad band centered at around 400 nm appears in the silver co-doped samples. It is important to note that no luminescence, other than that of erbium, is detected at around 1.5 μm after excitation at any frequency. As shown in the inset, for an excitation at 420 nm in the weak broad band and therefore not resonant with Er^{3+} excitations, the luminescence intensity goes to zero on the two sides of the Er^{3+} luminescence band. Furthermore, the

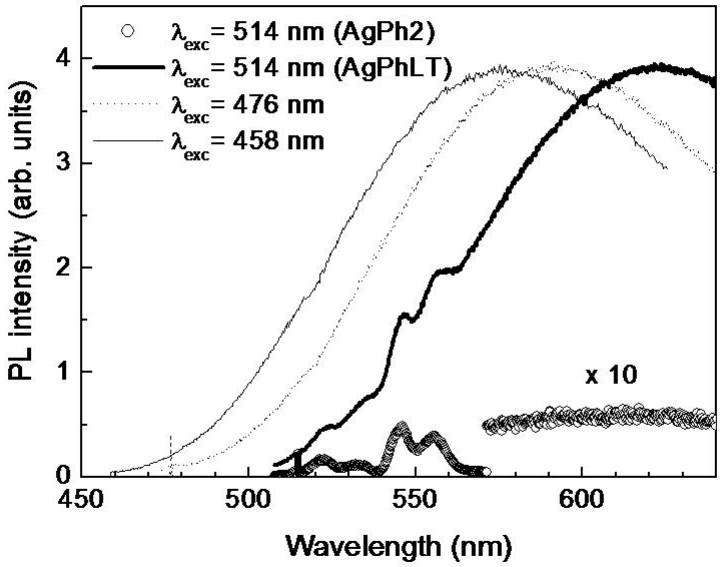

Figure 3.12: PL spectra of sample AgPh2 upon 514.5 nm laser excitation and of the laser treated sample AgPhLT upon 458, 476 and 514.5 nm laser excitation.

shape of the luminescence band was the same for the different excitations. Figure 3.12 shows the PL spectra of the silver doped glasses before and after the laser treatment. After excitation at 514.5 nm, on the high energy tail of the $^4I_{15/2} \longrightarrow {}^2H_{11/2}$ Er^{3+} transition, a broad band emission appears together with the $^2H_{11/2} \longrightarrow {}^4I_{15/2}$ and $^4S_{3/2} \longrightarrow 4I_{15/2}$ lines of Er^{3+} luminescence. The intensity of the band is very weak both in the untreated and in thermally treated samples. It increases by a factor of about 50 after the laser treatment, while position and shape are scarcely effected. By exciting the AgPhLT sample at 476 nm and 458 nm, the band progressively blue-shifts, indicating the presence of different centers, which absorb and emit at different frequencies [24].

Figure 3.13 shows the excitation spectrum (λ_{coll} = 515 nm), together with the PL spectrum ($\lambda_{exc} = 350$ nm) and the absorption spectrum for sample AgPhLT. The PL band is further shifted to shorter wavelengths, with respect to those of figure 3.12, obtained

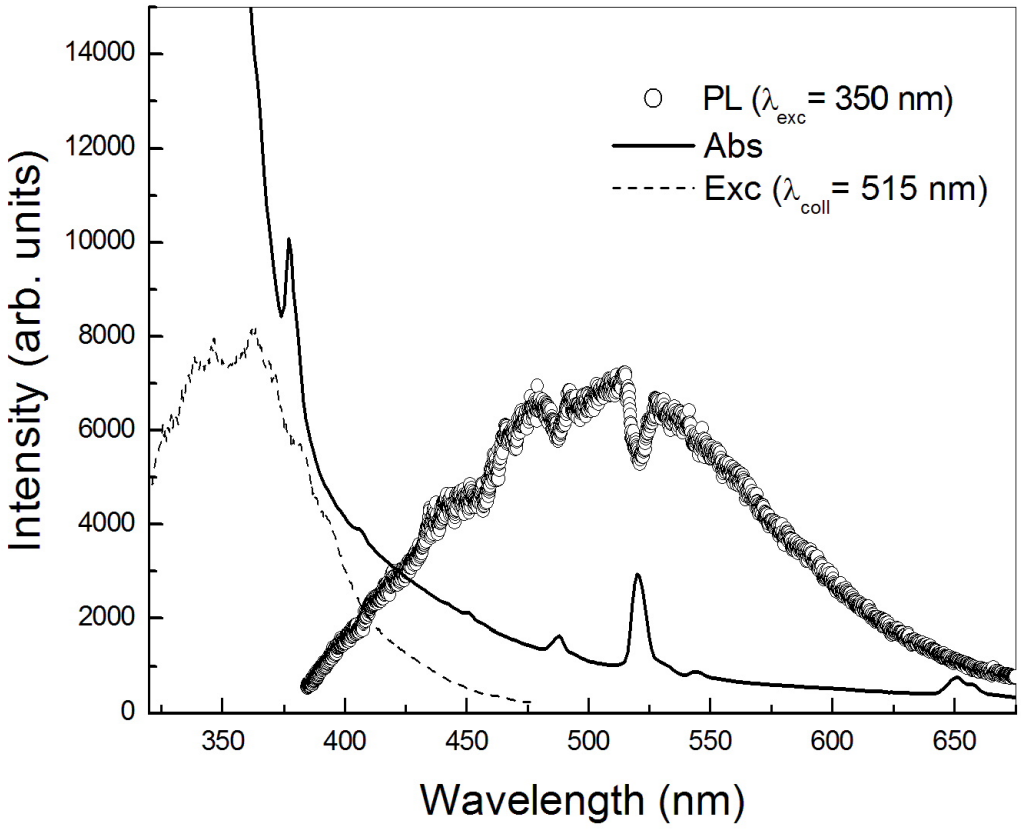

Figure 3.13: Excitation spectrum collected at 515 nm, PL spectrum upon 350 nm excitation by a Xe lamp and absorption spectra of the laser treated sample AgPhLT.

by excitation in the visible. The excitation at 350 nm is obtained by a Xe lamp, and therefore, the excited volume is not confined near the surface like with laser excitation. The PL has to travel a longer path inside the sample to reach the surface. The dips in the PL band in correspondence with the erbium absorption lines, the strongest one being around 520 nm ($^2H_{11/2}$ level), are a clear evidence of radiative energy transfer from silver aggregate to Er^{3+} ions, i.e. reabsorption of the luminescence.

In silver-doped silicate glasses it is possible to promote the formation of silver aggregates by heat treatments in air at temperatures above 450 ^{o}C [27]. Instead, in metaphosphate glasses the heat treatments seem to have smaller effects. The AgPh3 sample, annealed at 300 ^{o}C, shows a very weak luminescence band from silver aggregates, of intensity comparable with the one of AgPh2 (figure 3.12). When heated at higher temperatures, the glass tends to devitrificate before showing important silver clustering. On the other hand, the laser treatment at 355 nm is more effective and the luminescence of silver aggregates increases of about two order of magnitude. This is probably due to a selective excitation of the silver ions, which induces the silver clustering without affecting the glassy structure. The shape of observed luminescence, in particular the frequency position of its maximum, shifts with the excitation frequency. This is a clear indication that different centers are co-existent, probably Ag^+Ag^+ and Ag^+Ag^0 dimers, trimers and other small aggregates, as already observed in silicate glasses[24]. The increase of the broad band PL intensity in the laser treated sample can be associated to the increase of the Er^{3+} PL upon non-resonant excitation. However, the energy transfer process is weaker than in silicate[13]. The presence of dips in correspondence to Er absorption in the PL bands of silver aggregates clearly indicates that radiative transfer plays some role. This effect mainly depends on the geometry of the samples. Massive samples, as those of the present work, should show larger reabsorption effects than the thinner glasses used in previous studies [13]. On the contrary, the non-radiative transfer depends on the microscopic structure and spatial distribution of acceptor and donor species. In this respect,

the property of good solution with large separation among the doping species, which make phosphate glasses favored for high doping level active materials [28], is a drawback. In fact, metaphosphate glasses are constituted of long polyphosphate chains, which allow the clustering in pair of ions that are coordinated to a small number of oxygen ions (3 for Ag^+, 5 for Na^+), but prevent it for high coordination number ions such as rare earth [26, 29]. This physical constrain suggests that in phosphate glasses thermal annealing produces few Ag small aggregates, which should act as donors in the process of energy transfer to erbium ions [12, 13]. Laser annealing is more efficient in producing them, but energy transfer from the Ag aggregates to Er ions is less effective than in silicate glasses, probably because of a larger mean distance between donors and acceptors induced by the phosphate structure. A very weak energy transfer is observed and an important part of it is probably due to radiative reabsorption.

3.4 Effect of Silver Concentration on Er Luminescence enhancement:

In order to distinguish between the different excitation mechanisms, samples with different silver doping concentration were subjected to heat treatments to change the relative concentration of the silver related species in a erbium doped soda-lime glass in-order to correlate the visible fluorescence of these species with the erbium excitation. A part from the technological interest, erbium has a practical advantage over europium, as the efficient radiative emission at 1.5 μm is completely separated from the silver luminescence, which is centered in the visible region.

The set-up for the detection of the infrared signal consisted in a 320 mm single-grating monochromator with a resolution of 2 nm connected to an InGaAs photodiode, while for the visible range it consisted in a double monochromator with a resolution of 10 cm^{-1} connected to a photon counting system. The excitation spectra were corrected dividing

by the spectral output of the source collected by a calibrated photodiode. Photoluminescence measurements in the visible and infrared region (in particular around the $^4I_{13/2} \rightarrow {}^4I_{15/2}$ transition of the Er^{3+} ions) were obtained upon several excitation wavelengths. Time resolved PL measurements were carried on in the visible range exciting the samples by the third harmonic (355 nm) of a Q-switched Nd:YAG laser with a pulse width of 6 ns and a repetition rate of 10 Hz. The luminescence decay was collected at several wavenumbers with the set-up previously described and recorded by a multichannel analyzer. Further information was obtained by polarization spectroscopy. The polarized beam of an Ar^+ laser, operating at 488 nm, was used for the excitation and the luminescence with parallel (VV) or with perpendicular (VH) polarization was detected. A scrambler was inserted between the polarizer and the spectrometer for equalizing the set-up response. All measurements were taken at room temperature.

Figure 3.14 shows the absorption spectra of the silicate samples. The sharp weak peaks are due to Er^{3+} absorption. They should be common to all samples, but in fact it seems that their intensity decreases after the ion exchange. This process exchanges Na^+ ions with Ag^+ ions, but probably also some Er^{3+} ion diffuses to the solution and is lost for the glass. The plasmon band at 420 nm, typical of the spheroidal silver nanoparticles, is well observable in the sample Ag05 heated at 600 ^{o}C in air, but does not appear for annealing at T $<$ 400 ^{o}C. The other silver species are not easily discernible in the absorption spectra [24, 30]. The differential absorption measurements in the inset of Figure 3.14, where the absorption of the reference sample is subtracted, can help in the detection of the contribution of different silver aggregates. Neglecting the sharp dips due to the Er^{3+} absorption, the spectra look different in the blue and UV ranges, where the absorption becomes strong. We attribute this absorption to Ag^+ ions, whose absorption is centered at about 250 nm [24]. As expected, the absorption is higher in the Ag15 than in the Ag05 sample. Unfortunately, the measurement in the Ag50 is not significant, since the metallic silver on the surface greatly reduces the transmission in all the visible

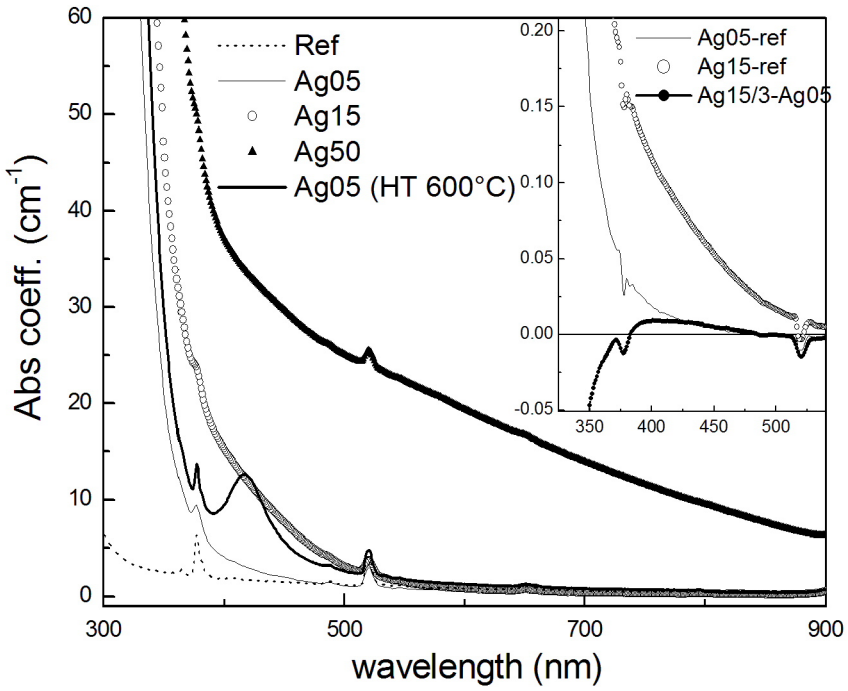

Figure 3.14: Room temperature absorption coefficient of the silicate samples. Inset: Differential spectra, which highlight the silver species absorption.

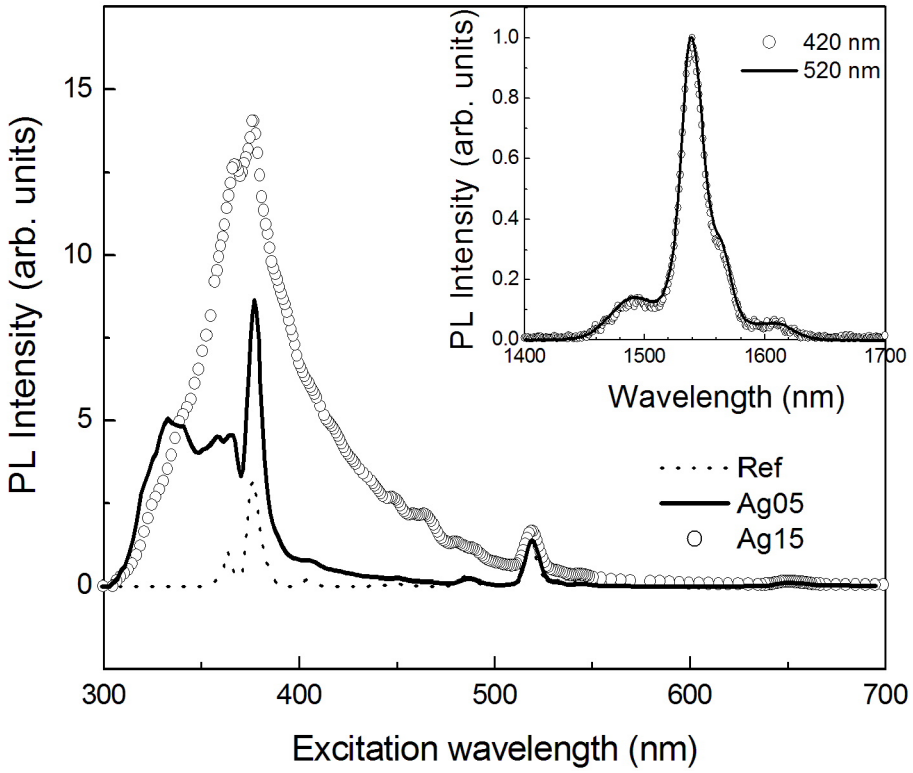

Figure 3.15: PL Excitation spectra collected at 1532 nm from Er^{3+} $^4I_{13/2} \rightarrow {}^4I_{15/2}$. Inset: Normalized PL spectrum of Ag05 upon excitation resonant (520 nm) and non resonant (420 nm) with erbium energy levels.

range. Apart from the intensity, also the shapes of the absorption profile in the Ag5 and Ag15 seem to be different, the latter presenting a shoulder at about 400 nm. If the exchange process would simply replace Na^+ with Ag^+ ions, without the formation of any silver aggregate, the absorption spectra of all as exchanged samples should have the same shape, with an intensity proportional to the Ag^+ concentration. The difference spectrum, $\alpha(Ag15)/3 - \alpha(Ag5)$, shows that this is not the case and that silver tend to aggregate already during the exchange process. This is reflected in a reduction of the absorption at low wavelengths and in the presence of the now clearly observable band, at about 400 nm, attributed to silver dimers or larger aggregates [24].

Figure 3.15 shows the excitation spectra of the exchanged silicate glasses collecting

the signal at 1532 nm, i.e. from the maximum of Er^{3+} $^4I_{13/2} \rightarrow {}^4I_{15/2}$ emission. It is important to note that no luminescence, other than that of erbium, is detected at around 1.5 μm after excitation in the visible. As shown in the inset for an excitation at 420 nm, the luminescence intensity goes to zero on the two sides of the Er band. The excitation spectra were normalized to the intensity of the line at 650 nm, which corresponds to the $^4F_{9/2} \rightarrow {}^4I_{15/2}$ of the Er^{3+} ions. This allows to compare more reliably the excitation spectra of different samples in presence of some unavoidable changes in the experimental conditions. In fact, the samples have different refractive index and different surface roughness, induced by the deep ion exchange. The excitation spectrum of the Ref sample shows only the sharp lines due to the direct excitation of the inhomogeneously broadened erbium levels. In the exchanged samples, also a broad band contribution appears. It is remarkable that not only the intensity but also the shape of this continuous contribution changes as the silver content is increased. As already observed [12, 14, 13, 15], the excitation out of the electronic energy levels of the erbium ions is a clear indication of the presence of an energy transfer process. In comparing the shapes of the excitation spectra of different samples, we have to consider not only the presence of different energy transfer mechanisms through which the erbium ions are excited but also that the samples are thick and the absorption is strong at low wavelength. Therefore, the excited volume is sample and wavelength dependent, causing a non-linearity of the excitation response.

Some centers that absorb the light and transfer the excitation to the erbium. Their spectroscopy and their activity in the transfer process can be studied by a detailed comparison of the excitation spectra taken at different emission frequencies and of the luminescence spectra obtained by exciting at different frequencies, possibly in time resolved experiments. Figure 3.16 shows the PL spectra of the Ag15 sample excited at different wavelengths between 410 and 595 nm. All spectra show a very broad band whose maximum shifts with the excitation frequency. A positive contribution to the PL from the erbium ions in this scale is visible only for the excitation at 520 nm, which is

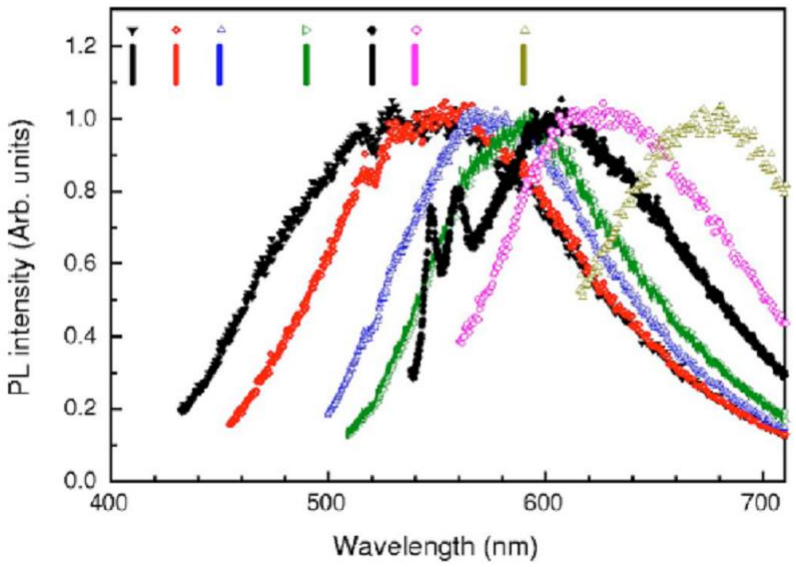

Figure 3.16: Normalized PL spectra of Ag15 sample upon excitation by a Xe lamp at several wavelengths (indicated in figure).

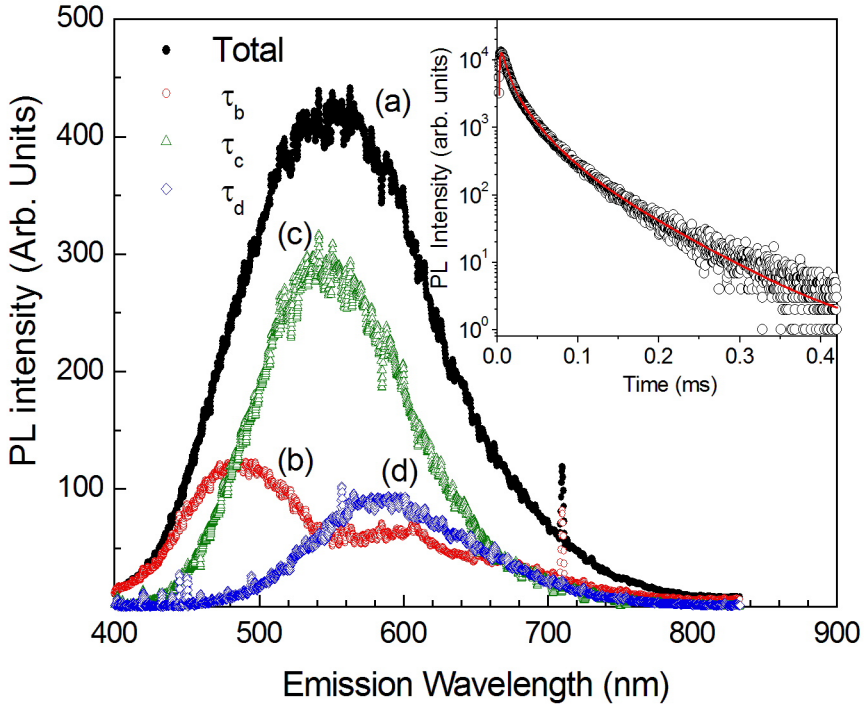

Figure 3.17: a) PL spectrum of sample Ag05 upon pulsed excitation at 355 nm; b), c), d) decomposition of spectrum a) in components with different decay time. Inset: Decay curve collected at 455 nm.

resonant with the $^4I_{15/2} \rightarrow {}^2H_{11/2}$. For the other excitations, not resonant with erbium transitions, a dip in the broad band appears always at 520 nm. This dip is attributed to reabsorption by the Er ions of the luminescence from silver aggregates.

Time resolved spectroscopy upon 355nm pulsed excitation shows that different centers contribute to the broad band luminescence. Figure 3.17 shows an attempt to separate three contributions with lifetimes in the ranges of about 10 μs, 50 μs and higher than 100 μs. The procedure used to obtain figure 3.17 is described in the following. The decay curve of the luminescence has been measured at different wavelengths. The inset shows the curve of decay taken at 455 nm, together with a fit by three exponentials, whose parameters are reported in Table 3.4. The three decay times needed for the best fit

Table 3.4: Lifetimes (μs) of the bands (see figure 3.17) which constitute the visible luminescence of the silver species, collected upon 355 nm pulsed excitation

Sample	τ_b	τ_c	τ_d	rise $\tau(b,d)$	rise $\tau(c)$
Ag05	10	50	100	1	6
Ag15	5	30	80	1	4
Ag50	3	10	50	1	2

slightly change with the detection frequency, but remain in ranges around the values of Table 3.4. Delayed spectra in different time windows were measured and the integrated luminescence was attributed to three contributions with the decay times of Table 3.4. The result has to be taken as purely indicative, since it is evident that a continuous distribution of lifetimes is actually present and the shapes of the bands depend on the choice of the three characteristic lifetimes.

In any case, the shape of the band (3.17(d)) with the longer decay-time is similar to that observed in ref. [24, 31] and attributed to small Ag^0 clusters. A band in the blue, similar in form of the blue component of figure 3.17(b) with fast decay time, was attributed to Ag_3^{2+} species [32]. Other centers with silver ions bound to silver atoms in dimers or trimers are expected to be present and they could explain the presence of the low frequency band of figure 3.17(b) and of the band of figure 3.17(c) [24]. In particular, Paje *et al.* [33] evidenced that in soda lime glasses Ag^+-Ag^+ dimers have a broad luminescence centered at about 525 nm, i.e. practically coinciding with band 3.17(c), while mixed species of Ag^0 and Ag^+ in dimers or trimers should emit at longer wavelength.

By increasing the silver content, in Ag15 and Ag50 samples, the fast decay components become stronger in comparison with the others and all lifetimes become shorter. On the contrary, the shapes of the bands of figure 3.16 do not change very much. These results could indicate that energy transfer between different active centers is present and becomes more and more important with the increasing of the silver content. This hypothesis is supported also by the behavior of the rise time of the luminescence, which is different at

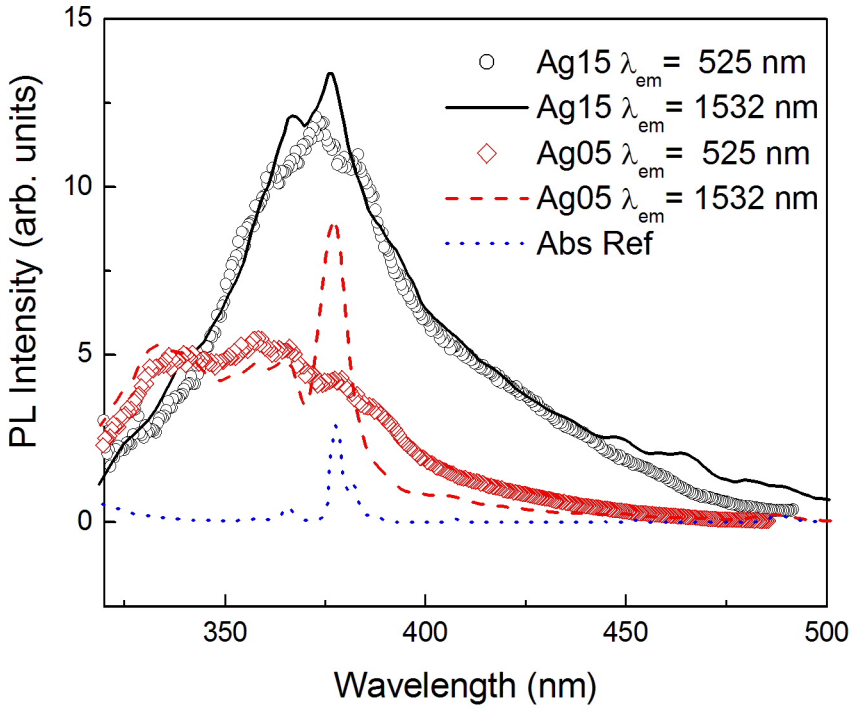

Figure 3.18: Comparison of the excitation spectra of sample Ag05 and Ag15 collected at 525 nm (Ag species luminescence) and 1532 nm (erbium luminescence). The absorption spectrum of sample Ref is reported to locate the absorption lines of erbium

different wavelengths (1 μs at 445 nm and 625 nm, 6 μs at 555 nm for Ag05). This seems to indicate that at 355 nm we do not excite directly the emitting centers and that different channels are active in the excitation of the other centers. Furthermore, the rise-time of the emission at 555 nm is close to the fast decay time of the luminescence at 445 nm. This could indicate that centers that produce luminescence at 445 nm also can transfer the excitation to other centers that have luminescence at 555 nm. In polarized measurements, the visible luminescence band of the Ag05 sample, shows a ratio of intensity I_{VH}/I_{VV} $\sim 1/3$. This low value is distinctive of centers with an oriented dipole, which can absorb and emit light only polarized along the axis [34]. This property is typical of dimers [35], but other small clusters with a preferential axis cannot be excluded.

Figure 3.18 shows the excitation spectra of the Ag05 and Ag15 samples collected at

515 nm from the broad luminescence band of the silver centers. (Compare figure 3.16 and note that, as there are several emitting center, the excitation spectra from the silver aggregates acquired at different wavelengths may substantially differ). At this frequency we are sure that there is no luminescence from excited states of Er^{3+} ions. The shapes of the excitation bands of figure 3.18 are practically coincident with those of the broad band contribution observed in the excitation spectra of the Er^{3+} luminescence, detected at 1.5 μm. This result indicates that the channel through which the erbium ions are excited is the silver aggregates that emits at about 515 nm. The sharp lines of the Er^{3+} absorption do not appear in the excitation spectra of the silver aggregate, indicating that energy transfer from Er to silver is negligible. Therefore, the transfer appears to be unidirectional from silver to erbium.

3.5 Discussion

The luminescence and excitation spectra indicate that silver aggregates, showing absorption in the blue and a green luminescence, can transfer the excitation to erbium ions. The energy transfer mechanism is still to be discussed. The transfer probability is proportional to the superposition integral of the two spectral shapes of the cross-sections in the emission of donors (Ag aggregates) and in the absorption of acceptors (Er^{3+} ions)[36, 37]:

$$P^{Ag-Er} = C \int \sigma(\nu)^{Er}_{Abs}\, \sigma(\nu)^{Ag}_{Em}\, d\nu \tag{3.1}$$

Equation 3.1 describes both the radiative and non-radiative resonant energy transfer, i.e. with the exchange of real or virtual photons. In the latter case, C is a constant which measures the strength of the coupling and depends on the physical mechanism, as dipole-dipole, dipole-quadrapole, exchange coupling, and on the actual space distributions of donors and acceptors. Phonon assisted energy transfer processes are expected to be less probable. As the erbium absorption spectrum has a very intense transition, the

hypersensitive $^4I_{15/2} \rightarrow {}^2H_{11/2}$ transition centered at about 520 nm, which contribute to about 90 % of the whole visible absorption, P^{Ag-Er} is practically proportional to $\sigma(\nu)^{Er}_{Abs}$ evaluated at the frequency transition. Equation 3.1 can also explain why the transfer from erbium to silver is inhibited: there is no strong absorption of silver aggregates at the wavelengths at which the erbium emits.

In a phosphate glass, we observed that the radiative transfer, i.e reabsorption, dominates on the very weak non-radiative transfer. In fact, energy transfer was observed only in thick samples [13, 38], where reabsorption can be more effective. In silicate, on the contrary, energy transfer was observed not only in our 200 μm plates, but also in thin films [12, 15]. The radiative mechanism of transfer from silver to erbium is for sure active, as it is testified by the dip in the luminescence spectrum of figure 3.16, in correspondence with the $^2H_{11/2} \rightarrow {}^4I_{15/2}$ transition. However, the radiative mechanism is not very effective, given the poor erbium cross section, and probably it is dominant only in phosphate glasses[38], where the glass structure allows a very effective separation of the active centers [39], with small non radiative transfer rate. On the contrary the structure of silicate, which allows tighter packing of the erbium and silver ions, should favor the non radiative energy transfer.

Our spectroscopic study shows that several emitting centers coexist and can absorb the visible light and transfer the excitation to erbium ions. However, since the erbium ions can efficiently accept excitation only in a narrow range around 520 nm, only the centers that emit at this wavelength can efficiently transfer their excitation to erbium. In particular, according to the spectrum in figure 3.17, the centers with the strongest emission in this region are the silver dimers, which are therefore expected to be the favored channel for the erbium excitation. On the other hand, the transfer to erbium may involve also levels other than the $^2H_{11/2}$, even if less effectively. This may explain the shape of the excitation band of erbium, which is a weighted sum of different absorption bands of silver aggregates.

Looking only at the IR excitation spectra, it appears that, as often stated, the introduction of silver has beneficial effects on the erbium luminescence, which in the silver doped samples is always higher than in the non doped sample with an enhancement factor ranging between 1 and over 100, in the regions where the erbium does not absorb. However it seems more meaningful to consider what is the actual efficiency of the pumping mediated by silver. A rough estimation may be obtained comparing the absorption and IR excitation spectra. From the ratio between the continuous background and the erbium absorption peak, in the excitation spectrum of sample Ag15, we see in figure 3.15 that, by pumping at 520 nm, the erbium luminescence due to transfer from Ag specie is about 1/2 of that due to direct erbium excitation. At the same wavelength, 520 nm, the absorption of silver is about two times that of erbium. Therefore, about 1/4 of the silver species transfers the excitation to erbium. This transfer efficiency slight increases by lowering the excitation wavelength and it reaches a maximum of about 50% at 370 nm because the silver centers that absorb at this wavelength have the maximum of $\sigma(\nu)^{Ag}_{Em}$ at 520 nm in correspondence with the maximum of $\sigma(\nu)^{Er}_{Abs}$. Similar results are obtained for Ag05, the transfer efficiency being slightly smaller. Note that the donors lifetime $(10 - 100\mu\text{s})$ is quite larger than that of acceptors ($\sim 1\mu$s [40]) in the level $^2\text{H}_{11/2}$. This forbids detrimental back transfer effects.

3.6 Summary and Conclusions

Erbium-doped soda-lime-silicate and phosphate thin plates were co-doped with Ag by using silver-sodium ion-exchange and later submitted to various heat treatments in air. After two annealing processes of 30 min each at 500C, the Ag-exchanged silicate glass exhibited a shoulder in its absorption spectrum, between 400 and 500 nm. A stronger absorption band centered in the blue region was observed after the heat treatment was performed at higher temperature (600C). An enhancement of the 1.53 μm luminescence

in the annealed Ag-exchanged silicate glasses was observed.

TEM analysis shows that thermal treatments induce Ag atoms to condense into nanoparticles. The size of the nanoparticles depends on the annealing parameters.

XP spectra show that the Ag atoms inserted in the glassy network by ion exchange are in a non-oxidized form. Shifts seen in the BE in the XP spectra of the Ag 3d can be correlated with the Ag cluster dimensions, i.e. the strength of the thermal treatments. The longer the annealing, the higher the cluster size and the lower the BE shift.

By the light of the results presented above, it seems significant to re-discuss the results [8, 10] which led to attribute the Eu luminescence enhancement to silver nanoparticles, in order to evaluate if our explanation, which does not consider the influence of the plasmon band, may apply also there.

In the work of Malta et al.[8], we notice that the differential absorption spectrum shows a peak at 320 nm that is due not only to silver colloids (it should be centered at longer wavelength) but also to ions or multimers that are known absorbing at these wavelengths and whose influence cannot therefore be excluded. Also in the works of Hayakawa, Selvan and Nogami [10, 11] the luminescence enhancement could be related to the presence of these small silver clusters. In fact, for short delay times they find a broad visible luminescence, which moreover presents dips in correspondence of the europium absorption bands [11]. Additionally, they do not find the decrease of the europium decay time that should be connected with the increase of the oscillation strength of the transition, and this suggests that the PL intensity increase is due to a greater efficiency of the pumping.

The works of Strohhofer, Portales and Mazzoldi all agreed that the main mechanisms of the RE excitation had to be energy transfer, even if the donors nature was not determined exactly. However, in [12, 15] the sensitizing effect of the silver appears stronger and for excitation at lower wavelengths with respect to [13]. Two reasons may be given for this: the first one resides in the different format, planar waveguides and bulk, of the

samples. As a matter of fact, when lowering the excitation wavelength toward the Urbach edge, the absorption coefficient increases and, in bulk systems, only the first layer is excited, reducing the final excitation of the erbium. On the contrary, the extinction of the exciting beam is very weak in films and the spatial distribution of excitation does not depend on the wavelength. Moreover in bulk system, especially if prepared by melt-quenching technique, the silver content cannot be as high as in films. The second reason regards the solubility of the RE and silver in the various hosts. The capability to have a good separation between the active dopant ions, which makes phosphate glasses preferred to silicon oxide or borosilicate as matrix for highly doped devices [41], makes them unfit to promote the closeness between lanthanide ions and silver luminescent centers that is required to have an effective energy transfer. From this point of view, soda lime glasses appear to have intermediate properties.

We can conclude that in our case the enhancement of the erbium luminescence is not due to an increase in the absorption or in the emission cross section, but to an electric dipole induced energy transfer.

In particular, the enhancement of the erbium luminescence in a silver doped glass is due to a energy transfer process from silver species, especially dimers. The mechanism of transfer operates in the visible through the excitation of the high energy levels of the erbium. The infrared erbium luminescence upon visible excitation increases because of the high absorption cross section of the silver species which moreover may transfer the excitation with an efficiency up to 50%. Hosts where the doping ions are easily segregated allow to have stronger coupling between silver species and rare earths with increased non-radiative transfer efficiency.

Bibliography

[1] V. M. Shalaev, Nonlinear Optics of Random Media: Fractal Composites and Metal-Dielectric Films, Springer, Berlin Heidelberg, (2000).

[2] U. Kreibig and M. Vollmer, Optical Properties of Metal Clusters, Springer, Berlin Heidelberg, 1995.

[3] F. Gonella and P. Mazzoldi, Metal Nanocluster Composite Glasses, Handbook of Nanostructured Materialsand Nanotechnology, H. S. Nalwa, **4**, 81-158, Academic Press, San Diego, (2000).

[4] W.L. Barnes, J. Mod. Opt. **45**, 661 (1998).

[5] B. Di Bartolo, Optical interactions in solids, John Wiley and Sons, New York (1968).

[6] E. Yablonovitch, Phys. Rev. Lett. **58**, 2059 (1987).

[7] R. M. Amos and W. L. Barnes, Phys. Rev. B **55**, 7249 (1997).

[8] O.L. Malta , P.A. Santa-Cruz , G.F. De Sa, and F. Auzel J. Lumin. **33**, 261 (1985).

[9] M. Moskovits, Rev. Mod. Phys. **57**, 783 (1985).

[10] T. Hayakawa, S.T. Selvan, and M. Nogami, Appl. Phys. Lett. **74**, 1513 (1999)

[11] S.T. Selvan, T. Hayakawa, and M. Nogami, J. Phys. Chem. B **103**, 7064 (1999).

[12] C. Strohhofer and A. Polman, Appl. Phys. Lett. **81**, 1414 (2002).

[13] H. Portales, M. Mattarelli, M. Montagna, A. Chiasera, M. Ferrari, A. Martucci, P. Mazzoldi, S. Pelli, and G.C. Righini, J. Non-Cryst. Solids **351**, 1738 (2005).

[14] A. Chiasera, M. Ferrari, M. Mattarelli, M. Montagna, S. Pelli, H. Portales, J. Zheng, and G.C. Righini, Opt. Mater. **27**, 1743 (2005).

[15] P. Mazzoldi, S. Padovani, F. Enrichi, G. Mattei, C. Sada, E. Trave, M. Guglielmi, A. Martucci, G. Battaglin, E. Cattaruzza, F. Gonella, and C. Maurizio, Proceedings of SPIE **5451**, 311 (2004).

[16] S. Pelli, M. Bettinelli, M. Brenci, R. Calzolai, A. Chiasera, M. Ferrari, G. Nunzi Conti, A. Speghini, L. Zampedri, J. Zheng, and G. C. Righini, J.Non-Cryst. Solids, **345& 346**, 372-376, (2004).

[17] A. Chiasera, M. Ferrari, L. Zampedri, M. Mattarelli, M. Montagna, H. Portales, C. Tosello, S. Dir, S. Pelli, and G.C. Righini, SPIE **5451**, 574-584, (2004).

[18] NIST Chemistry Web Book, WEB Edition, http://webbook.nist.gov/

[19] Tomokatsu H, Selvan S T and Nogami M Appl. Phys. Lett., **74**, 1513(1999).

[20] G. Speranza , S.N. Bhaktha, A. Chiappini, A. Chiasera, M. Ferrari, C. Goyes, Y. Jestin, M. Mattarelli, L. Minati, M. Montagna, G. Nunzi Conti, S. Pelli, G.C. Righini, C. Tosello, and K.C. Vishunubhatla, J. Opt. A: Pure Appl. Opt. **8**, S450 (2006).

[21] Doniach S and Sunjic M, J. Phys. C: Solid State Phys. **3**, 285(1970).

[22] Wertheim G K and DiCenzo S B, Phys. Rev. B, **37** 844(1988).

[23] Wertheim G K, DiCenzo S B and Buchanan D N E, Phys. Rev. B, **33**, 5384 (1986).

[24] M. A. Villegas, J. M. Fernández Navarro, S. E. Paje, and J. Llopis, Phys. Chem. Glasses **37**, 248 (1996).

[25] P.E. Hart, M.G. Mesko, J.E. Shelby, J. Non-Cryst. Solids, **263& 264**, 305(2000).

[26] I. Belharouak, H. Aouad, M. Mesnaoui, M. Maazaz, C. Parent, B. Tanguy, P. Gravereau, and G. Le Flem J. Sol. State Chem. **145**, 97 (1999).

[27] E. Borsella, E. Cattaruzza, G. De Marchi, F. Gonella, G. Mattei, P. Mazzoldi, A. Quaranta, G. Battaglin, R. Polloni, J. Non-Cryst. Solids, **245**, 122(1999) .

[28] S. Jiang, T. Luo, B. Hwang, F. Smekatala, K. Seneschal, J. Lucas, N. Peyghambarian, J. Non-Cryst. Solids, **263& 264**, 364(2000).

[29] R.K. Brow, J. Non-Cryst. Solids, **263& 264**, 1(2000) .

[30] A.A. Ahmed, E.W. Abd Allah, J. Am. Ceram. Soc. **78**, 2777 (1995).

[31] P. Gangopadhyay, R. Kesavamoorthy, Santanu Bera, P. Magudapathy, K. G. M. Nair, B. K. Panigrahi, and S. V. Narasimhan, Phys. Rev. Lett. **94**, 047403 (2005).

[32] E. Borsella , F. Gonella , P. Mazzoldi , A. Quaranta , G. Battaglin , and R. Polloni, Chem. Phys. Lett. **284**, 429 (1998).

[33] S. E. Paje , M. A. Garcia, J. Llopis, and M. A. Villegas, JJ. Non-Cryst. Solids **318**, 239 (2003).

[34] P. Wahl in Biochemical fluorescence, ed. by R.F. Chen and H. Edelhoch, Marcel Dekker, Inc New York (1975).

[35] P. Boutinaud and H. Bill, J. Phys. Chem. Sol. **57**, 55 (1996).

[36] F. Auzel in Radiationless Processes, ed. by B. Di Bartolo, Plenum Press, New York (1980).

[37] M. Mattarelli, M. Montagna, L. Zampedri, A. Chiasera, M. Ferrari, G. C. Righini, L. M. Fortes, M. C. Goncalves, L. F. Santos, and R. M. Almeida, Europhys. Lett. **71** , 394 (2005).

[38] M.Mattarelli, M.Montagna, E. Moser, K.C. Vishnubhatla, C. Armellini, A.Chiasera, M.Ferrari, G.Speranza, M. Brenci, G. Nunzi Conti, and G.C. Righini., J. Non-Cryst. Solids, **353**, 498501, (2007).

[39] M. Karabulut, G. K. Marasinghe, E. Metwalli, A. K. Wittenauer, R. K. Brow, C. H. Booth and D. K. Shuh, Phys. Rev. B **65**, 104206 (2002).

[40] E. Desurvire, Erbium-Doped Fiber Amplifiers, Principles and Applications, John Wiley, New York (1994).

[41] C. Jiang, W. Hu, and Q. Zeng, IEEE Phot. Tech. Lett **16**, 774 (2004).

Chapter 4

Micro-Machining of structures and waveguides in glasses by Femto-second Laser Direct Writing

INTRODUCTION

Micro-optics enable the collection, guidance, or modification of light, in a way to shape and influence light with very small structures and Integrated-optics integrates these micro-optic elements and other electronic, opto-electronic components onto a small chip for device oriented applications. In line with the trend towards miniaturization and the need to reduce costs, traditional optical elements are being replaced by smaller and lower-cost components. Diffractive and refractive micro-optical elements complement and often exceed the functionality and performance of traditional lenses, prisms and mirrors. Refractive micro-optics makes conventional optical elements like lenses or prisms smaller. Most of the micro-optical elements are fabricated by the standard UV-Lithography. Laser Direct Writing (LDW) technique with its ability to create the micro/nano structures in 3D, is a fast growing field and is proving to be a good contender to standard lithography based methods in 3D laser micro/nano machining technologies [1]. The ability to pattern

(process, deposit, dispense, or remove) materials in three dimensions in a pre-determined manner is attractive for several important application in and microfluidics[2, 3]. Direct writing using ultra-short pulses offers novel prospects for miniaturization and integration of highly functional photonic and microfluidic devices directly inside transparent dielectric materials([4]- [60]). In contrast to standard manufacturing methods such as physical-vapor deposition or ion exchange, the direct write approach is not restricted to the surface and can yield truly three-dimensional (3-D) structures. Femtosecond (fs) pulses possess the unique ability to precisely deposit energy inside the material. This ultrafast interaction does not require specially prepared or photosensitive materials and has the capability of realizing 3-D photonic structures in diverse materials at arbitrary depth inside the bulk substrate. There are two major procedures of modifying the material with femtosecond pulses. In the first case the material is removed after irradiating with short laser pulses (surface ablation or irradiation followed by selective chemical etching) and in the second case the physical properties and hence the refractive index (RI) of the material are modified by the laser pulses. In the latter case, nonlinear absorption arising from high peak intensities induce strong refractive-index changes in sub-micron volumes that permit the generation of two/three dimensional refractive index modified (either positive or negative change) structures with the help of computer controlled motorized translation stages. The structural modification leads to the formation of waveguides in the case of positive index change and devices (e.g. optical memory) in case of negative index change.

Several devices reported till date using this technique and its variations include: (a) Optical storage devices (b) 3-D Waveguides (c) Splitters, Couplers (d) Waveguide amplifiers (e) Gratings including FBGs (f) Micro-optical components (lenses, fibers etc.) (g) Waveguide lasers (h) Microfluidic and Lab-on-a-chip devices (i) Photonic crystals (j) planar light wave circuits and (k) nanostructures([8]-[19]). Several materials have been investigated for their interaction of femtosecond pulses, leading to exceptional applications,

such as:(a) Waveguides in laser crystals such as Ti:Sapphire, Nd:YAG ceramics ([20]-[23]) (b) Variety of microfluidic structures in Foturan^{TM} leading to lab-on-a-chip devices([24]) (c) Polymeric photonic structures in PMMA (Poly Methylmethacrylate)([25], [26]) (d) Waveguides in periodically poled lithium niobate (PPLN)([27]- [29]) (e) Waveguide lasers in the telecom band ([11], [12]) (f) Micro and nano channels in variety of materials ([30], [31]) (g) Photonic crystal structures in glasses and polymers etc. ([32], [19]) The quality of structures fabricated in dielectrics depends on parameters like wavelength and repetition rate of the femtosecond source, focal conditions, pulse duration, pulse energy, and sample translation speed. The mechanism by which the refractive index is modified with femtosecond pulses is not completely understood. The commonly accepted explanation is of energy deposition into the matrix via non-linear or multi-photon absorption leading to restructuring of the material. It has also been proposed that densification results when the molten material re-solidifies. Some of the possible mechanisms responsible for refractive index changes resulting from femtosecond pulse interaction with glasses include (a) Densification (compaction) through bond breaking (b) Color center formation which alters refractive index (c) Thermal melting followed by re-solidification leading to higher index core required for waveguiding. Streltsov et al. have critically interpreted the above reasons and suggested that a combination of these effects could be present, depending on exposure conditions of the ultrafast laser. Three important regimes have been identified by Hnatovsky et al. [39, 48] in their recent work: (a) Type I damage: Homogenous modification associated with smooth RI change (b) sub-wavelength nano-gratings produced with linearly polarized laser and disordered nanostructures with circularly polarized laser and (c) Disruptive modification (e.g. voids, micro-explosions). The mechanism of ultrashort-pulse modification of transparent materials can be divided into several steps: (1) Production of initial seed electrons through non-linear photoionization of free electrons or excitation of impurity defects, (2) avalanche photoionization, (3) plasma formation, and (4) energy transfer from the plasma to the lattice[33, 58]

The results of the direct writing of microstructures in fused silica, GE124, zinc-tellurite, Foturan and Baccarat glasses are presented in this chapter.

4.1 Experimental:

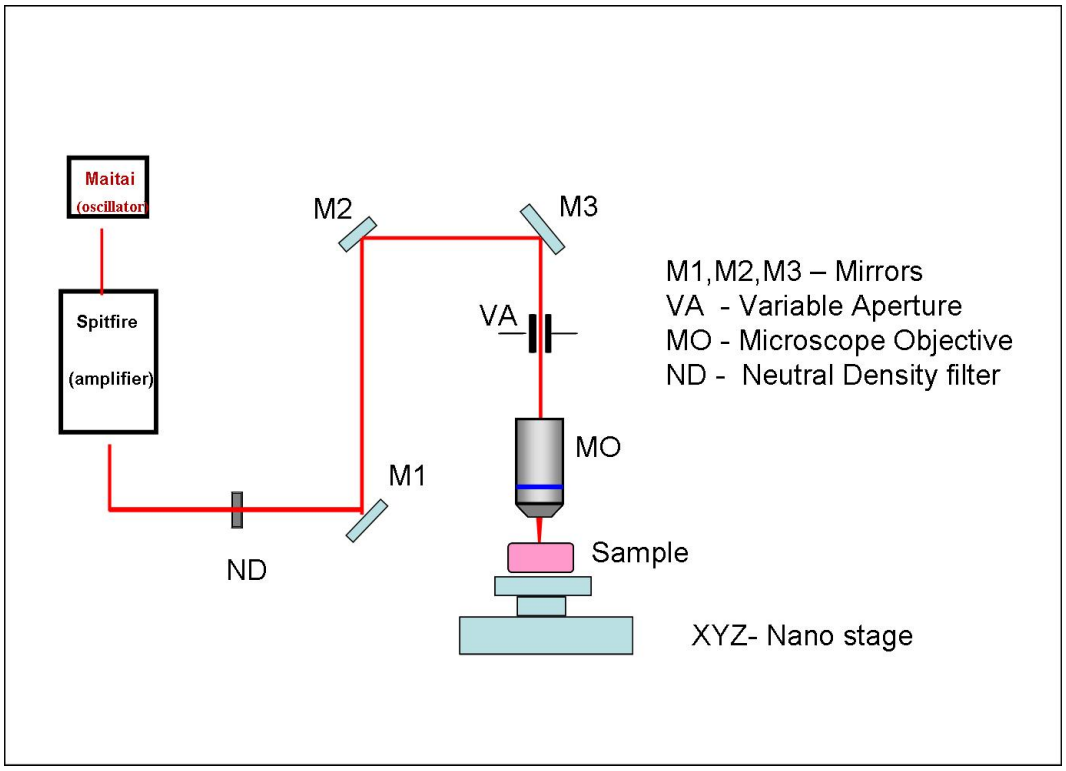

Figure 4.1: Schematic diagram of the experimental set-up for Laser Directed writing

Sample preparation: All the samples were typically cut to a dimension of 1cm X 2 cm for ease of use and all the 6 faces are optically polished. Sample were first cleaned using acetone and then with methanol to ensure that the surfaces are devoid of any stains and dust. The cleaned samples were placed on computer controlled XYZ nano-stages for better control over the structures to be written in them. Figure 4.1 shows the schematic of the experimental setup. The quality of the structures fabricated depends critically on the quality of the focused spot and the movement of the sample placed on XYZ stage.

Any aberration in the optics or un-wanted vibrations of the stage will affect the shape and size of the structures drastically. Typically 100 femtosecond amplified pulses were employed for direct writing at a wavelength of 800 nm with 1 KHz repetition rate. A spatial filter (pin hole) was used to produce a high spatial quality input beam which was then attenuated appropriately using neutral density filters for further use. The beam was steered such that it focuses downwards on to the sample after focussing with a microscope objective (typically 40X, 0.65 NA).

Inscription of grating: The procedure followed for inscribing grating is given below. A)Initially simple straight lines were inscribed into samples. Each line corresponds to a specific set of parameters (like the sample translation speed, intensity of the laser, and size of the aperture before the microscope objective). B) These structures were then imaged using Leica Scanning confocal Microscope. Images were obtained both in transmission mode and reflection mode. The imaging essentially takes advantage of differences in transmission and reflection properties of the samples in the regions exposed to the femto-second laser and the un-exposed regions. In the transmission mode the width of the structures is determined. In the reflection mode several snapshot of the structures are taken along the depth at definite intervals (typically the step size along the z is chosen to be around a micron). Each snapshot corresponds to a particular depth, all these snapshots are collated to obtain a 3-D (cross-sectional, depth profile) view of the structures written.

The lines/structure with desired width and depth profile were identified and with the corresponding writing parameters the structures/lines were written again and the images compared to ensure the repeatability (within the error limits). As an example in figure 4.2 shows the micro-line structures inscribed in Baccarat glass the line labeled as B2 was chosen and the parameters were used for inscribing a grating in the glass.

For further characterization of the lines/structures, micro-Raman microscopy, Ab-

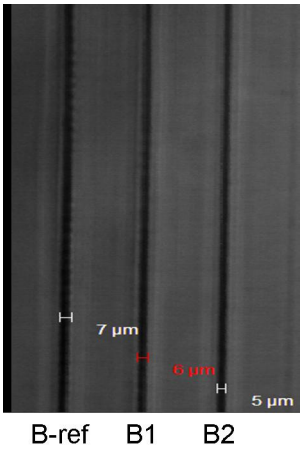

Figure 4.2: Confocal Microscope image of the micro-lines inscribed in Baccarat glass

sorption (Visible- NIR) spectroscopy and confocal Fluorescence spectroscopy were used for understanding of the basic process behind the LDW.

4.2 Results and discussion

4.2.1 Fused Silica:

Several research papers have been published on the nature of femtosecond interaction with fused silica leading to waveguiding properties, irradiation followed by chemical etching for microchannel/microfluidic applications([31]-[66]). Even though fused silica is a single-component glass, its properties can differ slightly depending on its thermal history and trace levels of impurities, and hence the parameters for LDW also are sample specific[67]. Here we have investigated two kinds of samples commercially available fused silica (purchased from Heraeus Ltd.,henceforth will be referred as fused silica) and GE124 (also a kind of fused silica) As mentioned earlier the aspect ratio of the structures can be varied by modifying the parameters like the intensity of the incident fsec laser, figure 4.3 shows the cross-sectional depth profile image of the structure for(a)110 μW, (b). 40 μW pulse energy. The aspect ratio can also be controlled easily varied by varying the input

aperture diameter before the microscope objective.

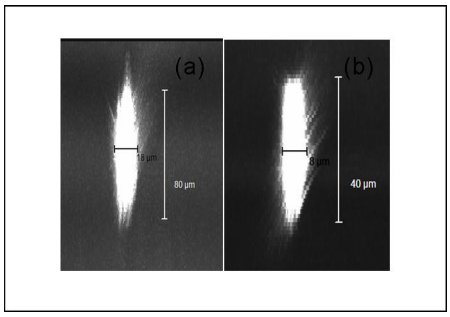

Figure 4.3: Confocal Microscope depth (cross-section) profile image of the structures

Inscription of gratings:

With the required parameters a micro-line was inscribed by focussing fsec laser pulses through the microscope objective (40 X, 0.65 NA, Olympus India). The sample was displaced perpendicularly to the written line by a definite distance and then another line (in parallel to the first line) was inscribed. In this way a set of 125 parallel lines were inscribed creating periodic alternating regions exposed and un-exposed to fsec laser irradiation. These set of lines act as grating. These grating-structures were inscribed in the glasses with the aim of obtaining an estimate of the change in refractive index induced by the fsec laser irradiation, from the grating efficiency measurements. Figure 4.4 shows the gratings inscribed in the fused silica (a) and GE124 (b) glasses. The inset shows the images of internal diffraction. A He-Ne laser (632nm) beam was incident perpendicular to the plane of the gratings, the internal diffraction images were recorded on a screen placed 10 cm away from the sample. The intensities of the different laser spots corresponding to the different orders of diffraction were measured using a Ophir power meter. The grating diffraction efficiency (η is the ratio of first order intensity to the zeroth order intensity) was calculated to be 20.3%. The change in the refractive index (Δn) is estimated to be

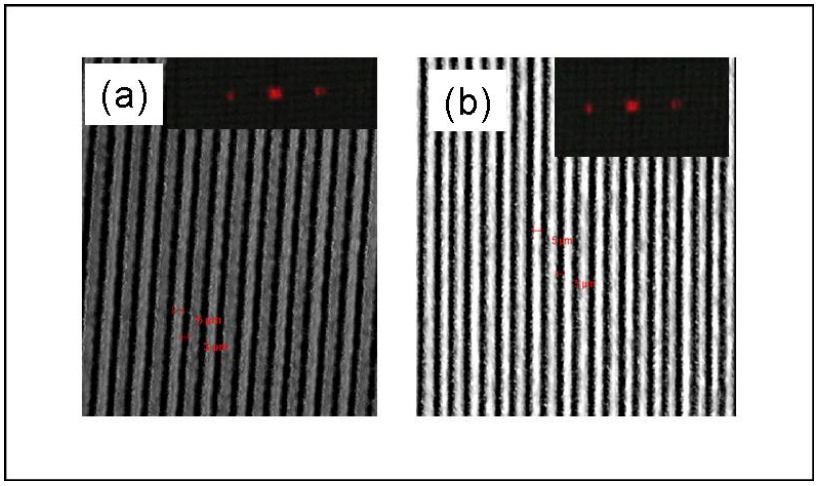

Figure 4.4: Confocal -Microscope images of gratings (a)fused silica (b)GE124 glasses;the inset shows the corresponding internal diffraction images

of the order of 10^{-3} using the equation 4.1.[68]

$$\Delta n = \lambda \; cos\theta \; tanh^{-1}(\sqrt{\eta})/ \; \pi \; d \tag{4.1}$$

Where η is the diffraction efficiency fraction of first order to the zeroth order, λ here is 632nm, θ = 90 degrees, d is the depth or the grating thickness. The Δn values of the gratings are listed in the table 4.1 The 2 D micro gratings (4.5 (a)) were realized by two sets of parallel lines written inside the bulk fused silica making an angle of 90 ^{o} with respect to each other. The 4.5 were realised by three sets of parallel lines inscribed making an angle of 60 ^{o} with respect to each other, (b)shows the formation of a star like structure having a central hexagon surrounded by small triangular structures, (c)shows the regular hexagon divided into six triangular structures. This is to demonstrate the ability of this process to create any structure, potentially leading to the fabrication of 2D-photonics crystals by LDW. This can be extended to 3d with effective control of the dimension of the structures by laser beam shaping. As expected the diffraction patterns (see the inset) are correspond to the structures written, the 2-d square grating show a

diffraction pattern having a square symmetry where as the other two structures display a hexagonal symmetry.

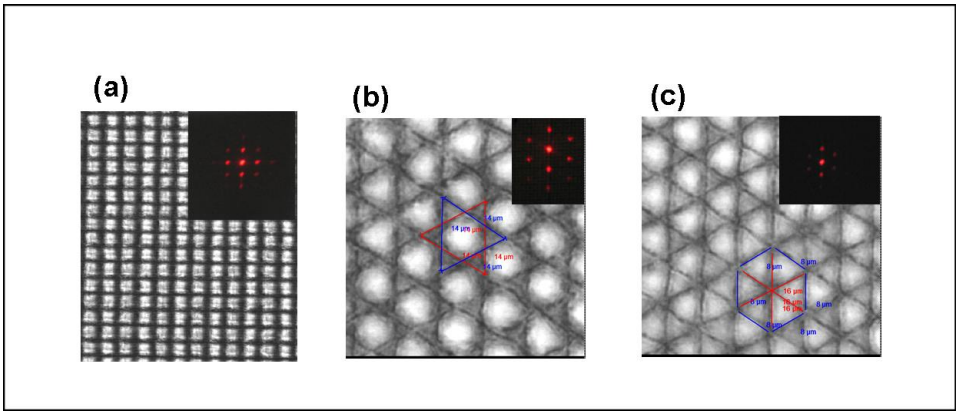

Figure 4.5: Confocal -Microscope images of 2-D gratings in fused silica, the insets show the corresponding diffraction patterns

Spectroscopic characterisation of the micro-structures:

To be able to obtain Absorption spectra in visible and NIR regions a set of 100 parallel lines are written in the samples, the spectra are obtained from the written region and un-irradiated regions. The spectra of the FS (4.6(a), (c)) and GE124 (4.6 (b), (d)) are similar, the increase in absorbance from the written region can be attributed to absorption due to the defects created during the process of LDW and also due to scattering losses (which also includes the losses due to diffraction from the grating).

To analyze the interaction of femtosecond pulses with fused silica glass network we performed micro-Raman measurements in the femtosecond laser-irradiated and non-irradiated regions of the sample. The samples were excited with 514 nm and figure shows the micro-Raman spectra obtained in two regions of the samples studied. Black curve represents the spectrum obtained from the region unexposed to fsec, red colored curve for region irradiated with fsec laser. The fused silica structural network typically

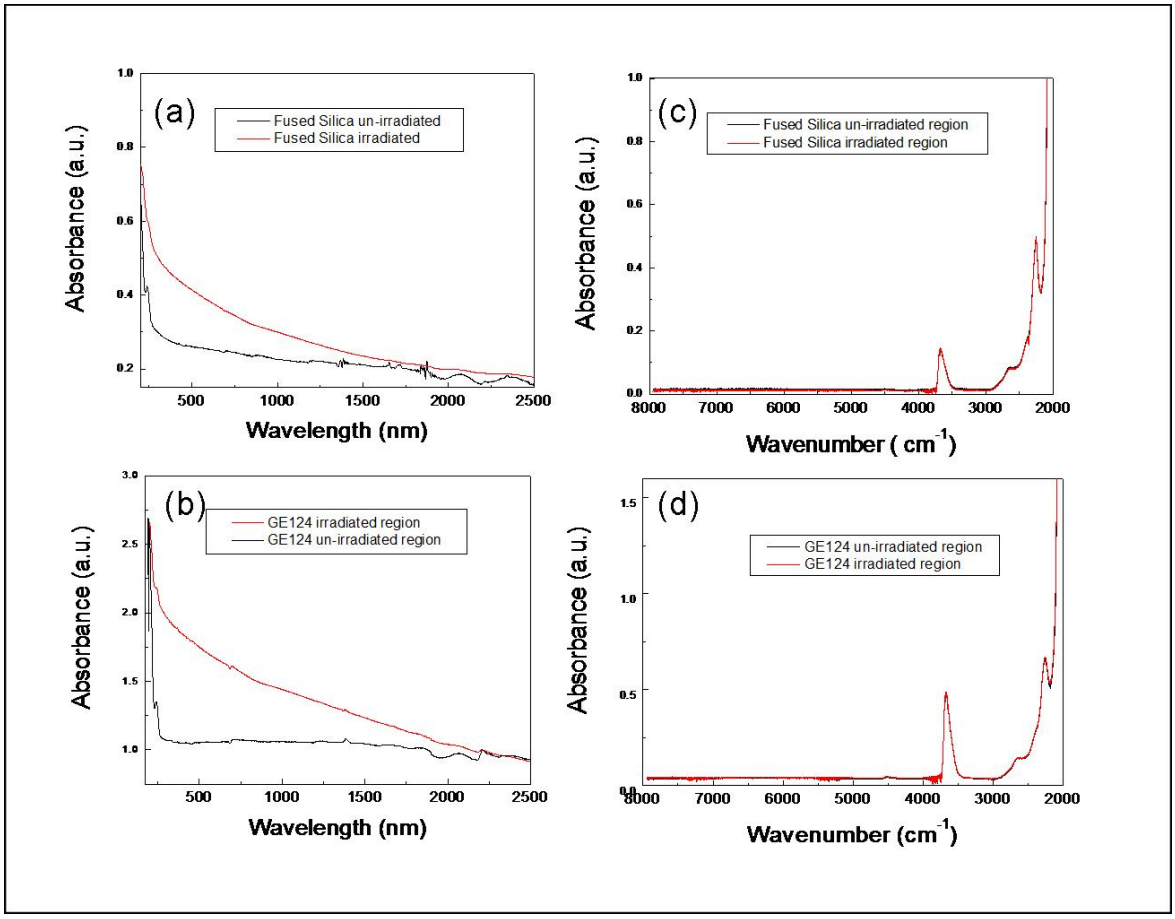

Figure 4.6: Absorbance spectra of fused silica [(a), (c)] and GE124 glass [(b), (d)] from the modified and un-modified region of the samples

has predominantly large 5- and 6-fold ring structures. The increase in the intensity of the peak at 600 cm^{-}1 is ascribed to the change in ring statistics where six-fold rings transform to threefold and fourfold rings after laser irradiation. An increase in the number of smaller 3- and 4-fold ring structures leads to a decrease in the overall bond angle and a densification of the glass. Earlier reports [40, 42, 59] also suggest that the possible mechanism of waveguiding in fused silica glass to be breakage of bonds in the network leading to densification and hence increase in refractive index in that region.

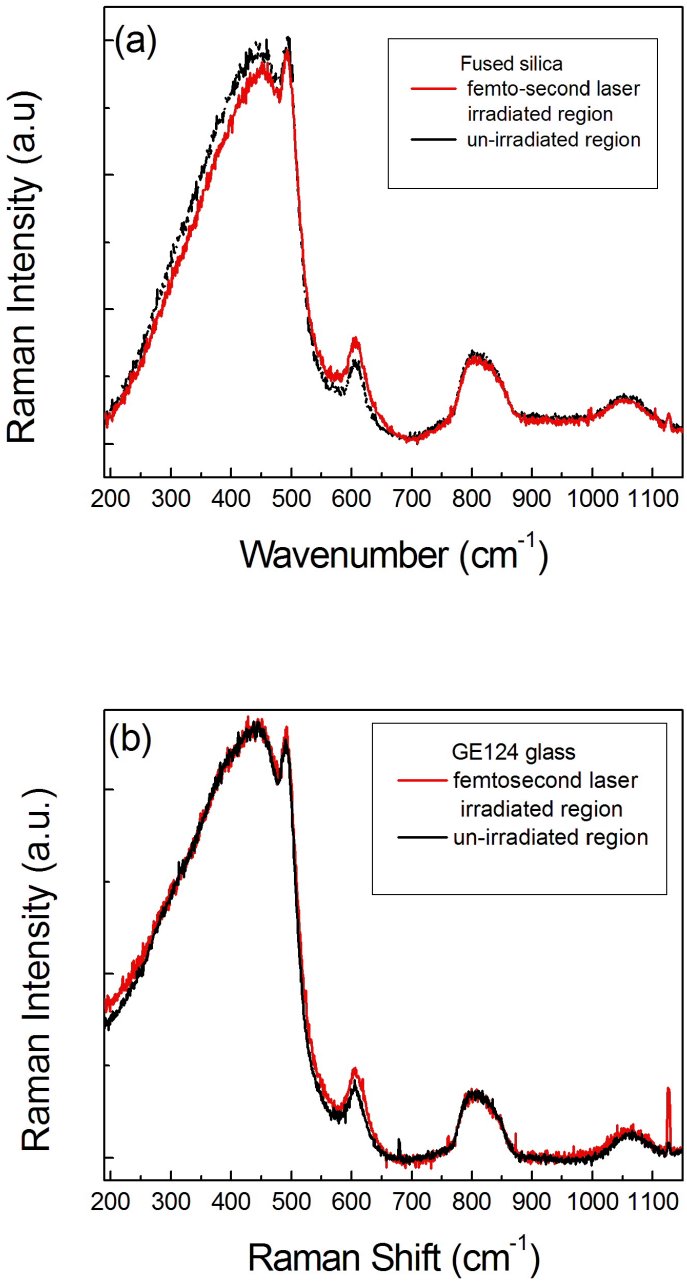

Figure 4.7: Raman Spectra of (a) Fused silica (b) GE124 samples

4.2.2 Zinc-Tellurite:

Tellurite glasses have high refractive index compared to silicate glasses. This induces the increase of local field around the rare earth ion causing the enhancement of the radiative transitions and a wider splitting of Stark sublevels. Consequently greater efficiency and broadening of the emission shape is observed. These properties prove to be valuable for WDM applications. The article by Tokuda et.al. [69] reports longitudinal writing of relatively short waveguides and positive refractive index change in niobium tellurite glasses. The work of Nandi et.al. has demonstrated the waveguiding in Er doped tellurite glasses co-doped with phosphate [70]. In contrast negative refractive index change has been reported making waveguiding impossible [71] In this section we concentrate on grating fabrication in zinc-tellurite glass ZT0 (the optical spectroscopic properties of the same were discussed in chapter2). The bandgap of tellurite based glasses being low as compared to silicate based glasses, the incident laser intensity required would be less as compared to silicate glasses which is evident from the table 4.1 , only a third of the pulse energy was used to inscribe structures. Micro gratings were inscribed in these tellurite glasses and the diffraction efficiencies are measured and the change in refractive index due to the laser irradiation is calculated (see Table 4.1). The confocal-microscope image of the grating and its internal diffraction is show in the figure 4.2.2 (a). Unlike the fused silica, the absorption spectrum from the laser irradiated region follows the spectrum of the un-irradiated region 4.2.2(b).

Table 4.1: Grating efficiency of various gratings in glasses

Sample	Intensity (Pulse energy μ J)	Dimension of structure (μ)	Grating period (μ)	Efficiency (η)	Δ n (X10^{-3})
Fused Silica	60	4	4	0.20	2.42
Zinc-Tellurite	20	6	10	0.14	2.025
Foturan	65	4	4	0.18	2.24
GE124	65	5	5	0.21	2.49
Baccarat	65	4	6	0.17	2.22

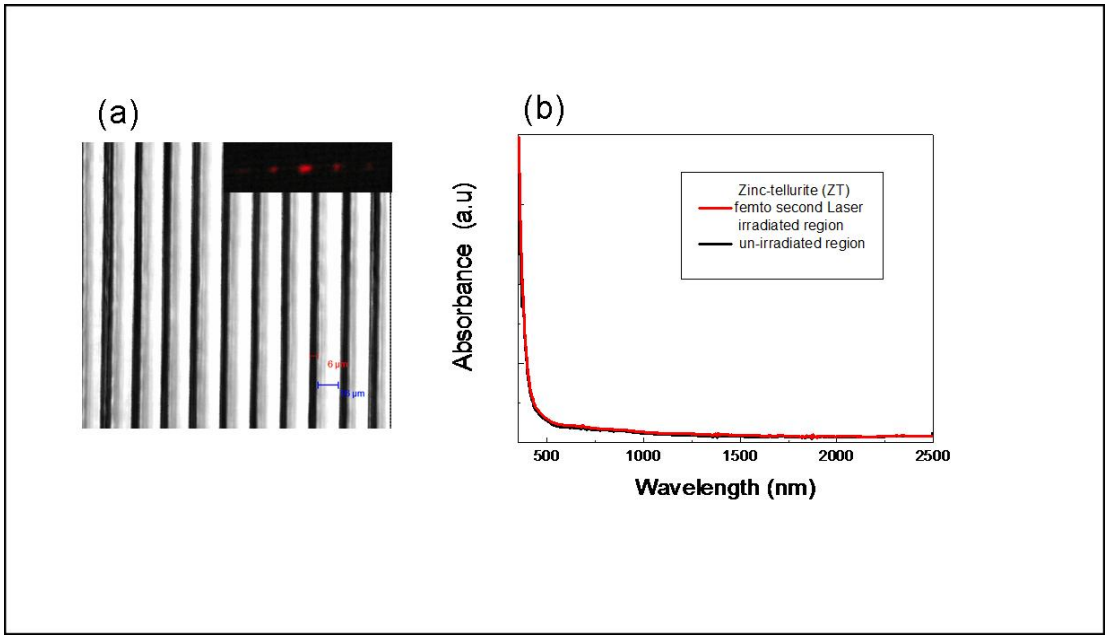

Figure 4.8: (a) Confocal-Microscope image of grating in ZT sample (inset shows the internal diffraction image); (b)Absorption spectrum in the region irradiated with femtosecond laser(red), un-irradiated region (black)

4.2.3 Foturan glass:

Foturan, a photosensitive glass is one of the most successfully commercialized glasses manufactured by Schott Glass Corporation. It comprises lithium aluminosilicate glass doped with trace amounts of silver and cerium. The cerium (Ce^{3+}) ion plays an important role as photosensitizer, which releases an electron to become Ce^{4+} with exposure to UV light. Some silver ions are reduced by the free electrons and silver atoms are created. However, in the case of fs laser irradiation, free electrons are generated by inter-band excitation due to multi-photon absorption for silver atom precipitation. Therefore, Ce^{3+} doping is not necessary for fsec laser micro-machining applications [72]. In a subsequent heat treatment, first the silver atoms diffuse and agglomerate to form nanoclusters at about 500 ^{o} C; then the crystalline phase of lithium meta-silicate grows in the amorphous glass matrix in the vicinity of the silver nanoclusters, which act as nucleus, at about 600 ^{o} C. As this crystalline phase of lithium meta-silicate has higher solubility in a dilute

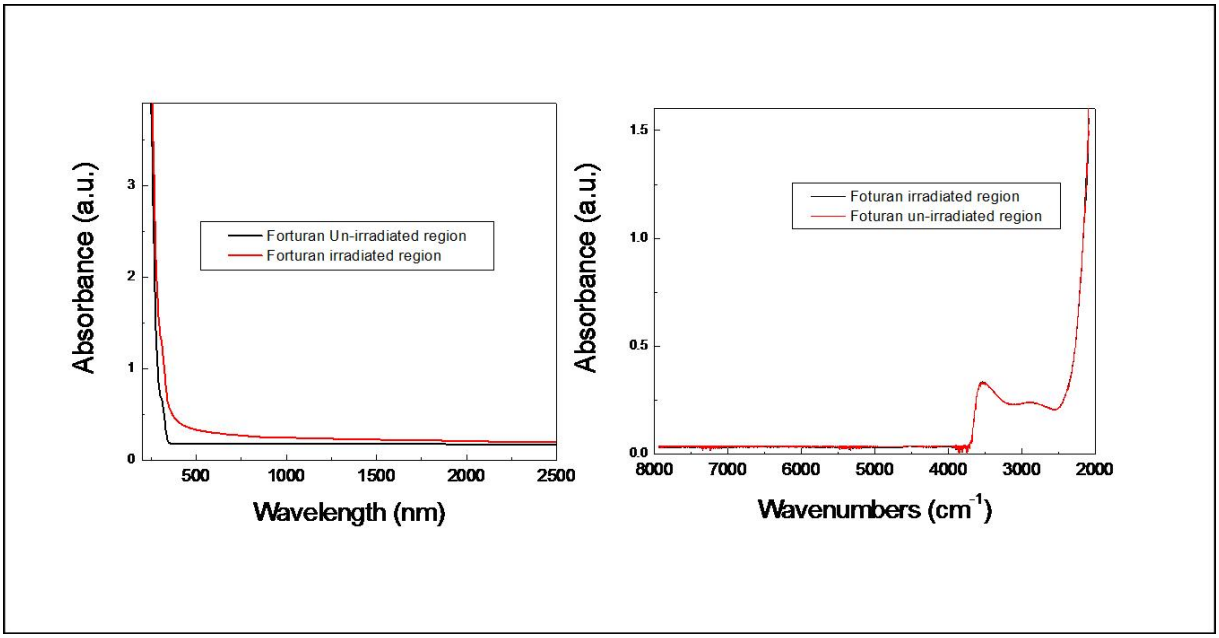

Figure 4.9: Absorbance spectra of Foturan glass from the modified and un-modified region of the samples

solution of HF acid than the glass matrix, it can be easily etched away. Midorikawas group has reported some excellent results of fsec modification in Foturan for applications in Lab-On-a-Chip and microfluidics([73]- [82]) Different structures fabricated in Foturan glass using femtosecond laser pulses include micro-mechanical and micro-optical components, microfluidic dye lasers, and microchannels, all integrated on a single chip leading to lab-on-a-chip device applications [16].

Micrograting were inscribed inside foturan glass, the change in refractive index is estimated to be 2.24 X 10^{-3} from the diffraction efficiency measurements. The absorption spectrum shows a apparent increase in absorbance in the laser irradiated region. This can be attributed to formation of color centers associated with Ag^{+} [66].

Raman spectrum from the laser-irradiated region could not be obtained as there was a strong fluorescence covering the raman bands. Confocal Photoluminescence was obtained by exciting the sample with 457nm, 488nm, 514nm. The Confocal Microscope was used

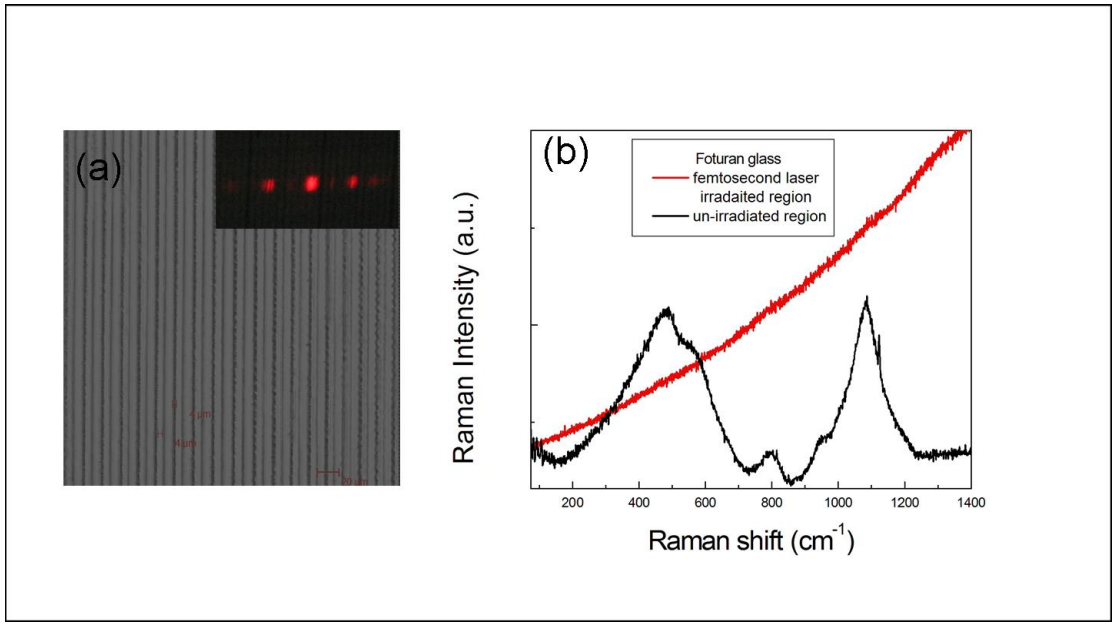

Figure 4.10: (a) Confocal -Microscope images of gratings in Foturan glass, (b) Micro-raman spectra from modified (red) and un-modified(black) regions of the sample

in the XY-lambda mode. In this mode the microscope collects the photoluminescence from the region of interest in the sample over the wavelength range specified. The typical interval width is 3 nm. The region of interest in the sample is excited with laser light and the Photoluminescence is collected for a specified time interval from the entire region of interest. The Photoluminescence in this 3nm band of wavelengths is stored as intensity pattern. The collection window then moves to next consecutive band of wavelength and the PL is recorded. This process is repeated until the entire specified range of wavelength is scanned by changing the collection window. Once the entire range is scanned the intensity patterns corresponding to the various wavelength intervals are integrated to obtain a intensity versus wavelength plot. Interestingly only the region irradiated with fsec laser shows clear photoluminescence band. The center of the band depends on the excitation source wavelength(see figure 4.11. Though this kind of PL was observed in Ag doped Phosphate glasses [66] , to our knowledge this is the first time being observed in Foturan glasses. As the PL is from only the region modified by the laser irradiation, as

the modified region has a relatively higher refractive index compared to the surroundings, it would act as a waveguide. Hence the PL can be confined and can be used as an internal probe when coupled to the microfluidic channels. This is significant as this PL having a broad band can be exploited for Integrated-optics applications. This kind of PL is not observed in the other samples presented in this thesis and as the other glasses do not contain any silver, this confirms that the PL in femtosecond laser irradiated region of Foturan glass is due to the silver-related colour centers.

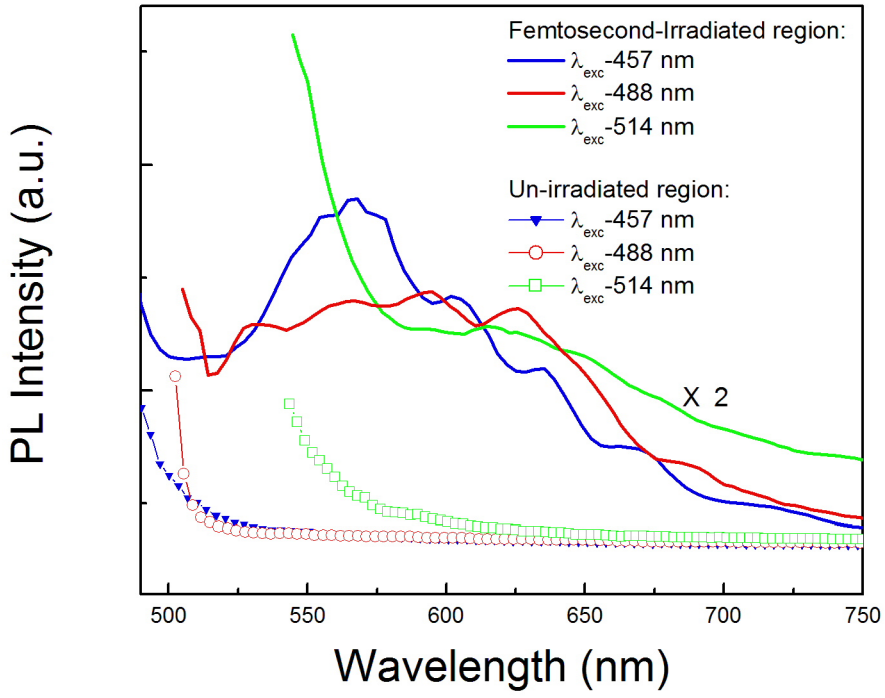

Figure 4.11: PL spectra of Foturan glass.

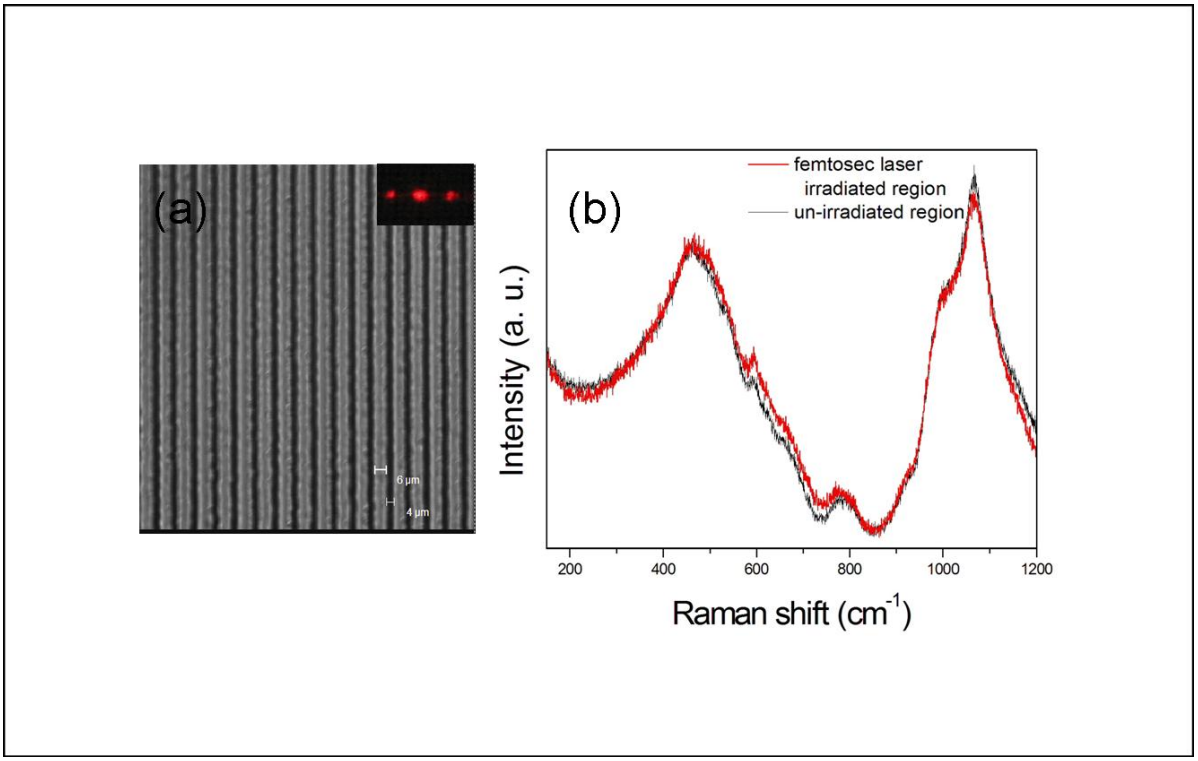

Figure 4.12: (a)confocal-microscope image of the grating structure inscribed in Baccarat glass (b)Micro-Raman spectra from femtosecond laser irradiated(red) and un-irradiated (black) regions

4.2.4 Baccarat glass

The detailed optical spectroscopic characterisation of this high quantum efficiency glass has been described in chapter 2. The results of the femtosecond LDW are discussed here. Figure 4.12(a) shows the gratings inscribed in the glass and the also the internal diffraction images. The absorption spectra shows an increase in absorbance in the visible region similar to fused silica, which can be attributed to scattering losses and absorption due to the defects created during the process of LDW. The modified was studied by micro-Raman. The sample was excited by a 632 nm He-Ne laser. Two main differences between irradiated and not irradiated lines were observed:

(1) an increase of the sharp defect band at 596 cm^{-1} and

(2) an increase of intensity and linewidth of the broad band at about 470 cm^{-1}. This

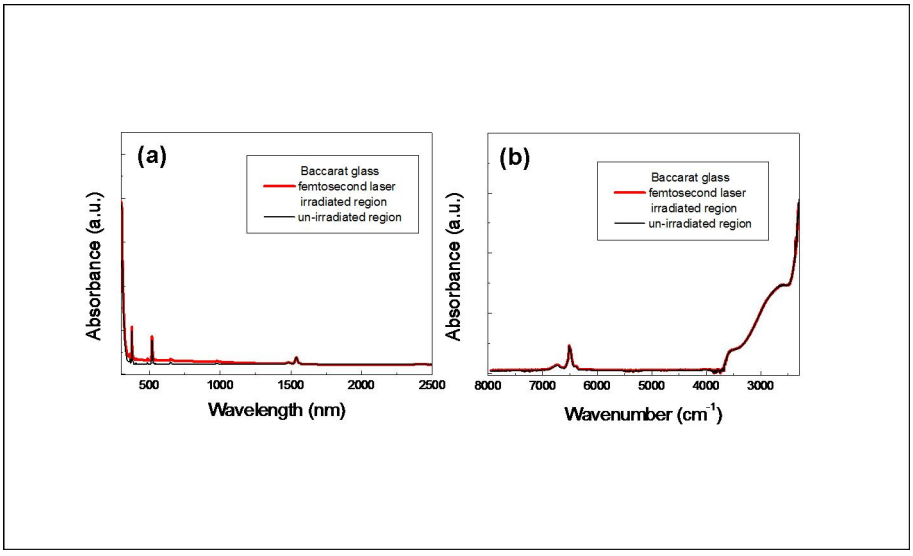

Figure 4.13: Absorption spectra of Baccarat glass(a)visible (b)NIR;obtained from femtosecond laser irradiated (red) and un-irradiate (black)

broad band is due to the bending and stretching of the bonds which connect the silica tetrahedra. Its width is related to the wide distribution of the O-Si-O angles of the disordered structure and increases with the hardening of the structure. The observed broadening of the band indicates an hardening of the glass, which is also the cause of a positive change of the refractive index. The micro-Raman mapping of the grating structure was done across three lines of the grating. The rectangle in the figure 4.14 (a) shows the region of the sample mapped and 4.14(b) shows the results of the mapping of raman intensity. Raman mapping was performed by mapping the intensity variation of the Raman feature at 590 cm^{-1}. The periodic variation of Raman intensity further proved the grating structure formation and also reflects the periodic refractive index variation across the grating structure.

Slit beam shaping for LDW to fabricate micro structures and waveguides

There are two principle ways of LDW

(a)Transverse: where the sample translation is perpendicular to laser propagation axis.

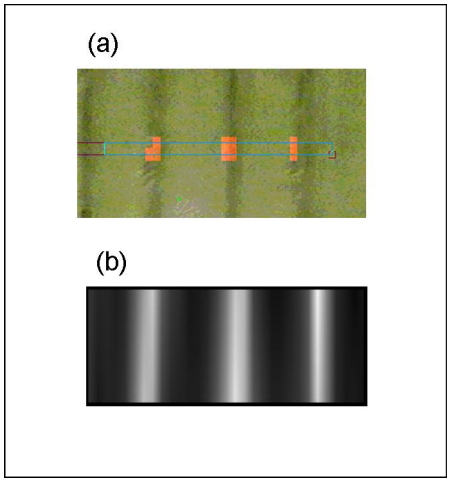

Figure 4.14: Micro-Raman mapping of the grating; (a)Optical image of the region mapped (identified by a rectangle) (b) raman intensity map of the rectangular region;bright region of the map indicates higher intensity

(b) Longitudinal: The sample translation and the laser beam propagation are parallel. Longitudinal LDW helps in fabrication of cylindrical waveguides but the length of the waveguides is limited by the working distance of the focussing objectives. The transverse writing geometry allows one to write waveguides and structures of arbitrary length and design, however this method produces waveguides and structures with strong core asymmetry and significant losses(in case of waveguides)[86]. This asymmetry can be explained as follows: perpendicularly to the beam propagation direction, the waveguide size is given approximately by the beam focal diameter $2\omega_0$, while along the propagation direction, it is given by the confocal parameter b = $2\pi(\omega_0)^2/\lambda$ [87]. For focused diameters of the order of a few micrometers, this results in a large difference in waveguide sizes in the two directions. This asymmetry becomes particularly severe when the waveguide size is increased, as required for waveguiding at the optical communication wavelength of 1.5 μm, thus greatly reducing the efficiency of fiber butt coupling in conventional telecommunications setups[87]. To circumvent this problem Osellame et.al. introduced a novel focusing geometry in which the femtosecond writing beam is astigmatically shaped by changing both the spot sizes in the tangential and sagittal planes and the relative posi-

tions of the beam waists. This shaping allowed the modification of the interaction volume in such a way that the waveguide cross section can be made circular and with arbitrary size[88]. Another simpler way is to use a rectangular slit oriented parallel to the writing direction [76]. In transverse LDW, by placing a rectangular slit close to the focussing objective acts as diffractive element and helps in redistribution of the laser intensity gradient around the focus [89]. Various structures were written by placing a rectangular slit of different dimensions (2mm, 1.5mm, 0.5mm) before the focussing microscope objective. For a particular slit width, line-structures were inscribed by varying the incident laser intensity and the translation speed of the samples, the process is repeated for all other slit widths mentioned above. The incident laser intensity shown in the figures was measured before the focussing by objective and after the slit was placed (the typical values of energy per pulse are varied from < 5 μ J to 75 μ J). The higher end was fixed at around 80-90 μ J, as energies above this were observed to damage samples. The typical speeds of the sample translation were 10, 25, 50, 100, 250 and 500 μm/second. To avoid sample damage, lower translation speed (< 50 μ m /second) were not employed while inscribing micro-structures at higher incident laser intensities (> 40 μ J). Similarly higher translation speed were not used at very low incident laser intensities (< 20 μ J) as the modifications induced by laser inscription in the samples at such experimental conditions were minimal or negligible, and the could not be imaged by the confocal microscope even when operated higher magnifications.

The confocal-microscope images of the structures written without a slit and with a slit of 500 μm placed before the focussing objective, are shown in the figures 4.15, 4.16. (The wobble seen in some of the structures can be avoided by using a vibration isolation optical tables for mounting the nano-positioner.)In every sub-figure, it can be seen that the incident femtosecond laser intensity (pulse energy) and the width of the slit used are mentioned on the top, while at the bottom of every figure the line structure label

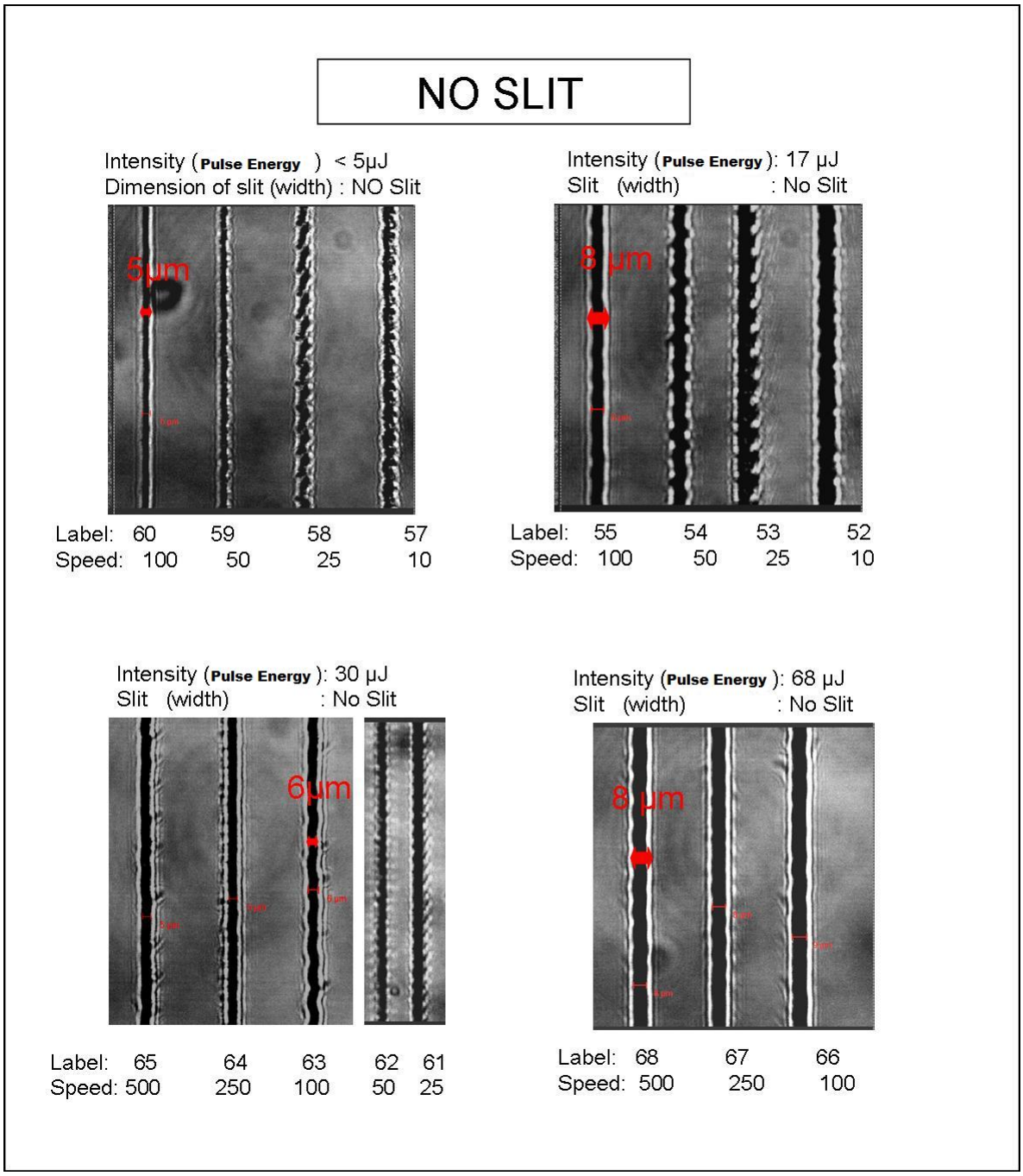

Figure 4.15: Confocal Microscope images of the waveguides inscribed in Baccarat glasses (rectangular Slit was not employed)

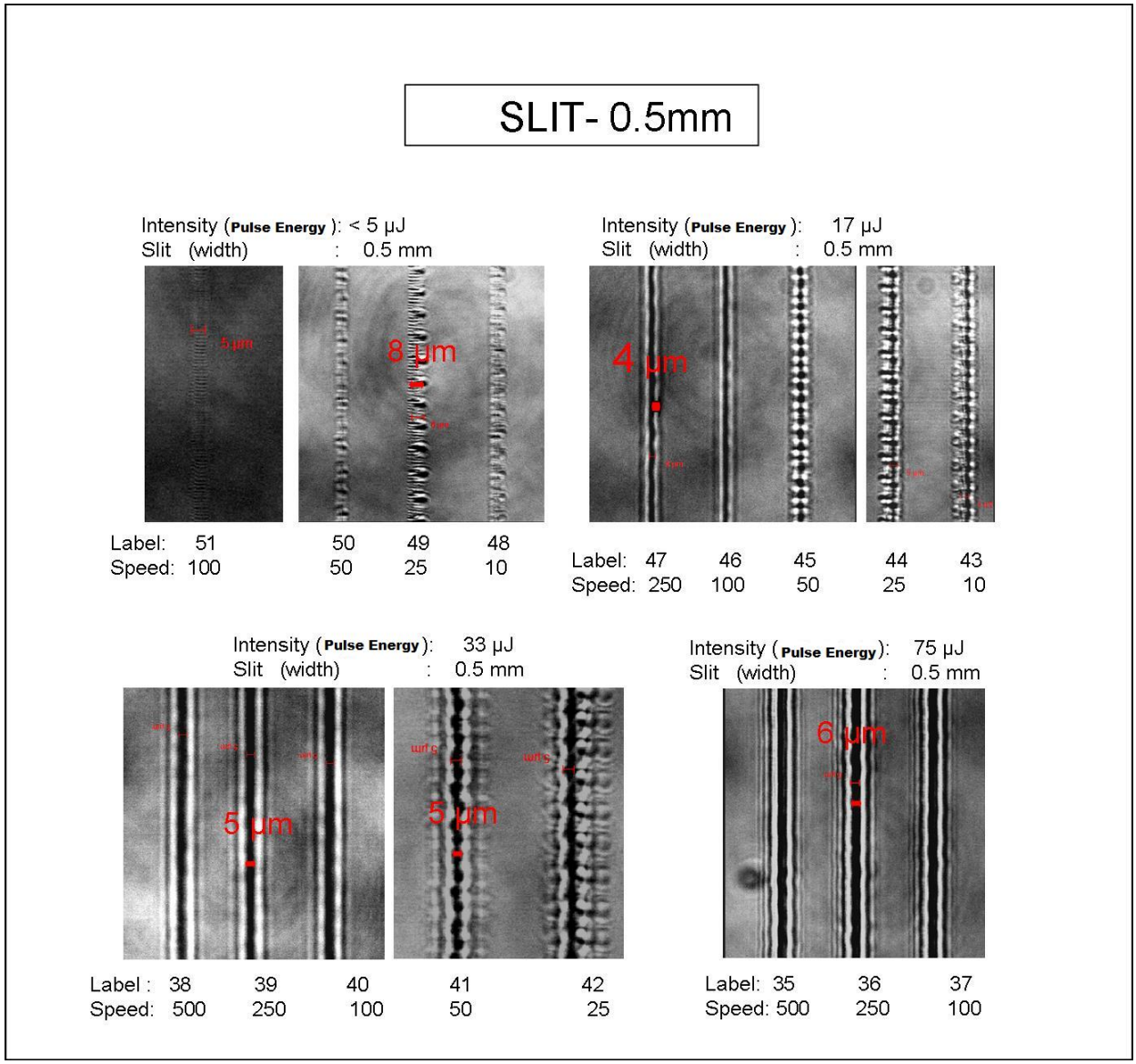

Figure 4.16: Confocal Microscope images of the waveguides inscribed in Baccarat glasses (a rectangular Slit of 0.5 mm was used for laser beam shaping)

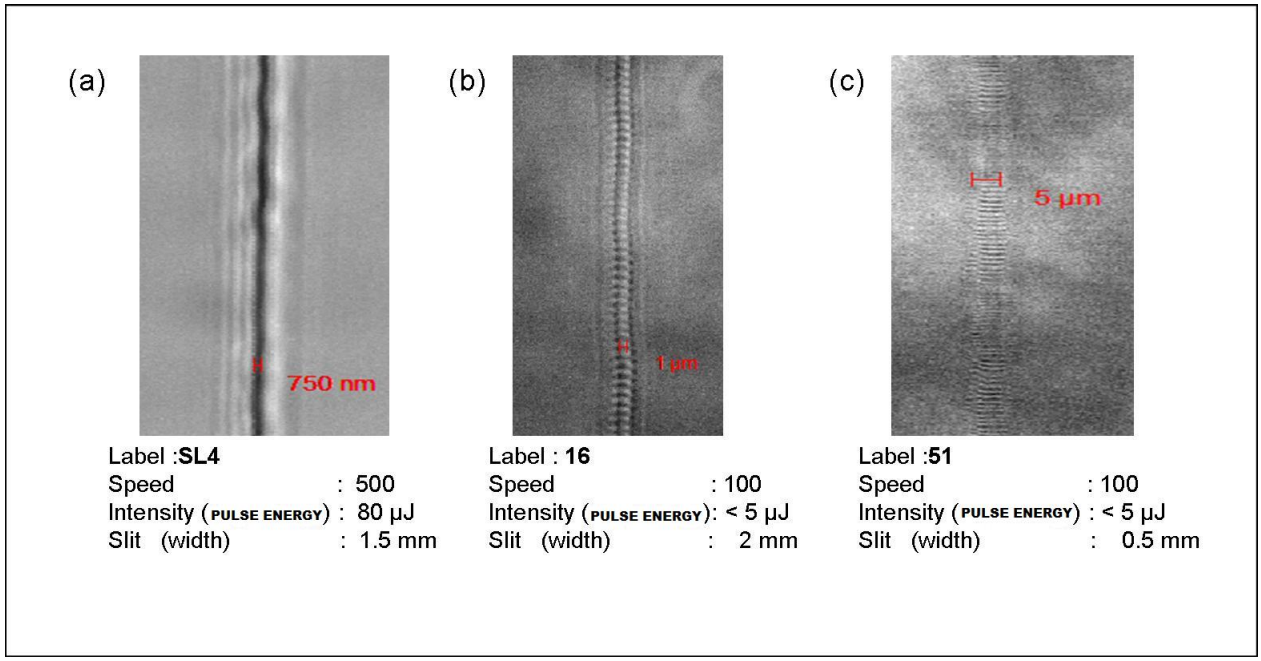

Figure 4.17: Microscope images of structures

number and the corresponding speeds(μ m /second) at which the sample was translated is mentioned. As seen from the figures the width of the structures written at lower speed are broader than those written at higher speed; in fact when the samples are moved at lower speeds a particular region is exposed to more number of laser shots, hence the area modified is more. The structures written using a slit at moderate laser intensities (around 20 , 30 μ J) and at speeds of (250, 500 μ m /second) on visual inspection through the microscope images appear more smooth as compared to structures written without using slit.

The diffraction from the rectangular slit combined with the effects due to repetitive exposure of a spot and the translation speeds, some interesting inscribed structures were observed. Figure4.17(a) shows a sub-micron structure with width of 750 nm. The contiguous pearl [4.17(b)] structured micro-line can be used as waveguide attenuators [15] as these structures scatter light. The modification seen in figure [4.17(c)] are parallel to scale bar, and are periodic. These modified planes are perpendicular to the line structure

are similar to the Fiber bragg gratings.

4.2.5 Near-filed Mode profiles and Loss measurements of Waveguide in Baccarat glass

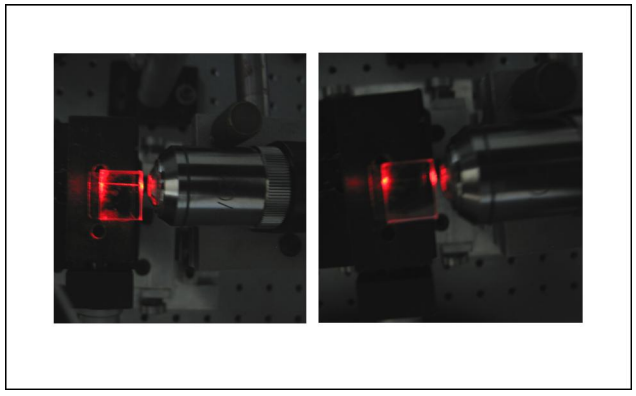

Figure 4.18: Demonstration of waveguiding in the waveguide inscribed in Baccarat, a He-Ne 632 nm cw laser was used.

Using the 'end-fire' (4.18 (a)) method 633 nm cw laser light was coupled into the waveguides. As expected the coupling was seen only in waveguide structures inscribed using a slit. The figure clearly indicates the streak of light guided along the waveguide whereas a small detuning of the laser beam path shows the streak vanishing [4.18 (b)]. This serves as an initial and fast test to verify whether a structure inscribed acts as a waveguide or not.

Near-field Waveguide Mode profile

The schematic diagram of the set-up for acquisition of near-field mode profiles of waveguides is shown in the figure 4.19. The laser source is a semiconductor tunable laser (ECL-200, Santec), with a fiber coupled output. The laser light from this fiber is butt-coupled into waveguides. The radiation from the exit face of the waveguide is collected

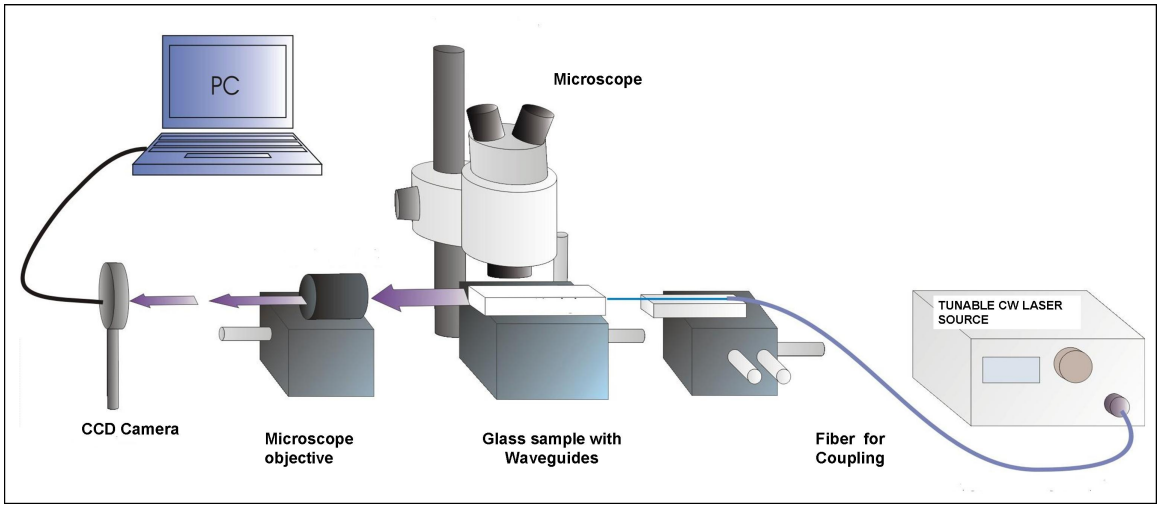

Figure 4.19: Schematic diagram of set-up for acquisition of near-field mode profiles of waveguides

by an 20 X objective and is focused on a Vidicon camera (C-2400, Hamamatsu). The near filed mode profiles are grabbed by a computer connected to the camera.

The optical properties of the structures were tested with the help of cw laser tuned to operate at 1600 nm (1600 nm was chosen in order to avoid absorption from the doped Er). The results show that there is indeed a positive refractive index change sufficient enough for light to be confined and guided through them. Figure 4.20(a) shows a typical mode profile of the output from a fiber. Figure 4.20 (b) shows the near field of the mode profile of a typical waveguide written using a slit of 1.5 mm while scanning the sample at a speed of 500μm /sec and an input energy of 30 μJ. The figure 4.20 (c) is the near field profile of a waveguide written with the same parameters as above but without a slit. The effect of the slit is clearly seen in the figure 4.20 as the mode profile is fairly circular and is comparable to fiber mode, whereas the wg profile without the slit is highly elliptical and it is bigger in size. The profile of the waveguide output 4.20 (b) clearly indicates single mode propagation.

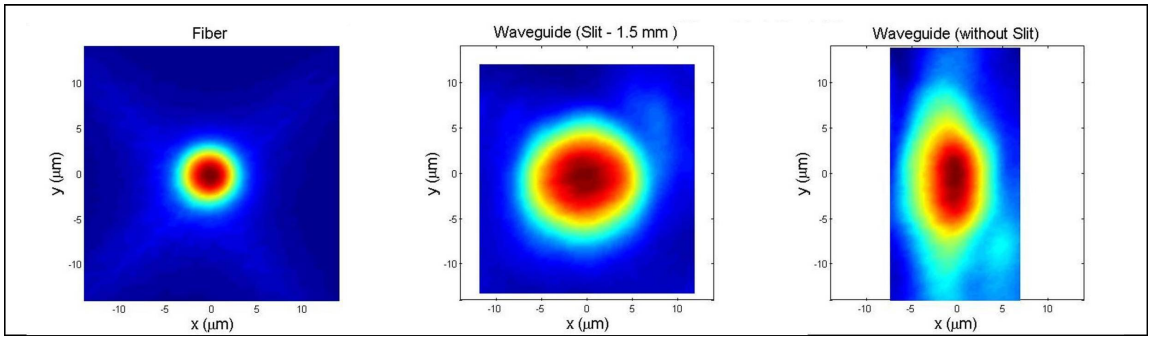

Figure 4.20: Comparison of near-field mode profiles of (a)Fiber , (b) Waveguide inscribed using a rectangular Slit and (c)Waveguide inscribed without a rectangular Slit

Propagation losses

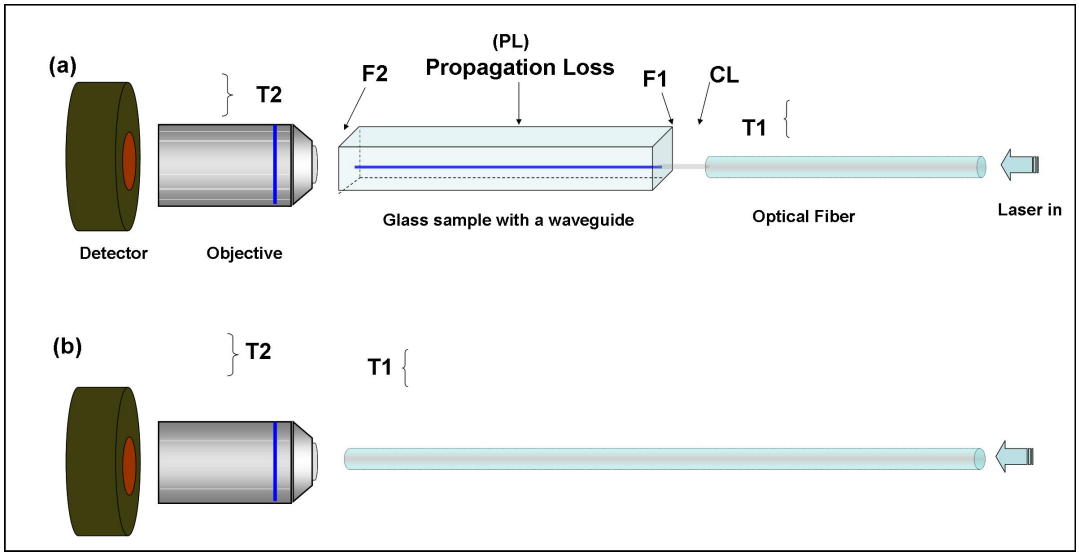

Figure 4.21: Propagation loss measurement in the waveguide(see the text for the description)

A very important parameter to asses the quality of the fabricated waveguides are propagation losses (PL). The set-up for waveguide loss measurement is similar to that of the mode-profile acquisition (see figure 4.19), the camera is replaced by a Germanium detector to measure the power output from the waveguide P_{out} and from the fiber P_{in}. Figure4.21 illustrates the various loss mechanisms involved. The laser light(1600 nm) is

butt-coupled into a waveguide using a fiber. An 20 X objective is placed such that the exit face of the waveguide is at the focus. The laser light at the exit face of the waveguide is collected by the objective and the intensity measured by the detector; this gives the output power P_{out}. As shown in the figure 4.21(b), the waveguide is removed and the fiber is moved close to the objective such that the fiber exit face is now in focus. The laser intensity from the fiber is measured and this gives the input power P_{in}. The total loss T_L is given by the equation

$$T_L = -10log_{10}\frac{P_{out}}{P_{in}} \tag{4.2}$$

T1 is the loss in the fiber used for waveguide coupling and T2 the loss due to the collection end (Objective, detector). The total loss T_L in the waveguide is the sum of the losses due to Fresnel losses (F1, F2), coupling loss (CL) between the fiber and waveguide and the Propagation loss (PL)

$$T_L\ (in\ dB) = [T1\ +\ T2 +\ F1 +\ F2 +\ CL +\ PL] -\ [T1 + T2] \tag{4.3}$$

assuming $F1\ =\ F2\ = FL$

$$Hence\ PL\ (in\ dB)\ =\ T_L - (\ 2\ FL)\ -\ CL \tag{4.4}$$

The near field profile of the waveguide written with a slit of 0.5 mm at a speed of 50 μ m / sec is shown in the figure 4.22. This waveguide has the lowest total loss (T_L) of 2 dB as compared to other waveguides. The CL is estimated from the extent of overlap of the fiber mode with that of the waveguide mode. The CL in this case is estimated to be 0.7 dB, the calculated Fresnel's loss (FL) are 0.2 dB. By using the equation 4.4 and inserting the values of CL and FL, the Propagation loss in the waveguide of 1 cm long is obtained to be $<$ 0.9 dB / cm (It was observed through a microscope that end surface

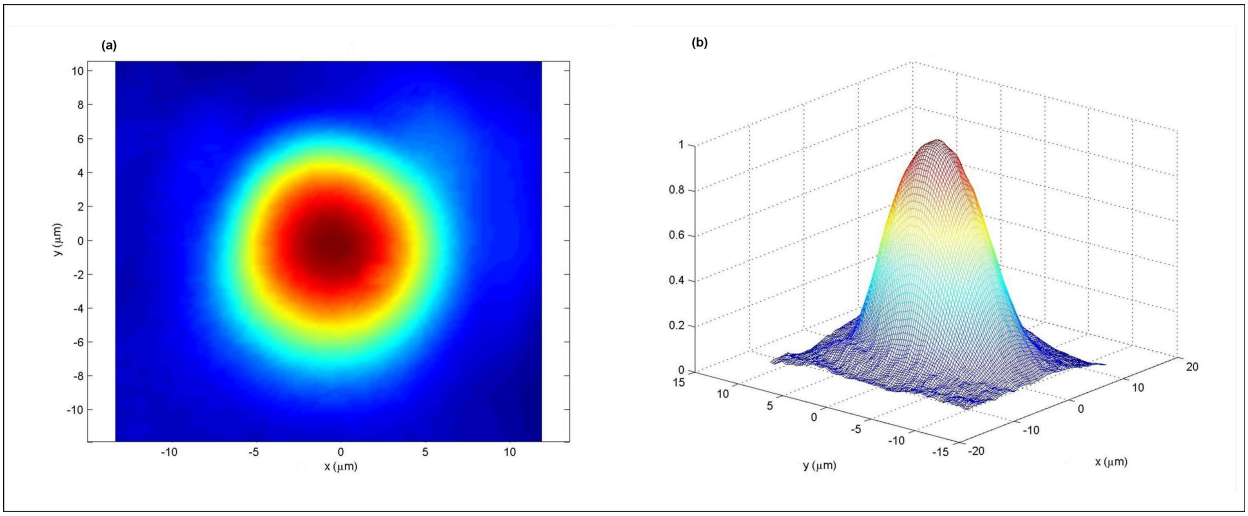

Figure 4.22: Near field mode profile of waveguide

of the waveguides are not polished to the desired level of smoothness). Since the PL value is strongly dependent on the CL, the estimated propagation loss value is expected to be much lower than the 0.9 dB / cm after better polishing of the end surfaces.)

The figure 4.23 shows the plot of the total loss in dB vs the sample translation speed. The graphs with circles (filled circles represent 75 μ joules pulse energy; circle represent 30 μ joules pulse energy) shows the loss of waveguides written using a slit of 0.5 mm and the triangles (filled triangles represent 75 μ joules pulse energy; triangles represent 30 μ joules pulse energy) show the loss of waveguides written with a slit of 1.5 mm width. The following conclusions can be drawn from the figure 4.23.

1) Effect of Slit width :

As can be seen from the graph the waveguides written using a slit of width 0.5 mm (circles) have lower losses as compared to those written using a slit of 1.5 mm (triangles).

2) Effect of Pulse energy

For any of the two slit width, the waveguides written at 30 μ joule pulse energy have relative low losses compared to the waveguides written with 75 μ joule pulse energy . This shows that the modification with pulse energy of 30 μ joule is optimal leading to

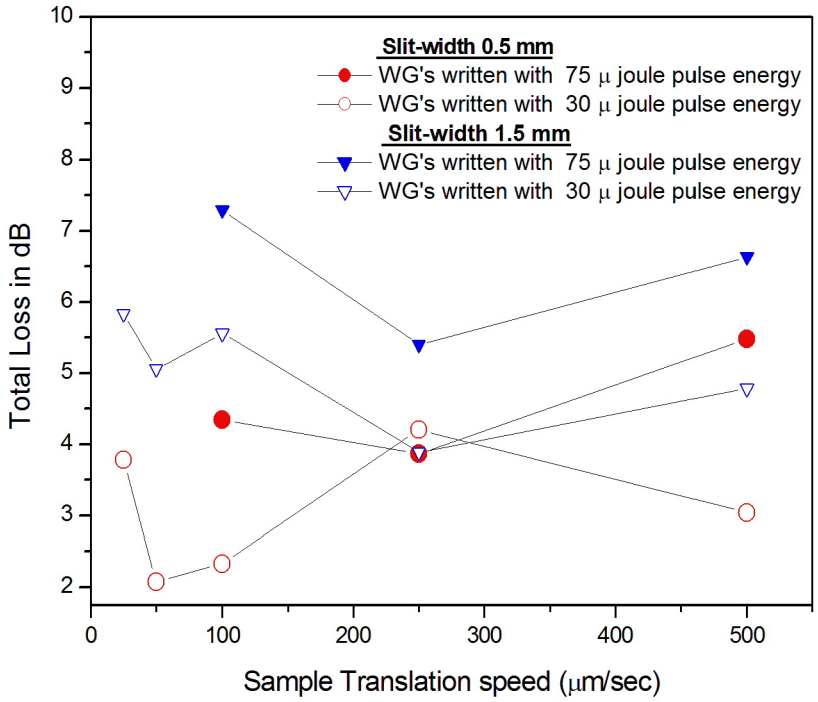

Figure 4.23: Waveguide losses Vs the LDW parameters

better confinement of the laser light and for pulse energies more than 75 μ joule seems to induce damages inside the waveguides leading to high losses.

3) Sample translation speed:

For a given slit width and pulse energy an optimal sample translation speed can be associated (50 μ m / sec in case of circles and 250 μ m / sec in case of triangles) leading to a low loss regime. At lower writing speeds, owing to the multiple exposure of a zone of the sample, the damage induced may be high leading to high losses in the waveguides. At higher speeds due to lack of proper overlapping between the modified zone, the confinement of the laser light may be poor leading to high losses. As stated previously the waveguide with relative low loss (PL of 0.9 dB / cm) was written with a slit of 0.5 mm at with a translation speed of 50 μ m / sec.

4.3 Conclusions

Various micro-structures of different shapes and width were inscribed into the Fused Silica, Foturan, Zinc-tellurite and Baccarat glasses. Micro gratings were fabricated in the above mentioned glasses using femtosecond direct writing. Refractive index change in these structures was estimated using optical diffraction technique and was found to be in the order of 10^{-3} sufficient for wave guiding applications. Confocal PL was observed from the LDW modified regions of in Foturan sample. Micro-Raman mapping of gratings in Baccarat confirmed the periodic refractive index change leading to the formation of grating . Waveguiding was demonstrated in the structures written in Baccarat glasses using a rectangular slit. With optimization of LDW parameters like the slit width, sample translation speeds and pulse energies, propagation loss $<$ 0.9 dB / cm is achieved in the waveguides in Baccarat.

Bibliography

[1] "3D Laser Microfabrication Principles and Applications", Edited by Hiroaki Misawa and Saulius Juodkazis, WILEY-VCH Verlag GmbH& Co. KGaA, Weinheim, 2006.

[2] J.A. Lewis, G.M. Gratson, Materials Today, 7(7-8), 32-39, 2004.

[3] D.B. Chrisey, Science 289, 879, 2000.

[4] K.M. Davis, K. Miura, N. Sugimoto, and K. Hirao, Opt. Lett. 21, 17291731, 1996.

[5] C.B. Schaffer, A. Brodeur, J.F. Garcia, and E. Mazur, Opt. Lett. 26, 9395 2001.

[6] J. Qiu, K. Kojima, K. Miura, T. Mitsuyu and K. Hirao, Opt. Lett., Vol. 24, pp. 786-788, 1999.

[7] E.N. Glezer and E. Mazur, Appl. Phys. Lett., Vol. 71, pp. 882- 884, 1997.

[8] Y. Shimotsuma, K. Hirao, J. Qiu, K. Miura, J. Non-Cryst. Solids 352, 646-656, 2006.

[9] Roberto Osellame, Nicola Chiodo, Giuseppe Della Valle, Giulio Cerullo, Roberta Ramponi, Paolo Laporta, Alexander Killi, Uwe Morgner, and Orazio Svelto, IEEE Journal of selceted topics in Quantum Electronics, VOL. 12, NO. 2, 2006.

[10] K. Itoh, W. Watanabe, Riken Review, 50, 90-94, 2003.

[11] S. Taccheo, G. Della Valle, R. Osellame, G. Cerullo, N. Chiodo, P. Laporta, O. Svelto, Alexander Killi, Uwe Morgner, Max Lederer and Daniel Kopf, Opt. Lett. Vol. 29, No. 22, 2004.

[12] G. Della Valle, R. Osellame, N. Chiodo, S. Taccheo, G. Cerullo, P. Laporta, A. Killi, U. Morgner, M. Lederer D. Kopf, Opt. Exp.Vol. 13, No. 16, 5976, 2005.

[13] K. Itoh, JLMN-Journal of Laser Micro/Nanoengineering, 1(1), 1-6, 2006.

[14] M. Kohtoku, T. Kominato, Y. Nasu, and T. Shibata, NTT Technical Review 3(7), July 2005.

[15] J. Qiu, The Chemical Record, 4, 50-58, 2004.

[16] K. Sugioka, Y. Cheng, and K. Midorikawa, Mater. Res. Soc. Symp. Proc. Vol. 850, MM1.3.1-MM1.3.12, 2005. (FOTURAN glass REVIEW)

[17] J. Kruger, W. Kautek, Adv. Poly. Sci. 168, 247-289, 2004.

[18] S. Kawata, H.-B. Sun, T. Tanaka, and K. Takada, Naturere 412, 697, 2001.

[19] H.B. Sun, S. Kawata, Adv. Polymer Sc. 170, 169-273, 2004.

[20] V. Apostolopoulos, L. Laversenne, T. Colomb, C. Depeursinge, R. P. Slath, M. Pollnau, R. Osellame, G. Cerullo and P. Laporta Appl. Phys. Lett. 85, 1122-1124, 2004.

[21] S. Juodkasis, K. Nishimura, S. Tanaka, H. Misawa, E.G. Gamaly, B. Luther-Davies, L. Hallo, P. Nicolai, V. T. Tikhonchuk, Phys. Rev. Lett. 96, 166101, 2006.

[22] G. A. Torchia, P. F. Meiln, A. Rodenas, D. Jaque, C. Mendez, and L. Roso, Opt. Express 15, 13266-13271, 2007.

[23] J. Lamela, A. Rodenas, D. Jaque and F. Jaque, Opt. Express 15, 3285-3290, 2007.

[24] A. Saliminia, N.T. Nguyen, M.-C. Nadeau, S. Petit, S.L. Chin, R. Valle , Journal of Applied Physics , 93 , 3724-3728 (2003)

[25] A. Zoubir, C. Lopez, M. Richardson, and K. Richardson, Opt. Lett. 29, 1840-1842, 2004.

[26] W. Watanabe, S. Sowa, T. Tamaki, K. Itoh , J. Nishii, panese Journal of Applied Physics 45(29), L765-L767, 2006.

[27] R.R. Thomson, S. Campbell, I.J. Blewett, A.K. Kar, D.T. Reid, Appl. Phys. Lett. 88, 111109, 2006.

[28] R. Osellame, M. Lobino, N. Chiodo, M. Marangoni, G. Cerullo, R. Ramponi, H.T. Bookey, R.R. Thomson, N. D. Psaila and A.K. Kar, Appl. Phys. Lett. 90, 241107, 2007.

[29] A. Rdenas, J. A. Sanz Garca, D. Jaque, G. A. Torchia, C. Mendez, I. Arias, L. Roso and F. Agull-Rueda, J. Appl. Phys. 100, 033521, 2006.

[30] D. Day and M. Gu, Opt. Exp. 12(16), 5939-5945, 2005.

[31] V. Maselli, R. Osellame, G. Cerullo, R. Ramponi, P. Laporta, L. Magagnin and P. L. Cavallotti, Appl. Phys. Lett., 88, 191107, 2006.

[32] S. Nolte, D. Blomer, J. Burghoff, A. Szameit, M. Will, A. Tunnermann, Glass Science and Technology 78, 141-147, Suppl. C, 2005.

[33] J.W. Chan, T. Huser, S. Risbud, and D. Krol, Opt. Lett. 26, 17261728, 2001.

[34] J. W. Chan, T. R. Huster, S. H. Risbud, and D. M. Krol, Appl. Phys. A: Mater. Sci. Process. 76, 367-372, 2003.

[35] M. Kamata, M. Obara, Appl. Phys. A. 78, 85-88, 2004.

[36] A. Saliminia, N.T. Nguyen, S.L. Chin and R. Valle, Optics Communications, 241(4-6), 529-538, 2004.

[37] A. Saliminia, N.T. Nguyen, S.L. Chin and R. Valle, Opt. Commun., 241(4-6), 529-538, 2004.

[38] J. Liu, Z. Zhang, S. Chang, C. Flueraru, C.P. Grover, Opt. Commun. 253(4-6), 315-319, 2005.

[39] C. Hnatovsky, R.S. Taylor, P.P. Rajeev, E. Simova, V.R. Bhardwaj, D.M. Rayner, and P.B. Corkum, Appl. Phys. Lett. 87, 014104, 2005.

[40] L. Shah, A.Y. Arai, Opt. Exp. 13(6), 1999-2006, 2005.

[41] A.Q. Wu, I.H. Chowdhury, and X. Xu, Phys. Rev. B 72, 085128, 2005.

[42] E. Toratani, M. Kamata, and M. Obara, Appl. Phys. Lett. 87, 171103, 2005.

[43] Q. Sun, H. Jiang, Y. Liu, Y. Zhou, H. Yang, and Q. Gong, J. Opt. A: Pure Appl. Opt. 7, 655-659, 2005.

[44] H. Zhang, S.M. Eaton, P.R. Herman, Opt. Exp. 14(11) 4826-4834, 2006.

[45] G. Matthaus, J. Burghoff, M. Will, S. Nolte, A. Tunnermann, Appl. Phys. A. 83, 347-350, 2006.

[46] A. Szameit, D. Blomer, J. Burghoff, T. Schreiber, T. Pertsch, S. Nolte, A. Tunnermann, F. Lederer, Opt. Exp. 13(26), 10552-10557, 2005.

[47] M. Will, S. Nolte, B. N. Chichkov, A. Tunnermann, Appl. Opt. 41, 4360-4364, 2002.

[48] C. Hnatovsky, R.S. Taylor, E. Simova, V.R. Bhardwaj, D.M. Rayner, P.B. Corkum, J. Appl. Phys. 98, 013517, 2005.

[49] V.R. Bhardwaj, E. Simova, P.P. Rajeev, C. Hnatovsky, R.S. Taylor, D.M. Rayner, P.B. Corkum, Phys. Rev. Lett. 96, 057404, 2006.

[50] J.R. Vazquez de Aldana, C. Mendez, L. Roso, Opt. Exp. 14(3), 1329-1338, 2006.

[51] A. Zoubir, M. Richardson, L. Canioni, A. Brocas, L. Sarger, J. Opt. Soc. Am. B. 22(10), 21382143, 2005.

[52] D. Blmer, A. Szameit, F. Dreisow, T. Schreiber, S. Nolte, A. Tnnermann, Opt. Exp. 14, 2151-2157, 2006

[53] A.Q. Wu, I.H. Chowdhury, X. Xu, Appl. Phys. Lett. 88, 111502, 2006.

[54] T.Q. Jia, H.X. Chen, M. Huang, F.L. Zhao, X.X. Li, S.Z. Xu, H.Y. Sun, D.H. Feng, C.B. Li, X.F. Wang, R.X. Li, Z.Z. Xu, X.K. He, H. Kuroda, Phys. Rev. B 73, 054105, 2006.

[55] A. Szameit, J. Burghoff, T. Pertsch, S. Nolte, A. Tnnermann, and F. Lederer, Opt. Express 14, 6055-6062, 2006.

[56] A. Zoubir, C. Rivero, R. Grodsky, K. Richardson, M. Richardson, T. Cardinal, M. Couzi, Phys. Rev. B. 73, 224117, 2006.

[57] G. Li, K.A. Winick, A.A. Said, M. Dugan, P. Bado, Opt. Lett. 31(6), 739-741, 2006.

[58] W.J. Reichman, D.M. Krol, L. Shah, F. Yoshino, A. Arai, S.M. Eaton, P.R. Herman, J. Appl. Phys. 99, 123112, 2006.

[59] N. T. Nguyen, A. Saliminia, W. Liu, S. L. Chin, R. Vallee , Opt. Lett., 28 , 1591-1593, 2003.

[60] A. Marcinkeviius, S. Juodkazis, M. Watanabe, M. Miwa, S. Matsuo, H. Misawa, and J. Nishii, Opt. Lett. 26, 277-279, 2001.

[61] K. Miura, J. Qiu, H. Inouye, T. Mitsuyu and K. Hirao, App. Phys. Lett., Vol. 71, pp. 3329-3331, 1997.

[62] J.W. Chan, T.R. Huser, S.H. Risbud and D.M. Krol, Appl. Phys. A, Vol. 76, pp. 367-372, 2003.

[63] O.M. Efimov, L.B. Glebov, K.A. Richardson, E. van Stryland, T. Cardinal, S.H. Park, M. Couzi and J.L. Bruneel, Optical Mater., Vol. 17, pp. 379-386, 2001.

[64] Y. Sikorski, A..A. Said, P. Bado, R. Maynard, C. Florea and K.A. Winick, Electron. Lett., Vol. 36, pp. 226-227, 2000.

[65] D. Homoelle, S. Wielandy, A.L. Gaeta, N.F. Borrelli and C. Smith, Opt. Lett., Vol. 24, pp. 1311-1313, 1999.

[66] Quan-Zhong Zhao, Jian-Rong Qiu, Xiong-Wei Jiang, Chong-Jun Zhao and Cong-Shan Zhu, Opt. Express, 12, 4035, 2004.

[67] K.C. Vishnubhatla, R. Sai Santosh Kumar, D. Narayana Rao, S. Venugopal Rao, (IOD-12) Proceedings of Photonics2006, Eighth International Conference on Opto-electronics, Fiber Optics and Photonics, University of Hyderabad, December 13-16, 2006.

[68] P J Scully, D Jones and D A Jaroszynski, J. Opt. A: Pure Appl. Opt. 5 S92-S96, 2003.

[69] Y.Tokuda, M.Saito.M.Takahashi, K.Yamada, W.Watanabe, K.Itoh, T.Yoko, Journal of Non-Crystalline Solids326& 327, 472-475 (2003).

[70] P.Nandi, G.Jose, C.Jayakrishna, S.Debbarma, K.Chalapathi, K.Alti, A.K.Dharmadhikari, J.A.Dharmadhikari and D.Mathur, Optics Express, vol. 14, No.25, 12145-12150 (2006).

[71] G.C.Righini, I.Banyasz, S.Barneschi, M.brenci, M.Cremona, D.Ehrt, M.Ferrari, R.M. Montereali, G.N.Conti, S.Pelli, S.Sebastiani and C.Tosello, Proc. SPIE 5840, 649-657(2005).

[72] Y.Dai, J.Qui, X.Hu, L.Yang, X.Jiang.C.Zhu, B.Yu, Appl.Phys.B, 84, 501-506, 2006.

[73] Z. L. Li, D. K. Y. Low, M. K. Ho, G. C. Lim, and K. J. Moh, J. Laser Appl. 18, 320, 2006.

[74] Y. Cheng, K. Sugioka, and K. Midorikawa, Opt. Express 13, 7225-7232, 2005.

[75] M. Masuda, K. Sugioka, Y. Cheng, N. Aoki, M. Kawachi, K. Shihoyama, K. Toyoda, H. Helvajian, and K. Midorikawa, Appl. Phys. A76, 857-860, 2003.

[76] Y. Cheng, K. Sugioka, K. Midorikawa, M. Masuda, K. Toyoda, M. Kawachi, K. Shihoyama, Opt. Lett. 28, 55-57, 2003.

[77] Y. Cheng, K. Sugioka, K. Midorikawa, M. Masuda, K. Toyoda, M. Kawachi, and K. Shihoyama, Opt. Lett. 28, 1144-1146, 2003

[78] K. Sugioka, M. Masuda, T. Hongo, Y. Cheng, K. Shihoyama, K. Midorikawa, Appl. Phys. A79, 815-817, 2004.

[79] Y. Cheng, K. Sugioka, and K. Midorikawa, Opt. Lett. 29, 2007, 2004.

[80] Y. Cheng, K. Sugioka, M. Masuda, K. Shihoyama, K. Toyoda, and K. Midorikawa, Opt. Express 11, 1809, 2003,

[81] T. Hongo, K. Sugioka, H. Niino, Y. Cheng, M. Masuda, J. Miyamoto, H. Takai, and K. Midorikawa, J. Appl. Phys. 97, 063517, 2005

[82] S. Ho, P. R. Herman, Y. Cheng, K. Sugioka, and K. Midorikawa, in Conference on Lasers and Electro-Optics (CLEO), Vol. 97 of OSA Trends in Optics and Photonics Series (Optical Society of America, Washington, D.C., 2004), paper CThD6.

[83] D. Ye, Y. Bing-Kun, L. Bo, Q. Jian-Rong, Y. Xiao-Na, J. Xiong-Wei, and Z. Cong-Shan, Chinese Physics Letters 22, 2626-2629, 2005.

[84] V.R. Bhardwaj, E. Simova, P.B. Corkum, D.M. Rayner, C. Hnatovsky, R.S. Taylor, B. Schreder, M. Kluge, J. Zimmer, J. Appl. Phys. 97, 083102, 2005.

[85] B. Yu, B. Chen, B. Lu, X. Yan, J. Qiu, C. Zhu, X. Jinag, Proc. SPIE 6171, 61710G1-61710G15, 2006.

[86] M.Ams, G.D.Marshall, D.J.Spence and M.J.Withford, Optics express, vol.13, No.15, 5676-5681(2005).

[87] R. Osellame, S. Taccheo, M. Marangoni, R. Ramponi, and Paolo Laporta, D. Polli, S. De Silvestri, and G. Cerullo, J. Opt. Soc. Am. B, Vol. 20, No. 7, 2003.

[88] G. Cerullo, R. Osellame, S. Taccheo, M. Marangoni, D. Polli, R. Ramponi, P. Laporta, and S. De Silvestri, Opt. Lett. 27, 19381941, 2002.

[89] K.J.Moh, Y.Y.Tan, X.C.Yuan, D.K.Y.Low, and Z.l.Li, Optics express, vol.13, No.19, 7288-72979, 2005.

Chapter 5

Conclusions & Future perspectives

5.1 Materials and Characterisation techniques

The research work was carried out with the following main objectives,

- to find novel suitable host material for Er^{3+} ions,
- to achieve Er^{3+} luminescence enhancement using Silver as sensitizer, and
- to fabricate waveguides, micro-structures by LDW in various glasses.

The results of the same were presented in previous chapters in detail. The summary of the results highlighting the most important results are presented here. The following are the list of samples which were characterised

Materials worked on:

- Modified Silica Baccarat glasses activated with Er
- Zinc-Tellurite glasses activated with Er
- Silver as sensitizer: Er doped Ag ion-exchanged silicate glasses
- Ag ion exchanged Phosphate glasses co-activated with Er

- Sodium phosphate glasses activated with Er 3+ co-doped with silver
- Fused Silica, Foturan^{TM}, GE124, Zinc-Tellurite and Baccarat glass: Direct-writing of optical waveguides, and microstructures using a femtosecond Laser

The following are the main characterization techniques/tools used to characterize the refractive index, thickness, propagation losses, emission properties and the quantum efficiency of the emission of the Er^{3+} activated glasses under investigation. **Characterization Techniques:**

- m-line (for Refractive index, waveguide loss measurements)
- Laser Scanning Confocal Microscopy
- Luminescence, Excitation spectroscopy, and lifetime measurements
- Raman spectroscopy (Micro/Macro)
- XPS
- UV-Visible, FTIR absorption spectroscopy
- TEM

5.2 Summary of results

The **Baccarat glasses**, with molar composition: 77.29 SiO2: 11.86 K2O: 10.37 PbO: 0.48 Sb2O3, have been produced by a conventional melt-quenching technique. Two different sets of samples were produced, containing 0.2 and 0.5 mol% of Er^{3+} ions. Optical spectroscopic characterisation of these glasses reveals that the glasses have these salient features

- **High transparency:** Raman and Absorption measurements show high transparency of glass

- **Low OH content:** The OH concentration from FTIR absorption spectra are estimated to be low as 3.6 X 10^{18} cm^{-3}.

- **No NIR-to-visible upconversion:** implies (a)Er3+ ions are homogeneously distributed in the glass matrix signal has been detected. The non-appearance of upconversion in Baccarat glasses indicates that most of and that (b) absence of interaction clusters as well as chemical clusters are practically absent.

- **Lifetimes:**The $^4I_{13/2}$ metastable of the Er3+ ions decay curves present a single exponential profiles; with a lifetime value of 11.5 ms, 14.2 ms for the sample doped with 0.5 mol %, 0.2 mol % of erbium respectively

- **High Quantum efficiency:**quantum efficiency reaches very high values, up to 79.8 % in the case of a calculation based on the Judd-Ofelt theory, for the 0.2 mol % Er3+ − activated glass and remains among the highest quantum efficiencies estimated in pure or modified-silica host glasses

Erbium-doped soda-lime-silicate and phosphate thin plates were co-doped with Ag by using silver-sodium ion-exchange and later submitted to various heat treatments in air. Bulk Sodium phosphate glass activated with Er and codoped with silver were prepared, these glasses were subjected to heat treatments. The most important results are as follows

- **Luminescence Enhancement:** The Er3+ PL at 1.5 μ m is found to be increased for nearly all excitation wavelengths from 400 to 500 nm in the Ag -ion exchanged annealed Silicate samples

- **Bulk Phosphate glasses:**The radiative transfer, i.e reabsorption, dominates on the very weak non-radiative transfer.

- **Silicate samples:** Though radiative mechanism of energy transfer is active, the non-radiative mechanisms are dominant, the enhancement of the erbium lumines-

cence in a silver doped glass is due to a energy transfer process from silver species, especially dimers.

With the focuses on the development of Laser Direct writing for inscription of micro-structures and waveguides and setup was home-built and optimized. Various micro-structures , micro gratings, waveguides were inscribed into glasses.

- **Micro-gratings:**Gratings were inscribed in fused silica, foturan, ge124, zinc-tellurite and Baccarat glasses. The change in refractive index is calculated to be of the order of 10^{-3} from the diffraction efficiency measurements.

- **Sub-micron structure:**By placing a slit (of appropriate dimension) before the microscope objective, a structure of width 750 nm (less than diffraction limit) is written in Baccarat glass

- **Demonstration of Waveguiding:**Waveguiding was demonstrated in the structures written in Baccarat glasses using a rectangular slit. The lowest estimated propagation loss in the waveguide achieved is 0.9 dB / cm

5.3 Future perspectives: Direct application to the Industry

The optical and spectroscopic properties of this modified-silica glass make it well adapted as host medium for the light propagation and a good candidate for many applications in telecommunication systems. The laser action shown by the micro-spheres of Baccarat glass fabricated by plasma torch method amply substantiates the fact that Baccarat is a good glass. Research aimed to demonstrate correlation of silver nanoparticles and/or multimers with 1.5 μ m luminescence enhancement has to taken advantage.

The development of erbium-doped integrated optical amplifiers so far has followed three main manufacturing routes:

(a)local doping of a bulk glass or of a glass thin film with rare-earth ions by diffusion or ion-implantation; the process leads to a local increase of the refractive index, and therefore also produces a waveguide;

(b) fabrication of a rare-earthdoped bulk glass by conventional melting process or by sol-gel, and subsequent fabrication of the waveguide by diffusion processes (by ion-exchange, in particular);

(c)deposition of a glass thin-film waveguide containing rare-earth ions by RF magnetron sputtering, chemical vapour deposition (CVD), electron-beam vapour deposition, flame hydrolysis deposition (FHD), or sol-gel processes .

The LDW using femtosecond laser has openend new vistas in this field, efforts are in the direction to fabricate waveguide amplifiers in Baccarat , zinc-tellurite glasses. Micro-fluidic channels are to be inscribed into the Foturan glass and integrate them with the waveguides written by LDW with the aim of developing waveguide sensors for Integrated optic applications and to realize the 'Lab on Chip' concept.

Publications List:

1. " Photoluminescence characterisation of Femtosecond laser direct written microstructures and gratings in fused silica and Foturan glasses " , manuscript under preparation (to be submitted to Journal Applied Physics A: Material Science and Processing).

2. " Femto-second laser direct writing parameters Vs propagation losses of buried waveguides in high Quantum efficiency Er doped Baccarat glass" , to be communicated to the Applied Physics Letters.

3. **K.C. Vishnubhatla**, S. Venugopal Rao, R. Sai Santosh Kumar, K. Shiva Prasad, P.S.R.Prasad and D. Narayana Rao, "Inscription and characterization of micro-structures in silicate, FOTURAN^{TM} and tellurite glasses by femtosecond laser direct writing" , Proc. of SPIE Vol. 6881 688113-1, (2008).

4. **K.C. Vishnubhatla**, S. Venugopal Rao, R. Sai Santosh Kumar, S.N.B. Bhaktha, A. Chiappini, A. Chiasera, J. Laureyns, M. Ferrari, M. Mattarelli, M. Montagna, R.Osellame, R. Ramponi, G.C. Righini , S. Turrell, and D. Narayana Rao, "Micro-Raman mapping of micro-gratings in BACCARAT glass directly written using femtosecond laser" , Proc. of SPIE Vol. 6881 688114-1, (2008).

5. S. Venugopal Rao, A. A. Bettiol, **K. C. Vishnubhatla**, S. N. B. Bhaktha, and D. Narayana Rao, F. Watt, " Fabrication and characterization of microcavity lasers in rhodamine B doped SU8 using high energy proton beam " , Appl. Phys. Lett., 90, 101115 (2007).

6. M. Mattarelli, M. Montagna, **K.C. Vishnubhatla**, A. Chiasera, M.Ferrari, G.C.

Righini, " Mechanisms of Ag to Er energy transfer in silicate glasses: A photoluminescence study " , Physical Review B 75, 125102(2007).

7. M Bouazaoui, B Capoen, A P Caricato, A Chiasera, A Fazzi, M Ferrari, G Leggieri, M Martino, M Mattarelli, M Montagna, F Romano, T Tunno, S Turrel and **K.C. Vishnubhatla**, " Pulsed Laser Deposition of Er doped tellurite films on large area " , Journal of Physics: Conference Series, 59 , 475478, (2007).

8. M.Mattarelli, M.Montagna, E. Moser, **K.C. Vishnubhatla**, C. Armellini, A.Chiasera, M.Ferrari, G.Speranza, M. Brenci, G. Nunzi Conti, G.C. Righini, " Silver to Erbium energy transfer in phosphate glasses " , Journal of Non Crystalline Solids 353, 498501(2007)

9. S.N.B. Bhaktha, B. Boulard, S. Chaussedent, A. Chiappini, A. Chiasera, E. Duval, C. Duverger, S. Etienne, M. Ferrari, Y. Jestin, M. Mattarelli, M. Montagna, A. Monteil, E. Moser, H. Portales, **K.C. Vishunubhatla**, " Erbium-activated modified silica glasses with high $^4I_{13/2}$ luminescence quantum yield " , Opt. Mat., 28, 1325-1328(2006).

10. G.Speranza, S.N.B. Bhaktha, A. Chiappini, A. Chiasera, M. Ferrari, C. Goyes, Y. Jestin, M. Mattarelli, L. Minati, M. Montagna, G. Nunzi Conti, S. Pelli, G.C. Righini, C. Tosello, **K.C. Vishunubhatla**, " Nanocomposite Er-Ag silicate glasses " , Journal of Optics A: Pure and Applied Optics, 8, S450 (2006).

11. Prasad P.S.R., Shiva Prasad K., **Krishna Chaitanya V.**, Babu, E.V.S.S.K., Sreedhar B. and Ramana MurthyS, " In situ FTIR study on the dehydration of natural goethite ", Journal of Asian Earth Sciences, 27, 4, 503-511(2006).

12. Vincent Benoit, Shivakiran Narasimha Bantwal Bhaktha, Brigitte Boulard, Stphane Chaussedent, Andrea Chiappini, Alessandro Chiasera, Eugene Duval, Serge Etienne, Maurizio Ferrari, Bruno Gaillard-Allemand, Yoann Jestin, Maurizio Mattarelli, Maurizio Montagna, Andr Monteil, Enrico Moser, Gualtiero Nunzi Conti, Stefano Pelli, Herv Portales, Desai N. Rao, Giancarlo C. Righini, **Krishna Chaitanya Vishunubhatla**, " Optical and spectroscopic properties of erbium-activated modified silica glass with 1.54 μ m high quantum efficiency " , SPIE Proc. (Photonics West), 5723, 79-88(2005).

13. Shivakiran N. Bhaktha B., Roberto Calzolai, Andrea Chiappini, Alessandro Chiasera, Maurizio Ferrari, Yoann Jestin, Maurizio Mattarelli, Maurizio Montagna, Enrico Moser, Gualtiero Nunzi Conti, Stefano Pelli, Herve Portales, Desai N. Rao, Giancarlo C. Righini, Cristiana Tosello, **Krishna C. Vishunubhatla**, Jie Zheng, " Spectroscopic properties of Er^{3+}-activated Ag-exchanged silicate and phosphate glasses " , SPIE Proc. (Photonics West), 5723, 139-146(2005).

14. M. Martino, A.P. Caricato, A. Fazzi, F. Romano, V.K. Tikhomirov , A.B. Seddon, M. Mattarelli, A. Chiappini , **Krishna C. Vishnubhatla**, " Pulsed Laser Deposition of Er^{3+} - doped Oxyfluoride Thin Films ", Journal of Non-Crystalline Solids, 351 , 18101813, (2005).

15. P.S.R. Prasad, **V. Krishna Chaitanya**, K. Shiva Prasad and D. Narayana Rao, " Direct formation of the -CaSO4 phase in dehydration process of gypsum: In situ FTIR study " , American Mineralogist, 90, 4, 672-678 (2005)

Conferences Presentations (International / National):

1. **K.C. Vishnubhatla**, R. Sai Santosh Kumar, K. Shiva Prasad, P.S.R. Prasad . Narayana Rao, S. Venugopal Rao, " Inscription and characterization of micro-structures in silicate, FOTURANTM and tellurite glasses by femtosecond laser direct writing ", selected for ORAL presentation at LASE 2008 (SPIE-Photonics West), California, U.S.A, January 2008.

2. **K.C. Vishnubhatla**, R. Sai Santosh Kumar, S.N.B. Bhaktha, A. Chiappini, A. Chiasera, J. Laureyns, M. Ferrari, M. Mattarelli, M. Montagna, S. Turrell, , S. Venugopal Rao, D. Narayana Rao , " Micro-Raman mapping of micro-gratings in BACCARAT glass directly written using femtosecond laser ", selected for ORAL presentation at LASE 2008 (SPIE-Photonics West), California, U.S.A, January 2008.

3. **K.C. Vishnubhatla**, R. Sai Santosh Kumar, D. Narayana Rao, S. Venugopal Rao, " Femtosecond laser direct writing of waveguides and microstructures in borate, modified-silicate, and FOTURAN glasses." , (IOD-12) Proceedings of Photonics2006, Eighth International Conference on Optoelectronics, Fiber Optics and Photonics, University of Hyderabad, December 13-16, 2006.

4. **K. C. Vishnubhatla**, M. Mattarelli, C. Armellini, S. N. B. Bhaktha, A. Chiasera, A. Chiappini, M. Montagna, E. Moser, G. Speranza, M. Ferrari, G. C. Reghini, D. N. Rao, " Silver to Erbium energy transfer in Phosphate glasses.", (PMD-31) Proceedings of Photonics2006, Eighth International Conference on Optoelectronics, Fiber Optics and Photonics, University of Hyderabad, December 13-16, 2006.

5. C. Armellini, R. Belli, S.N.B. Bhaktha, A. Chiappini, A. Chiasera, M. Ferrari, V.

Foglietti, Y. Jestin, M. Montagna, A. Minotti, E. Moser, S. Pelli, D.N. Rao, G.C. Righini, C. Tosello, **K.C. Vishnubhatla**, " RF-sputtering fabricated silicahafnia planar waveguides activated with Er^{3+}/Yb^{3+} for integrated optics. " , (IOD-22) Proceedings of Photonics2006, Eighth International Conference on Optoelectronics, Fiber Optics and Photonics, University of Hyderabad, December 13-16, 2006.

6. S.N.B. Bhaktha, A. Chiappini, A. Chiasera, M. Ferrari, C. Goyes, Y. Jestin, M. Mattarelli, L. Minati, M. Montagna, G. Nunzi Conti, S. Pelli, G.C. Righini, G. Speranza, C. Tosello, **K.C. Vishunubhatla**, " Nanocomposite Er-Ag silicate glasses " , European Optical Society Topical Meeting, Optical Microsystems, Capri, Italy (15-18th Sep 2005) 18.

7. A. Chiappini, S.N.B. Bhaktha, M. Montagna, E. Moser, C. Tosello, **K.C. Vishunubhatla**, S. Dir, C. Armellini, A. Chiasera, M. Ferrari, C. Goyes, Y. Jestin, G. Nunzi Conti, S. Pelli, G.C. Righini, " Synthesis, Properties and Structural Investigation of Colloidal Silica Particles for Photonic Applications " , Proceedings of the Workshop Italiano Sol-Gel, Milano 22-23 June, 2006, pp. 58-59.

8. Y. Jestin, C. Armellini, S.N.B. Bhaktha, A. Chiappini, A. Chiasera, S. Dir, M. Ferrari, C. Goyes, M. Montagna, E. Moser, G. Nunzi Conti, S. Pelli, G.C. Righini, C. Tosello, **K.C. Vishunubhatla**, " Sol-Gel Derived Glass-Ceramic Waveguides for Optical Amplification ", Proccedings of the V Workshop I